DTIC
SELECTED
DEC 1 1 1995
F

TECHNICAL REPORT SIT-DL-93-9-2695

JUNE, 1993

A LABORATORY INVESTIGATION OF
SEA ICE DYNAMICS
IN A
STRATIFIED WATERBODY
Preliminary Results

by

Jennifer Kehl Waters
Michael S. Bruno
Thomas O. Herrington
Kelly L. Rankin

19951208 062

TECHNICAL REPORT SIT-DL-93-9-2695

JUNE, 1993

A LABORATORY INVESTIGATION OF
SEA ICE DYNAMICS
IN A
STRATIFIED WATERBODY
Preliminary Results

by

Jennifer Kehl Waters
Michael S. Bruno
Thomas O. Herrington
Kelly L. Rankin

Table of Contents

1

Appendix A:
        Test Data

Appendix B:
        Internal Wave Strip Chart Recordings

Appendix C:
        Salinity Profile Data and Plots

2

List of Figures

3

List of Tables

4

Introduction

The movement of Arctic ice floes is receiving greater interest today than ever before. While the tracking of ice floes is important to aiding in Arctic navigation, a knowledge of the dynamics of sea ice is also vital to understanding critical environmental issues such as global warming.

Although for many years, ice observations were obtained primarily under proprietary government studies, several marginal ice zone experiments have recently been conducted which have provided accessible, enlightening data of ice floe tracks, ice compositions and floe geometries. In addition to large projects, such as the Marginal Ice Zone Experiment (MIZEX), the Coordinated Eastern Arctic Experiment (CEAREX), and the Antarctic Marine Ecosystem Research in the Ice Edge Zone (AMERIEZ), there have also been many smaller studies. The relatively new data from these studies has made it possible to more accurately model ice floe movement physically and numerically. The effect is actually two-fold, since the site data has provided critical information needed to prepare and perform relevant model tank tests. The availability of the tank test data, in addition to the site data, allows validation and further refinement of numerical prediction methods.

One of the primary difficulties in modelling (both physically and numerically) ice floe movement is the numerous independent parameters which significantly affect floe behavior. In addition to geometric parameters, such as length, beam, draft, and under-ice topography, the salinity profile of the water body in which the ice floe moves has been shown to have a large effect on the ice-water resistance, and thus the floe's motion (e.g. Morison, et. al., 1987).

The tests described in this thesis investigate the additional resistance that internal wave creation induces on an ice floe moving in a two-layer, density stratified water body. Stratified conditions exist in what is referred to as the Marginal Ice Zone (MIZ) during the spring melt season. The stratification is created when the ice floes, which have very little salt content, melt and create a layer of relatively warm, low salinity (and low density) water on top of the existing water, which has typical open-ocean salinity, Arctic temperature, and thus higher density values. The stratification is remarkably stable, with a sharp pycnocline lasting for long periods of time.

5

Previous Laboratory and Field work

Laboratory Experiments

There have been a limited number of laboratory experiments undertaken which investigate the added resistance due to internal wave creation on moving bodies. However, each experiment described here contains useful information for further studies which incorporate similar tank experiments.

Perhaps the most well-known laboratory experiments of the type were conducted by Ekman (1904). His study was motivated by field observations of a phenomenon that he referred to as "dead water." The study illustrated and explained the vertical momentum transfer from a body moving on the surface to the generation of internal waves. It was not until much later that similar studies were conducted and their results published.

Muench and Hachmeister's laboratory study (1984) modelled sea ice keels in a stratified tank, 15 m long, 0.5 m wide, and 1 m deep. The study was similar to the one discussed in this report; the additional drag that internal wave generation induced on the travelling ice keel was extracted and plotted versus non-dimensional velocity, U/C_1, where C_1 is the first-mode interfacial phase speed. (This is discussed later in the Analysis section.) Some of the significant differences between Muench and Hachmeister's study and the Davidson Laboratory study include the modelled floe geometries, as well as the parameters varied during the tests.

Ma and Tulin's (1992) study investigated the internal wave wake geometry and amplitude generated by a spheroid (simulating a ship) moving faster than the fastest internal wave phase speed (the supersonic case) in a stratified tank, 12 ft (3.7 m) long, 8 ft (2.4 m) wide, with a 2 ft (0.61 m) depth. Although the relevance of this study to Arctic ice floe movement is limited, the report contains some interesting experimental setup information.

Helfrich and Melville's (1985) paper discusses an experimental and theoretical study of long, nonlinear internal waves over slope-shelf topography. The laboratory experiments were conducted in a salt-stratified tank, 24 m long, 0.38 m wide with a 0.6 m water depth. Although the waves in this experiment were created by an internal-wave maker, not a moving disturbance on the free surface, the information contained in the report may be quite valuable for further

studies. The shadowgraph photographs of the internal waves are particularly impressive. The experimental results compared very well with their KdV model predictions. However, problems with use of the theoretical model to study actual oceanographic situations are discussed.

Field Studies

As stated earlier, there now exist a great deal of field observations which may be applied toward modelling ice floe dynamics. The studies mentioned here represent a mere sampling of the literature that has been published to date.

The study by Morison et. al. (1987) is perhaps one of the most comprehensive studies of the parameters affecting ice floe drag in the summer MIZ of the Greenland Sea. The study, performed during MIZEX '84, found the ocean conditions to be highly variable. Data collected from the two drifting ice stations include observations of ocean boundary layer turbulence, profiles of water temperature, salinity, and velocity, as well as ice ablation, ice concentration, solar radiation and spectral albedos. The stratification's impact on the ice floe drag and heat transfer is discussed. It was found that for high stratification, the drag increased dramatically, possibly due to internal wave generation by ice bottom roughness. Correlation with Muench and Hachmeister's (1984) results is also discussed. In the report it is stressed that more laboratory experiments need to be conducted to provide more data to validate theoretical models. McPhee and Kantha's (1989) paper later discussed these field observations in their study of internal wave generation by sea ice.

Sandven and Johannessen's (1987) paper on internal wave observations in the MIZ states two possible internal wave generators: tidal oscillation over a topographic feature, or ice keels moving in relation to the water. The internal wave characteristics and wave energy levels of the observed waves are discussed; and a dispersion relation is solved numerically and compared with the observations. They conclude that the internal waves observed may be modelled, to a good first approximation, as horizontally propagating plane gravity waves in an inviscid fluid.

There are also several field studies of internal wave dynamics outside of the Marginal Ice Zone. For example, Watson, et. al. (1992) discuss measurements of a novel experiment in which three ships were used to generate internal wave wakes in a stratified sea loch. Valuable results are obtained, particularly in

7

reference to the dependence of disturbing-body length to generated internal wave characteristics.

Previous Theoretical and Numerical Work

Internal Wave Theory

The effect of internal waves on ice floe movement is discussed by Bruno (1991). The assumptions in his development of the internal wave equations are applicable to the study addressed in this thesis. Therefore, the rigorous derivations provided of the equations governing internal wave generation should provide guidance in further analyses of the results found in the Davidson Laboratory study.

Yih (1960) presents a model of wave motion in a stratified, inviscid fluid obtained by reducing the governing equations to a Sturm-Liouville system. The paper provides applications for continuously stratified fluids, as well as those containing density discontinuities. The result is a very versatile numerical model with broad applicability.

Zhu, et. al. (1987) present and discuss two theoretical models of dispersive long waves propagating in a stratified fluid. One is an inhomogeneous KdV (IKdV) model, while the other is a Boussinesq-class model. Both models were developed for predicting the internal waves generated by a pressure disturbance moving in incompressible, inviscid and stratified fluid systems. The two methods are compared to each other and to experimental data. Although their discussions of two-layer stratified systems is limited, their findings show potential for application to this ice floe study.

There are also many other studies which investigate internal wave energy and internal wave creation by specific types of forcings. Ball's (1963) paper discusses the transfer of a surface wave's energy to an internal wave, with detailed derivations for the shallow water case. It may be possible to draw an analogy of the surface wave's impartation of energy to an internal wave field to that of an ice floe. However, complications arising due to wave field coupling, which are nonexistent in ice floe dynamics, may hinder comparisons of the two phenomena.

Ice Floe Numerical Modelling

Several ice-ocean numerical models have been developed. The types of models vary widely, from short-term (order of hours or days) to long term (order of months or years). However, none have included the additional resistive and coupling effects attributable to internal wave creation.

Some of the recent models which incorporate ice-ocean coupling effects include Bruno and Madsen (1989), Kantha and Mellor (1989), and Pritchard et. al. (1990). Coupling of the ice and ocean affects the ice motion and the dynamics of the upper ocean. The ice-water resistance, which is the source of the coupling, remains largely unresolved. The resistance at the ice-water interface is generally attributed to only two factors: skin friction resistance associated with the small-scale roughness of the under-ice topography, and form drag associated with pressure disturbances from large-scale features such as keels. However, in a stratified ocean, another coupling mechanism due to the generation of internal waves exists. It has been shown that this phenomenon may significantly affect the ice-water resistance and thus the ice motion (e.g. Muench and Hachmeister, 1984).

Separate studies of ice-water drag coefficient determination for implementation into ice floe numerical models also neglect internal wave generation effects. From studies such as Madsen and Bruno's (1987) relatively simple methodology for calculating ice floe drag coefficients to McPhee's (1982) thorough analysis of ice-water dynamics, explicit incorporation of internal wave generation is not identified. In McPhee's (1982) report, a rigorous analysis of several parameters affecting ice-water drag, including boundary layer alteration due to rapid melting, is addressed. McPhee discusses deficiencies in ice-water drag treatment of other numerical models, and provides several methods for incorporating the momentum flux between the ice and the water in those models. However, later studies indicate the necessity of also including internal wave generation effects (e.g. McPhee and Kantha, 1989).

Although discussion of the numerical models in depth would transcend the scope of this thesis, it is important to emphasize that internal wave effects on ice-water drag, and therefore predictive models, still demand further attention.

The Davidson Laboratory Project

Introduction

The series of experiments discussed in this thesis investigated the increased drag exhibited by ice floes in salinity-stratified waters. The tests examined the dependence of the additional ice-water drag and the characteristics of the generated internal wave on parameters such as floe velocity, floe draft, upper layer thickness, and under-ice topography. These parameters were therefore varied in the test matrix to achieve information on the corresponding trends. Both non-stratified and stratified tests were performed.

The tests were conducted in Davidson Laboratory's Tank 3 Facility. The tank is 313 ft (95.4 m) long, 12 ft (3.6 m) wide, and permits water depths up to 6 ft (1.8 m). The tank was designed primarily as a high-speed naval architectural towing tank. However, many other hydrodynamic projects, including offshore structure wave impact studies, reef flow visualizations and coastal beach erosion studies have been conducted in this tank. The towing carriage permits velocities up to 100 ft/s (30 m/s) with a 0.01 ft/s (0.003 m/s) resolution. The towing mechanism provides extremely accurate and consistent low speed towing velocities.

For the stratified experiments, the tank was salinity-stratified by creating a saline water body and layering fresh water above the salt water. The stratification desired was a two-layer configuration, to simulate marginal ice zone conditions observed by Morison et. al. The stratification procedure is described and a sample achieved salinity profile is provided in the Large-Scale Experimental Setup section.

The ice floe models were constructed of extruded polystyrene and fitted with an interior wood frame to facilitate connection to the towing apparatus. A stiff spring balance with a maximum capacity of 10 lb, used to obtain drag measurements, connected the floe to the towing apparatus. Internal wave data was acquired through two methods: time-history wave wire records and VHS video tape recordings. (Both are also described further in the Large-Scale Experimental Setup and Instrumentation subsection.) See Figure 1 for sketch of the test setup.
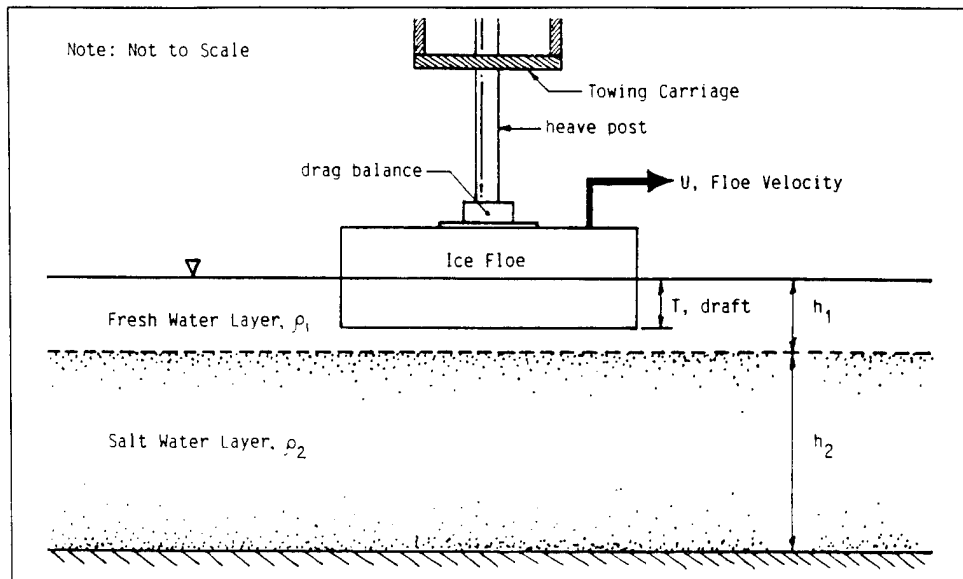
Figure 1: Sketch of Ice Floe Test Setup

Scaling

Standard naval architectural practices were followed in the scaling of the ice floe tests. Froude number similarity between full scale and model scale floes was assumed. Bruno (1992) discusses the impracticalities of Reynolds scaling, and gives further justification for employing Froude's hypothesis to this series of experiments.

The full scale floes were assumed to have the following idealized geometric characteristics:

$$length, L= 100 \text{ m}$$
$$beam, B= 100 \text{ m}$$
$$draft, T= 8.3 \text{ to } 16.6 \text{ m}.$$

A length scale ratio of 109 was used, which yielded model floe dimensions of:

$$length, L= 3 \text{ ft (0.91 m)}$$
$$beam, B= 3 \text{ ft (0.91 m)}$$
$$draft, T= 3 \text{ to } 6 \text{ in (7.6 to 15.2 cm)}.$$

12

The majority of the upper layer thicknesses modelled corresponded to full scale thicknesses between 19 m and 25 m, with one set of tests performed corresponding to a full-scale upper thickness of 33 m. Although the full-scale ice drafts are high compared to marginal ice zone observations (Bourke and McLaren, 1992), preliminary tank tests indicated that these corresponding higher model drafts were required to create quantifiable drag forces and internal wave disturbances in the experiments. In any case, it appears that the critical parameter is not the absolute floe draft, but rather the draft relative to the upper layer thickness, which was representative of full-scale conditions.

Non-dimensional total resistance coefficients were obtained by applying the following formula:

$$C_t = \frac{F_t}{\rho A U^2},$$

where F_t is the total measured drag force, A is the wetted surface area, and U is the towing speed. (Note the variation from some conventions of defining $C_t = \frac{F_t}{\frac{1}{2}\rho A U^2}$.)

Pursuant to common naval architectural practice, the total drag force acting on the ice floe was separated into two components: a frictional resistance component, F_f, and a residual resistance component, F_r:

$$F_t = F_f + F_r.$$

The residual resistance component includes the effects from all of the non-frictional drag contributors. The coefficients C_f and C_r are non-dimensionalized in a similar manner as C_t, employing the respective resistive component forces, F_f and F_r. Therefore, the total resistance coefficient may be written:

$$C_t = C_f + C_r.$$

Arctic ice floe observations have indicated that a moving ice floe creates extremely little to no measurable surface wave creation. The Froude number of the model tests was therefore limited to avoid creation of surface waves during the tank experiments. This condition then simplified the ice-water drag analyses by allowing assumption of zero surface wavemaking drag.

In the unstratified tests, the only sources of resistance were therefore assumed to be skin friction and form drag, hence the value of F_r is equal to the form drag, F_d, i.e. $F_r \equiv F_d$. Therefore, for unstratified tests, the above equation may be written:

$$F_{t,\,unstratified} = F_f + F_d.$$

13

It is recognized that most conventions non-dimensionalize the form drag coefficient, C_d, using the frontal projection area (i.e. beam $\times$ draft). However, in this thesis, continuity throughout all coefficients is preserved by non-dimensionalizing C_r using the *total* wetted surface area. To avoid any confusion, the coefficient C_d will not be used, and the form drag component of the total resistance will hereafter be referred to only as the "unstratified residual resistance," and the corresponding coefficient written as "$C_{r,\,unstratified}$." Therefore:

$$C_{t,\,unstratified} = C_f + C_{r,\,unstratified}.$$

In the stratified tests, the residual resistance included the additional drag caused by internal wave creation, i.e. $F_{r,\,stratified} = F_{r,\,unstratified} + F_{iw}$, where F_{iw} is the internal wave drag component. Therefore the total drag coefficient for the stratified tests was written:

$$C_{t,\,stratified} = C_f + C_{r,\,unstratified} + C_{iw}.$$

Flat Plate Tests

Before the ice floes were tested, flat plate tests were performed to determine the skin frictional resistance of the material used to construct the model ice floes. The "flat plate" used in such a test is actually a streamlined, thin board of the material of interest with tapered ends, which is mounted vertically and towed lengthways so as to minimize form drag and surface wave production. The assumption in flat plate tests is that the resistance due to skin friction is so proportionally greater than the other components of the resistance (such as wavemaking and form drag), that the total resistance measured is entirely attributable to skin friction resistance. Towing velocities are also limited so as to prevent surface wave creation.

Following these assumptions, a flat plate was created out of the material used to construct the ice floe models, and attached to the carriage with a draft of 9 in (23 cm). (A sketch of the flat plate used for these tests is shown in Figure 2.) A soft spring drag balance with a maximum capacity of 10 lb and a resolution of 0.01 lb was used to measure the plate's drag force. The friction coefficient for the floe material was determined from the flat plate tests as:

$$C_f = \frac{F_{total,\,flat\,plate}}{\rho A U^2} \,,$$

where $F_{total,\,flat\,plate}$ was the total measured drag force from the flat plate test.

14
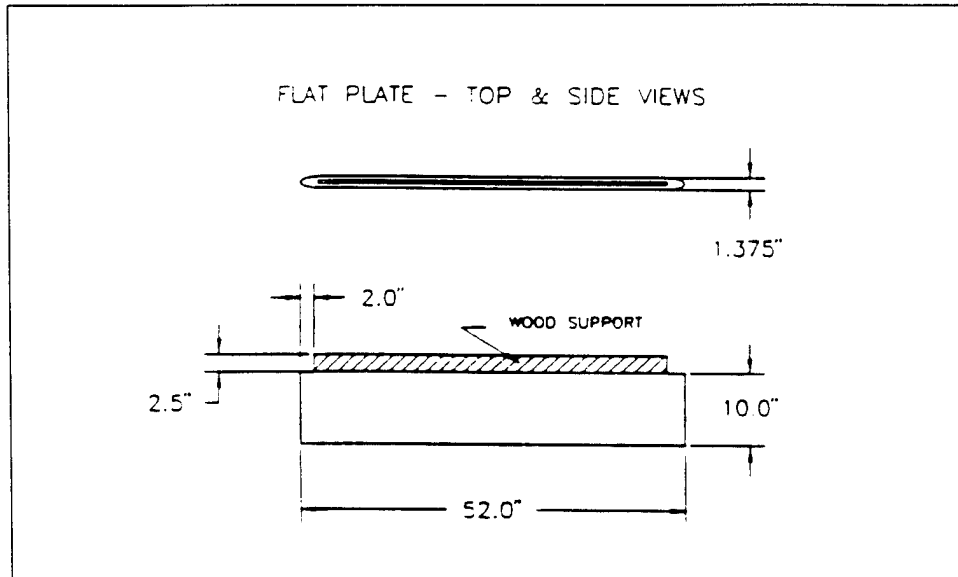
Figure 2: Flat Plate Model - Plan and Profile Views

The C_f values varied only slightly during the experiments, and an average value of $C_f = 4.5 \times 10^{-3}$ was adopted for the speed range of 0.3 to 0.6 m/s, which corresponds to a Reynolds number range of 3×10^5 to 6×10^5. This skin friction information was later used to extract the residual resistance component from the total resistance.

Small-Scale Experiments

A series of relatively small-scale qualitative experiments were conducted before the main tests in a Plexiglass tank (unofficially referred to as the "Davidson Laboratory Tank 4 Facility") measuring 8 ft (2.4 m) long by 2 ft (0.61 m) wide, with a variable water depth up to 1.8 ft (0.55 m). (See Figure 3.) This

15
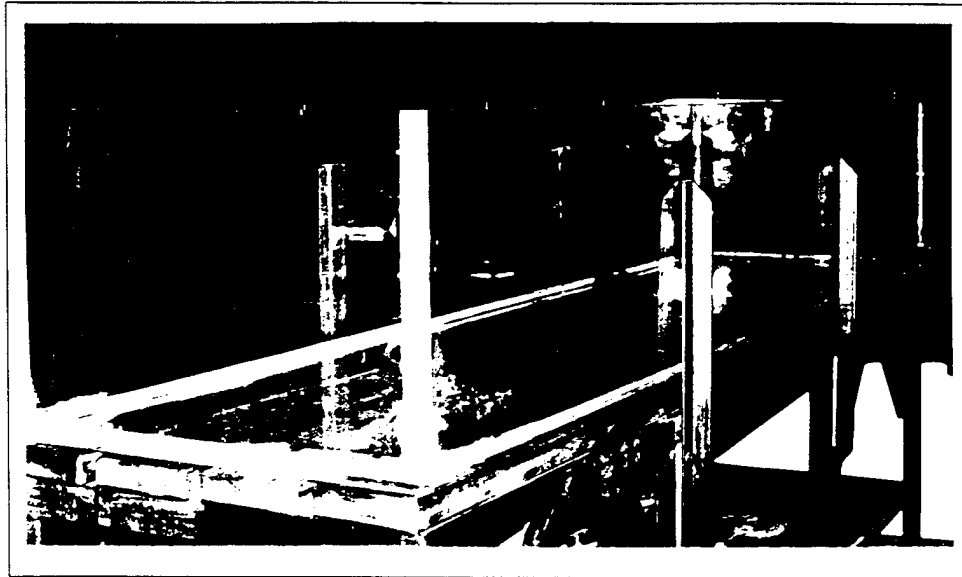
Figure 3: Small-Scale Experimental Tank

setup was ideal for experimenting with different methods of creating a stratified water column, as well as with methods for sharpening the interface between the two salinity layers. The volume of the tank was small enough to easily drain and refill several times per day as needed, while still representing a large enough scale to provide valid information on the behavior of the stratification and experimental methods in the larger tank. This smaller tank also provided a convenient setup in which to experiment with different internal wave observation techniques.

During these tests, several methods of creating a stably stratified water column in the laboratory setting were tested. The techniques included several methods which introduced fresh water on top of a tank of salt water, and some which introduced salt water at the bottom of a tank of fresh water. The latter methods were unsuccessful, due to excessive mixing of the two fluids at even very slow salt water input flow rates. A very gradual halocline resulted, which was unacceptable for these experiments.

The process decided upon for application in the larger tank is actually quite simple, and was easily implemented in the larger tank. The method requires a salt water layer to be established, and then introduces fresh water on top through hoses mounted perpendicular to plywood boards which are floating on the surface. The fresh water sheets off of the boards in a mostly horizontal

16

direction, and layers on top of the fluid beneath with very little disturbance to or mixing with the salt water layer. See Figure 4 for schematic.
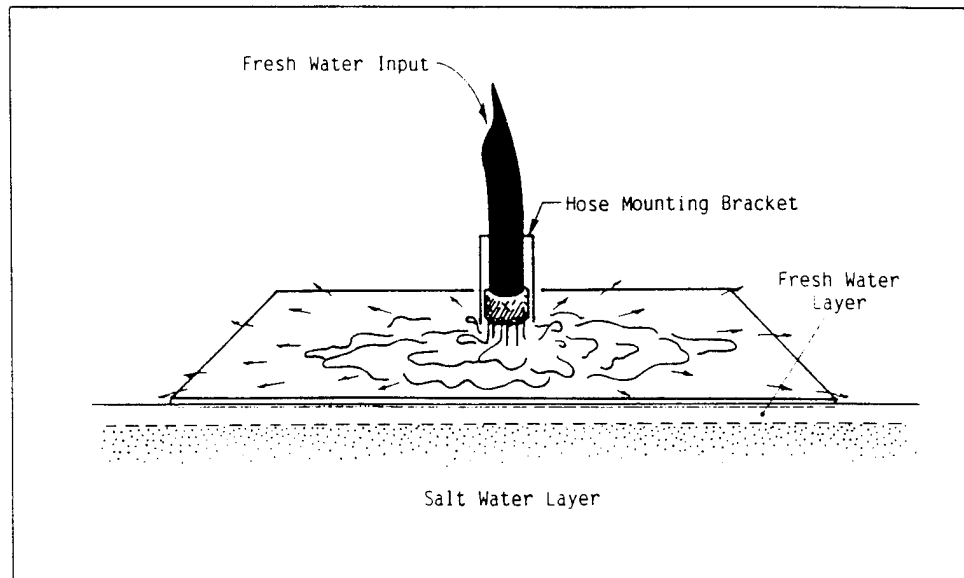
Figure 4: Sketch of Stratification Process

It was also during these tests in the smaller tank that the SIS (Stratification Intensification System) instrument was developed and a small prototype was built. The instrument intensifies the stratification of the water column (sharpens the halocline) by removing a horizontal "strip" of mixed salinity water. A schematic of its operation is shown in Figure 5. Figure 6 shows a photograph of the prototype, better known as "Little SIS."
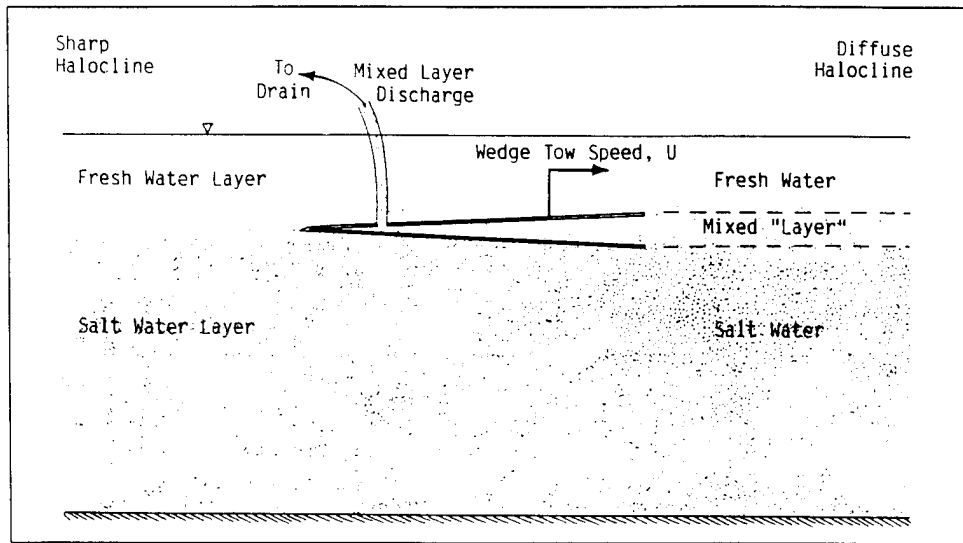
Figure 5: Schematic of SIS operation
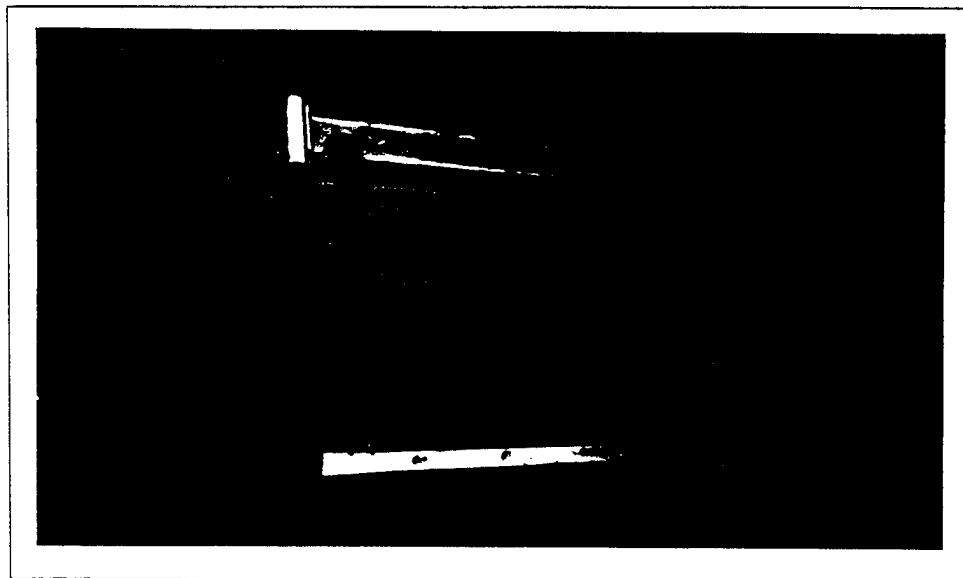
Figure 6: "Little SIS"

Large-Scale Experimental Setup and Instrumentation

At the commencement of the tests, the tank water level was lowered to the desired depth of the salt water layer, 4 ft (1.2 m). This water was then salinated to approximately 35 ppt, by adding 999 NaCl, 99.9% pure table salt. The water was

18

mixed thoroughly by mounting a "mixing mesh" on the tank carriage and towing it several times throughout the length of the tank.

The method developed in the small-scale tests for layering fresh water on top of the salt water proved to be very successful in the large tank. Five plywood sheets, each measuring 6 ft by 12 ft (1.8 m by 3.6 m) were distributed along the length of the tank. A freshwater discharge hose was mounted perpendicular to each board, and fresh water was introduced until a layer thickness between 7 and 9 in (18 to 23 cm) was achieved. The resulting salinity profile exhibited a sharp halocline, as desired. A sample salinity profile is shown in Figure 7.
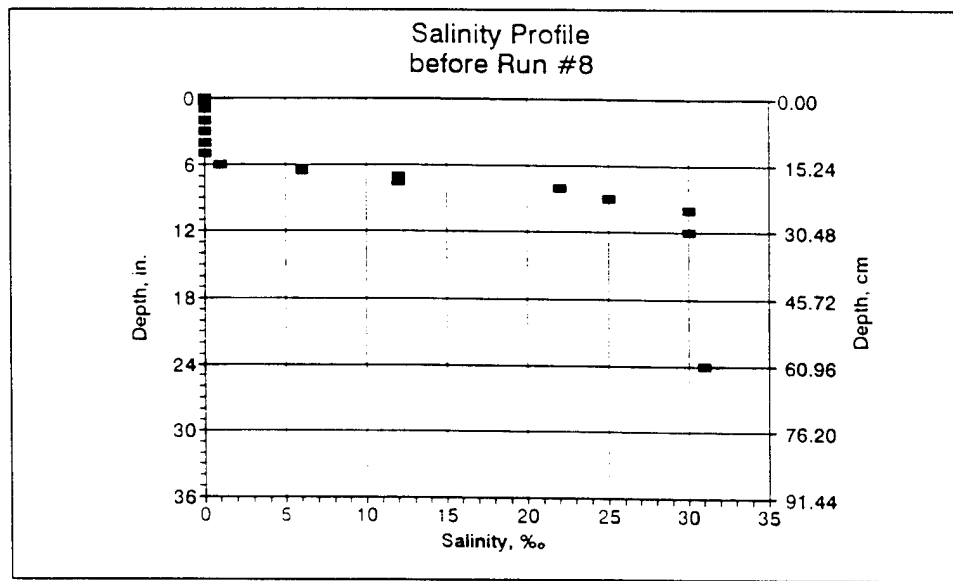
Figure 7: Sample Achieved Salinity Profile

The "Big SIS" was constructed of expanded PCP, and proved to be a successful method of sharpening the halocline in the larger tank. The instrument measured 11.5 ft wide (3.5 m), 3 ft (0.91m) long, and 3 in (7.6 cm) high at the inflow (leading) edge. (See Figure 8.) The hoses which exited from the trailing edge of the wedge were connected to a manifold which was then connected to a pump suspended from the towing carriage. The discharge from the pump was then sent to a large skimmer drain. The wedge itself was attached to the carriage and was towed the length of the tank, as needed to remove a strip of mixed salinity water. The tow speed was adjusted to balance the flow into the wedge with the flow out of the system so as to avoid disturbances. Symbolically:

$$Q_{in} = Q_{out} = A_{frontal, projected} \times U,$$

where $A_{frontal, projected}$ was the frontal projected area equal to the maximum (leading edge) thickness of the wedge, and U was the carriage towing speed. If necessary, additional fresh water was then introduced on the surface (by the method previously described) to replenish the discharged volume of water.
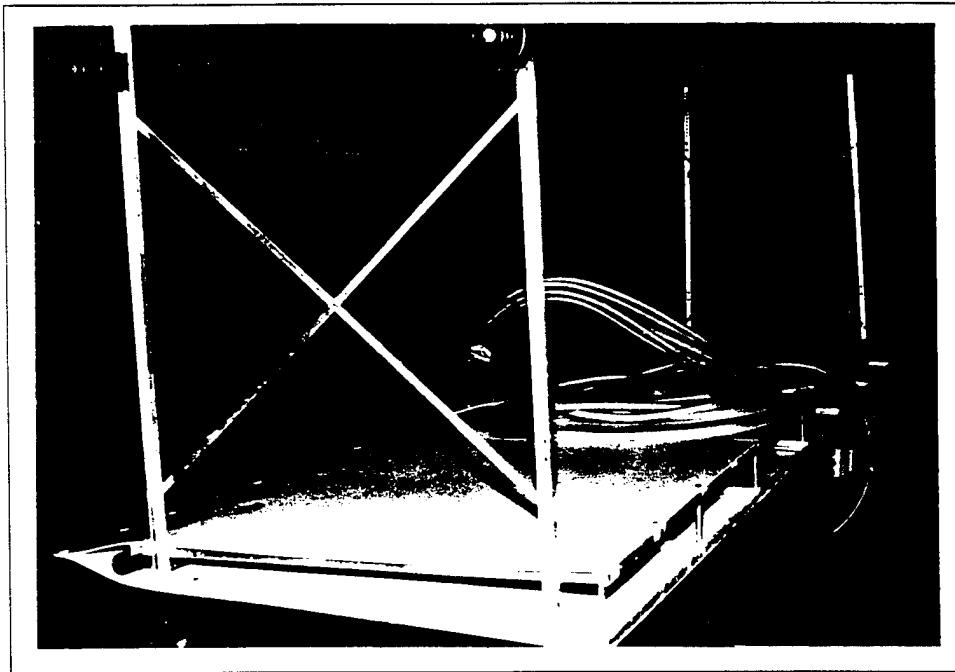
Figure 8: "Big SIS"

Several methods of obtaining internal wave recordings were tested. Some of the unsuccessful methods included dye-injection techniques, shadow photography visualization (from Mowbray, 1967), echo-sounder recordings, and traditional wave wire methods.

The problem with the dye-injection techniques arose from the high diffusivity of the dyes in both fresh and salt water. No dye was found that would either remain at the interface of the two layers, or stay primarily in one of the two layers for any reasonable time scale. Reports of other projects in which dye-injection techniques for internal wave visualization were successful incorporated density stratifications much greater (by at least a factor of 10) than in the Davidson Laboratory experiments.

The primary problem with implementation of Mowbray's (1967) Schlieren and Shadowgraph techniques in the Davidson Laboratory test series

20

was the requirement of "observation windows" within the test section, or preferably, an entirely glass-sided tank. Since Tank 3 has solid concrete walls and no observation windows, the numerous pieces of apparatus required to be installed inside of the tank to implement this method would have greatly disrupted the internal wave motion, so this method was therefore deemed impractical. Successful implementations of this technique may be seen in the results from Helfrich and Melville's (1985) laboratory experiments.

An echosounder was tested as well, and although this technique is promising for acquiring internal wave data in future studies, the particular instrument tested for these experiments unfortunately did not have enough sensitivity to accurately register the internal wave location. An echosounder with greater sensitivity and resolution appears to be an ideal instrument for this type of test because of its non-obtrusiveness.

Traditional wave wires were also impractical for use in this study, because of the severe corrosive nature of salt water. Virtually every wave wire instrument submerged into the tank corroded away within minutes.

However, two methods for internal wave observation proved to be successful, and provided accurate recordings of the internal wave created by the moving ice floe. The first method used an internal wave wire probe designed and built for this project, and the second method employed a submerged video camera to record observations of the internal wave.

The internal wave probe design was essentially a modified conventional wave wire design. The instrument consisted of a pair of platinum wires 22 in (55.9 cm) long, spaced 0.5 in (1.3 cm) apart, which were encased in a 1 in (2.54 cm) diameter hollow plastic tube. The tube had open slots which allowed free vertical movement of the fresh water / salt water interface. The internal wave wire's operation is analogous to a surface wave wire's. The internal wave instrument was submerged below the free surface with a portion of the probe penetrating below the salt water interface. The probe measured average conductivity of the fluid body, and converted this into a voltage. Changes in the level of the salt water produced an associated linear change in conductivity, and thus voltage reading. The output from the instrument was then fed into a strip chart recorder, and also branched into the Davidson Laboratory's computer data acquisition equipment. A schematic of the internal wave wire electronics is shown in Figure 9. A photograph of this internal wave wire is shown in Figure 10.
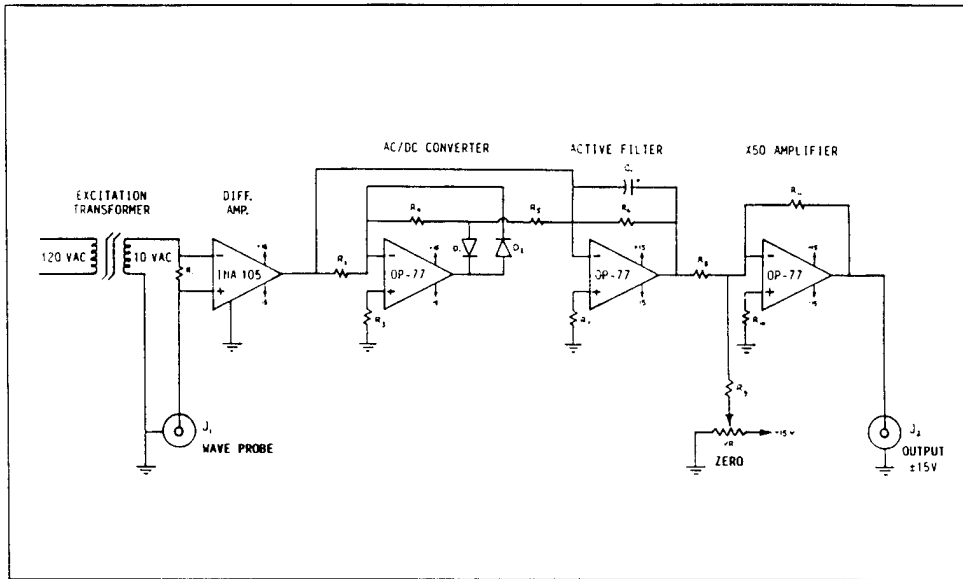
**Figure 9:** Electrical Schematic of Internal Wave Wire
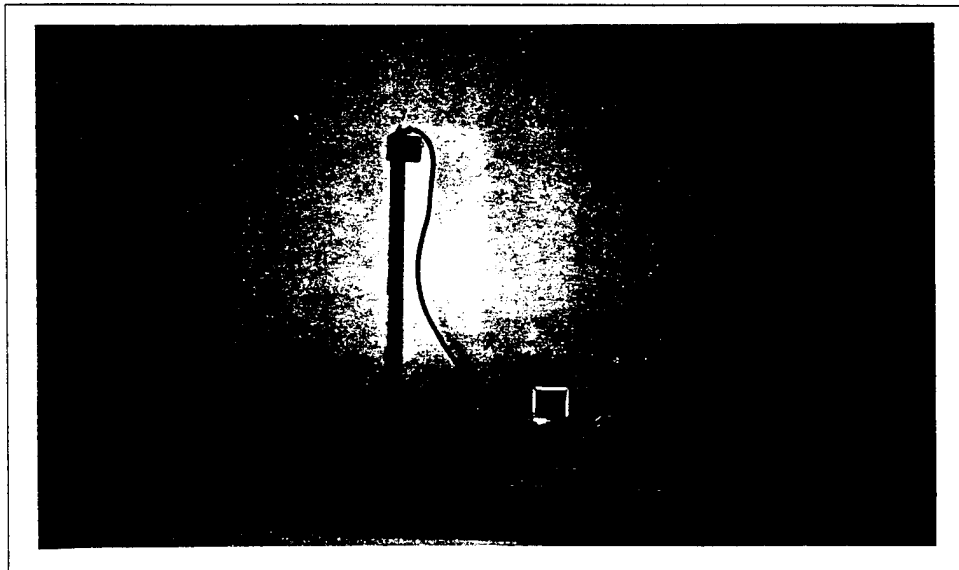
Figure 10: Internal Wave Wire

Additional internal wave observations were obtained through a submerged video camera, mounted on the side of the tank. During the small-scale tests, the lower, saltier layer was clouded due to dust particles in the salt which was used to salinate the water, while the upper, fresh water layer was clear. However, in the

22

larger scale tests, the salt used to create the salt water was extremely pure, and the layer was clear. However, after the fresh water was layered above, it was observed that the tiny air bubbles in the "newer" layer made the water appear cloudy when a bright light was shone from above, while the lower, saltier layer remained clear. This situation therefore facilitated easy visualization of the interface between the two layers when viewed through a camera mounted below the surface. This technique was therefore implemented, and provided excellent internal wave recordings.

Difficulties were also encountered with salinity profile measurement instruments. Although several electrical conductivity probes were designed and built during this project to measure the electrical conductivity and thus salinity through the water column, severe corrosion and non-linearity problems were encountered which required dismissal of these instruments.

A successful, although laborious, method was ultimately employed to obtain the salinity profiles. "Grab samples" were taken at different discrete levels through the water column; a hand-held refractometer was then used to measure the salinity of each sample.

The Test Matrix

Four different ice floes were tested, each with different under-ice topographies as described below:

Floe #1: flat bottom
Floe #2: low-frequency sinusoid bottom profile
Floe #3: higher-frequency sinusoid bottom profile
Floe #4: irregular bottom topography, typical of deformed first-year ice observations

The lower frequency sine wave of Floe #2's bottom topography had a wavelength of 1.5 ft (0.46 m). The higher frequency sine wave of Floe #3's topography had a wavelength of 1.0 ft (0.30 m). Each sine wave had an amplitude of 1.0 in (2.54 cm). Floe #4 had an irregular bottom modelled after Lange and Eicken's (1991) observations of class II ice. (See Figures 11 through 14 for profiles.) Each floe had a square-shaped plan view, 3 ft (0.91 m) side length, and a rectangular frontal projection with a height of 1 ft (0.30 m).
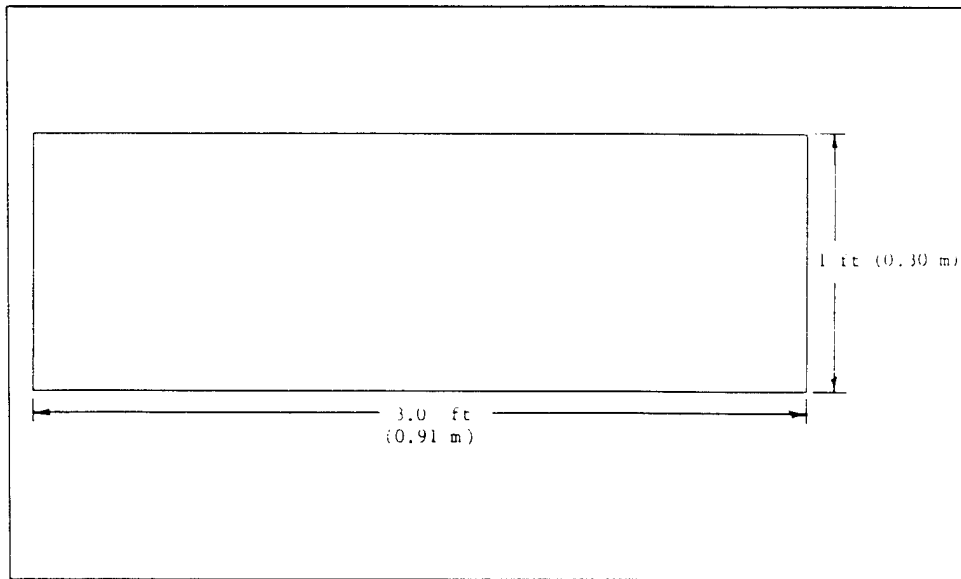

Figure 11: Profile View of Floe #1

24
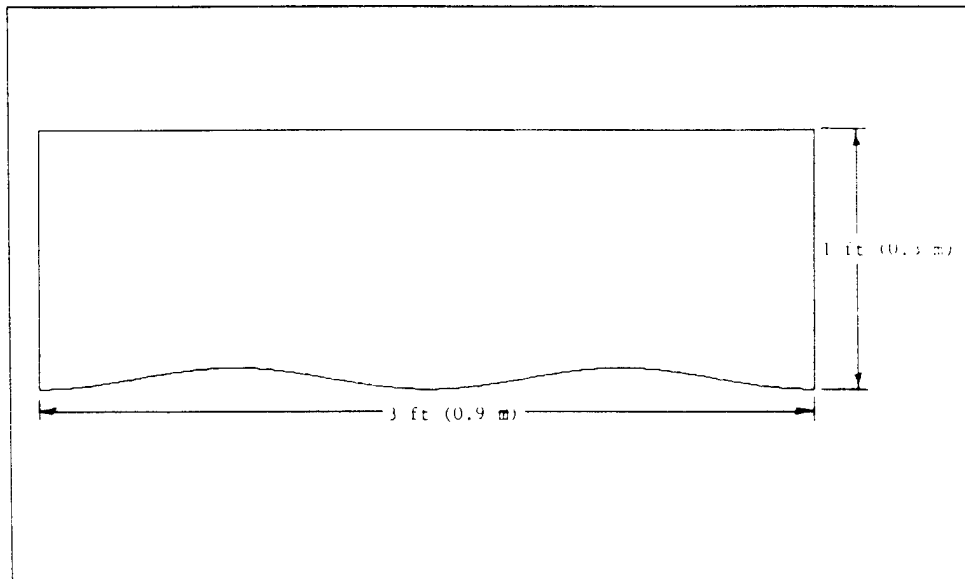
Figure 12: Profile View of Floe #2
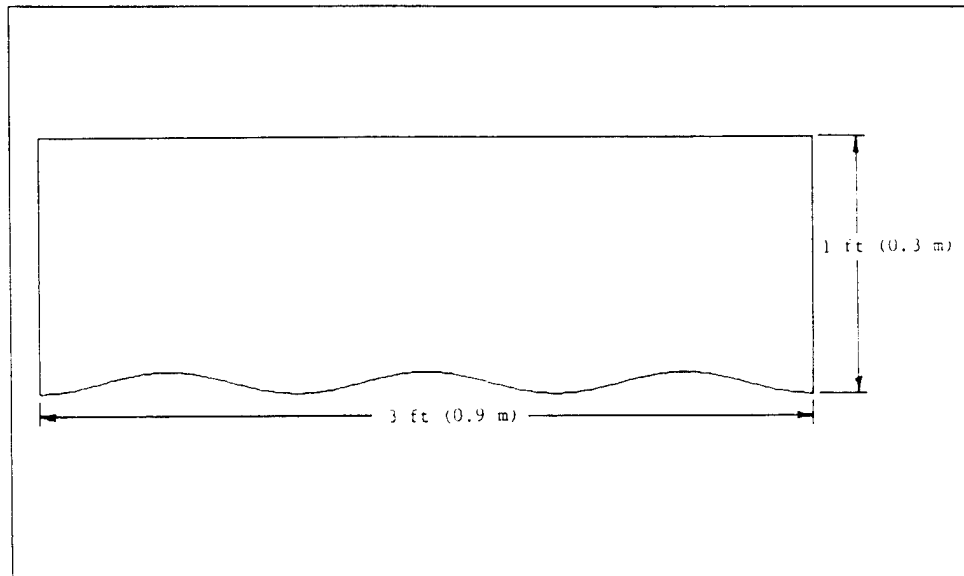
Figure 13: Profile View of Floe #3

25
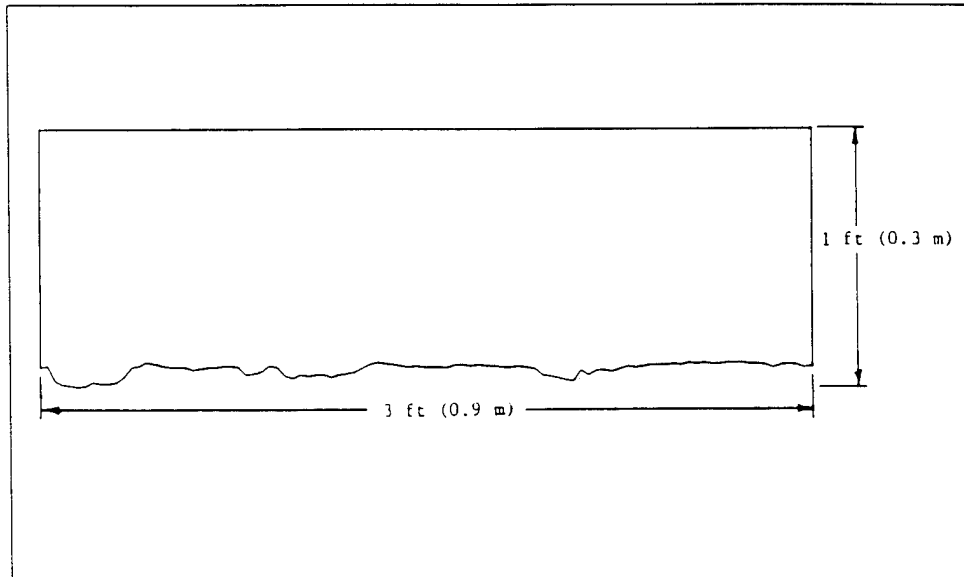
Figure 14: Profile View of Floe #4

Non-Stratified Test Matrix

The unstratified test matrix includes conditions similar to the stratified tests shown in Table 1 for each of the four ice floe models. Unfortunately, many of these tests were not completed at the time this thesis was written. (Floe #3 and Floe #4 have not been tested at all in the non-stratified condition.) However, all of the remaining tests will be performed during June of 1993, and a later paper will present the complete results.

Stratified Test Matrix

The stratified tests proved to be massively time consuming, due to the lengthy stratification establishment time requirements, and then limitations on the time during which the tank remained suitably stratified. Sharpening the interface through use of the SIS was also time consuming. In addition, after each run, very long internal waves propagated along the length of the tank; therefore more than a half hour time period between the end of one run and the beginning of the next was required to allow the internal waves to dissipate.

To simplify and streamline the test matrix, modifications were made to the originally intended stratified test matrix during the experiment based on observations of the internal wave behavior and drag trends. The resulting test matrix is displayed in Table 1, with the corresponding run numbers for each test point identified.

Table 1: Stratified Test Matrix

Run Numbers
Ice Floe #1

Ice Floe Draft (in)	(cm)	Upper Layer, h₁ (in)	(cm)	Velocity 0.1 ft/s 3 cm/s	0.2 ft/s 6 cm/s	0.3 ft/s 9 cm/s	0.4 ft/s 12 cm/s	0.5 ft/s 15 cm/s	0.6 ft/s 18 cm/s	0.7 ft/s 21 cm/s
3.0	7.6	6.0	15.2		Run 13			Run 14		Run 15
5.0	12.7	6.0	15.2			Run 12				
5.0	12.7	7.5	19.1						Run 11	
6.0	15.2	7.5	19.1		Runs 1,8		Runs 9,10			
6.0	15.2	9.0	22.8	Run 6	Runs 4,5	Run 7				

Run Numbers
Ice Floe #2

Ice Floe Draft (in)	(cm)	Upper Layer, h₁ (in)	(cm)	Velocity 0.2 ft/s 6 cm/s	0.3 ft/s 9 cm/s	0.4 ft/s 12 cm/s	0.5 ft/s 15 cm/s	0.6 ft/s 18 cm/s	0.7 ft/s 21 cm/s	0.8 ft/s 24 cm/s
2.0	5.1	5.5	14.0				Run 20	Run 21		Run 22
3.0	7.6	5.5	14.0	Run 16		Run 17	Run 19	Run 18		

Run Numbers
Ice Floe #3

Ice Floe Draft (in)	(cm)	Upper Layer, h₁ (in)	(cm)	Velocity 0.1 ft/s 3 cm/s	0.2 ft/s 6 cm/s	0.3 ft/s 9 cm/s	0.4 ft/s 12 cm/s	0.5 ft/s 15 cm/s	0.6 ft/s 18 cm/s	0.7 ft/s 21 cm/s
3.0	7.6	6.5	16.5				Run 25	Run 26		Run 27
3.0	7.6	7.0	17.8				Run 55			
4.0	10.2	6.5	16.5		Run 23		Run 24	Run 28		Run 29
4.0	10.2	7.0	17.8				Run 54			

Run Numbers
Ice Floe #4

Ice Floe Draft (in)	(cm)	Upper Layer, h₁ (in)	(cm)	Velocity 0.1 ft/s 3 cm/s	0.2 ft/s 6 cm/s	0.3 ft/s 9 cm/s	0.4 ft/s 12 cm/s	0.5 ft/s 15 cm/s	0.6 ft/s 18 cm/s	0.7 ft/s 21 cm/s
2.0	5.1	7.0	17.8				Run 53			
3.0	7.6	7.0	17.8				Run 52			
4.0	10.2	7.0	17.8		Run 48		Run 49	Run 50		Run 51

Test Results

Data Acquisition

Resistance and wave wire data were acquired by the Davidson Laboratory DAP5 data acquisition program. Data was acquired within a 50 ft (15 m) test length of the ice floe's travel. Liberal acceleration and stabilization allowances were incorporated before this data acquisition length. The resistance values obtained were calculated by averaging the input over the test length. Time history files of the wave wire data were also obtained. A summary of the test data is included in Appendix A. Strip chart recordings of the wave wire readings were also obtained and are included in Appendix B.

Salinity profiles within the data acquisition portion of the tank were taken before and after each test run. These results are presented in Appendix C.

VHS videotape recordings of the internal wave created by the ice floe were obtained by mounting a small camera on the side of the tank at the level of the halocline. Unfortunately, no still photographs were taken during the tests, since the number of intrusions in the water column was kept as small as possible.

Non-Stratified Test Results

At this time, only Floe #1 and Floe #2 have been tested in the non-stratified condition. Tables 2 and 3 include the total resistance coefficients ($C_{t,unstratified}$ values) from Floe #1 and Floe #2, while Tables 4 and 5 list the residual resistance coefficients ($C_{r,\ unstratified}$ values) for the two floes.

Table 2: Unstratified Test Total Resistance Coefficients, $C_{t,\,unstratified}$ values, from Floe #1

Non-Stratified Test
Total Resistance Coefficients, Floe #1

Ice Floe Draft, T		Velocity							
in	cm	0.1 ft/s 3 cm/s	0.2 ft/s 6 cm/s	0.3 ft/s 9 cm/s	0.4 ft/s 12 cm/s	0.5 ft/s 15 cm/s	0.6 ft/s 18 cm/s	0.7 ft/s 21 cm/s	0.8 ft/s 24 cm/s
2.0	5.1								
3.0	7.6			0.032	0.027	0.026	0.027		
4.0	10.2								
5.0	12.7			0.033	0.036	0.036	0.036		
6.0	15.2			0.044	0.031	0.039	0.043		

Table 3: Unstratified Test Total Resistance Coefficients, $C_{t,\,unstratified}$ values, from Floe #2

Non-Stratified Test
Total Resistance Coefficients, Floe #2

Ice Floe Draft, T		Velocity							
in	cm	0.1 ft/s 3 cm/s	0.2 ft/s 6 cm/s	0.3 ft/s 9 cm/s	0.4 ft/s 12 cm/s	0.5 ft/s 15 cm/s	0.6 ft/s 18 cm/s	0.7 ft/s 21 cm/s	0.8 ft/s 24 cm/s
2.0	5.1								
3.0	7.6			0.033	0.034	0.033	0.033		
4.0	10.2								
5.0	12.7			0.053	0.048	0.050	0.050		
6.0	15.2			0.059	0.060	0.060	0.058		

Table 4: Unstratified Test Residual Resistance Coefficients, $C_{r,\,unstratified}$ values, from Floe #1

Non-Stratified Test
Residual Resistance Coefficients, Floe #1

Ice Floe Draft, T		Velocity							
in	cm	0.1 ft/s 3 cm/s	0.2 ft/s 6 cm/s	0.3 ft/s 9 cm/s	0.4 ft/s 12 cm/s	0.5 ft/s 15 cm/s	0.6 ft/s 18 cm/s	0.7 ft/s 21 cm/s	0.8 ft/s 24 cm/s
2.0	5.1								
3.0	7.6			0.028	0.023	0.022	0.023		
4.0	10.2								
5.0	12.7			0.029	0.032	0.032	0.032		
6.0	15.2			0.040	0.027	0.035	0.039		

29

Table 5: Unstratified Test Residual Resistance Coefficients $C_{r,\text{unstratified}}$ values, from Floe #2

Non-Stratified Test
Residual Resistance Coefficients, Floe #2

Ice Floe Draft, T		Velocity							
in	cm	0.1 ft/s 3 cm/s	0.2 ft/s 6 cm/s	0.3 ft/s 9 cm/s	0.4 ft/s 12 cm/s	0.5 ft/s 15 cm/s	0.6 ft/s 18 cm/s	0.7 ft/s 21 cm/s	0.8 ft/s 24 cm/s
2.0	5.1								
3.0	7.6			0.029	0.030	0.029	0.029		
4.0	10.2								
5.0	12.7			0.049	0.044	0.046	0.046		
6.0	15.2			0.055	0.056	0.056	0.054		

Stratified Test Results

Tables 6 through 9 present the total resistance coefficients ($C_{t,\text{stratified}}$ values) from the stratified tests. Plots of the data appear in the Discussion and Preliminary Analysis section.

Table 6: Stratified Test Total Resistance Coefficients, $C_{t,\text{stratified}}$ values, from Floe #1

Stratified Test
Total Resistance Coefficients, Floe #1

Ice Floe Draft, T		T/h,	Velocity						
in	cm		0.1 ft/s 3 cm/s	0.2 ft/s 6 cm/s	0.3 ft/s 9 cm/s	0.4 ft/s 12 cm/s	0.5 ft/s 15 cm/s	0.6 ft/s 18 cm/s	0.7 ft/s 21 cm/s
3.0	7.6	0.50		0.054			0.072		0.030
5.0	12.7	0.83			0.090				
5.0	12.7	0.67						0.089	
6.0	15.2	0.80		0.095		0.140			
6.0	15.2	0.67	0.241	0.112	0.103				

30

Table 7: Stratified Test Total Resistance Coefficients, $C_{t,\,stratified}$ values, from Floe #2

Stratified Test
Total Resistance Coefficients, Floe #2

Ice Floe Draft, T in	cm	T/h,	Velocity						
			0.2 ft/s 6 cm/s	0.3 ft/s 9 cm/s	0.4 ft/s 12 cm/s	0.5 ft/s 15 cm/s	0.6 ft/s 18 cm/s	0.7 ft/s 21 cm/s	0.8 ft/s 24 cm/s
2.0	5.1	0.36				0.027	0.020		0.019
3.0	7.6	0.55	0.066		0.076	0.044	0.032		

Table 8: Stratified Test Total Resistance Coefficients, $C_{t,\,stratified}$ values, from Floe #3

Stratified Test
Total Resistance Coefficients, Floe #3

Ice Floe Draft in	cm	T/h,	Velocity						
			0.1 ft/s 3 cm/s	0.2 ft/s 6 cm/s	0.3 ft/s 9 cm/s	0.4 ft/s 12 cm/s	0.5 ft/s 15 cm/s	0.6 ft/s 18 cm/s	0.7 ft/s 21 cm/s
3.0	7.6	0.46				0.076	0.052		0.029
3.0	7.6	0.43				0.079			
4.0	10.2	0.62		0.202		0.103	0.069		0.037
4.0	10.2	0.57				0.113			

Table 9: Stratified Test Total Resistance Coefficients, $C_{t,\,stratified}$ values, from Floe #4

Stratified Test
Total Resistance Coefficients, Floe #4

Ice Floe Draft in	cm	T/h,	Velocity						
			0.1 ft/s 3 cm/s	0.2 ft/s 6 cm/s	0.3 ft/s 9 cm/s	0.4 ft/s 12 cm/s	0.5 ft/s 15 cm/s	0.6 ft/s 18 cm/s	0.7 ft/s 21 cm/s
2.0	5.1	0.29				0.033			
3.0	7.6	0.43				0.044			
4.0	10.2	0.57		0.060		0.103	0.063		0.030

Limited wave wire data was recorded. During a few of the tests, difficulties with the instrument were encountered due to corrosion of the wires. However, valid results were obtained for most of the stratified tests. Figure 15

31

shows a representative strip-chart recording of the internal wave disturbance. Appendix B includes all of the strip-chart recordings obtained.
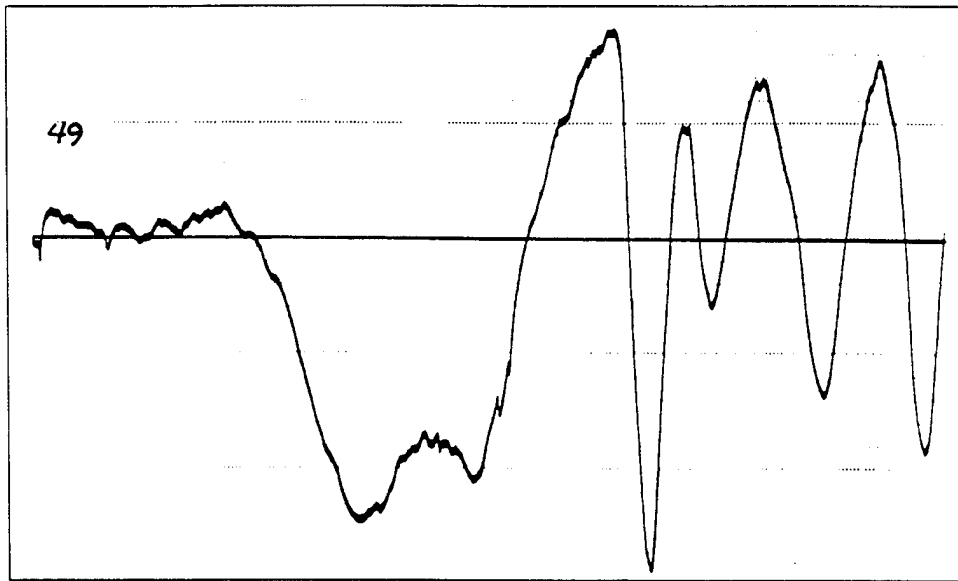

Figure 15: Sample Internal Wave Wire Strip-Chart Recording

In addition to the computer and strip-chart recordings of the internal waves, VHS videotape records of the tests were obtained which clearly show the creation and propagation of the internal wave as the ice floe moves through the tank. Unfortunately, this medium is not conducive for reproduction in a report. However, the visualization of the internal wave creation and behavior presented some interesting information. At the speeds where the resistance "peaked," the internal wave created by the moving ice floe seemed to attach to the aft end of the floe. This is contrasted to the two other conditions: before and after the peak. In slower runs (before the peak), the internal wave created was visible, but did not touch the ice floe. In faster runs (after the peak), the internal wave also did not touch the floe, and the wave created diminished with increasing floe velocity. See Figure 16 for sketches of the floe with internal wave profiles.
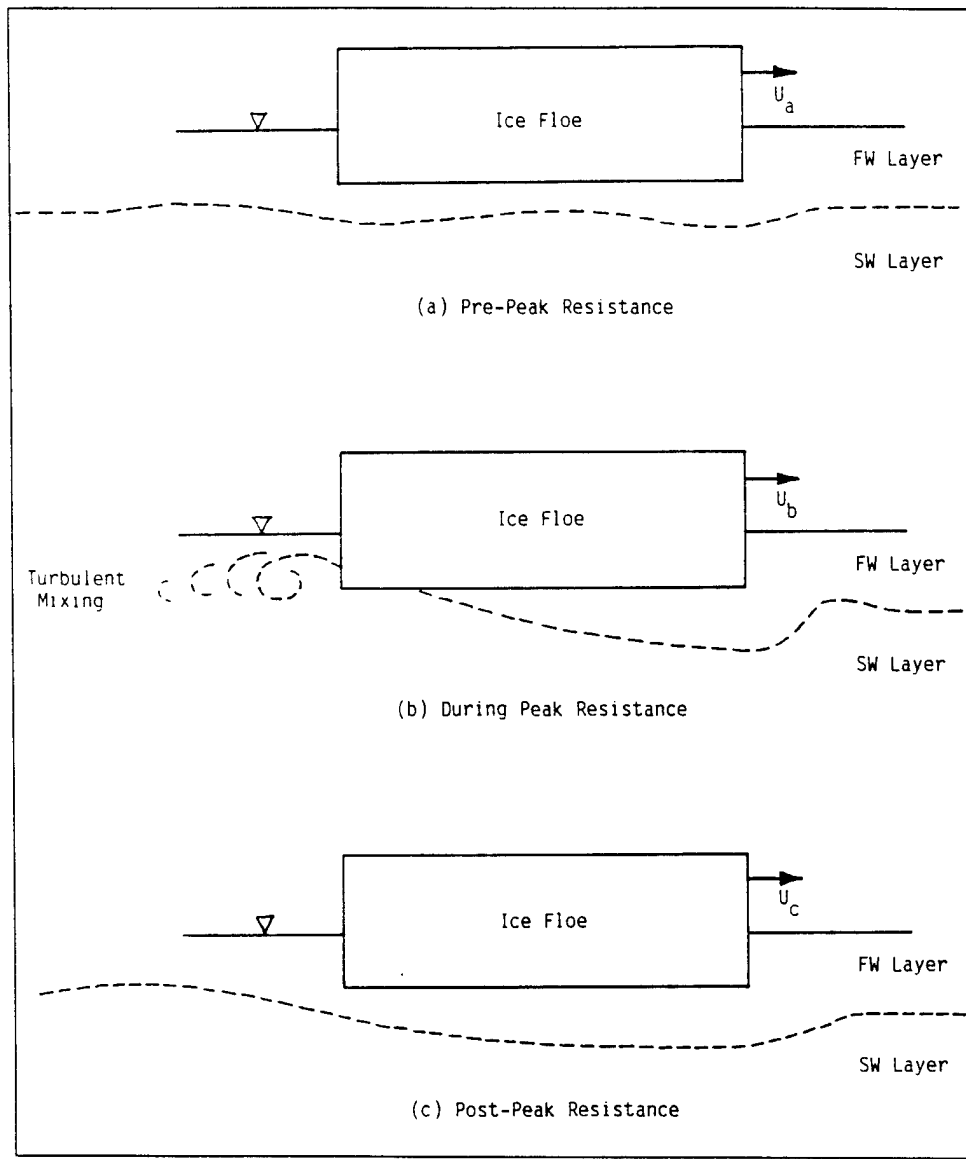
Figure 16: Internal Wave Profile Sketches for (a) Pre-Peak Resistance, (b) Peak Resistance, and (c) Post-Peak Resistance

33

Discussion and Preliminary Analysis

Non-Stratified Tests

Figures 17 and 18 show the residual resistance coefficients obtained from the unstratified tests of Floe #1 and Floe #2 plotted versus Reynolds number. The non-dimensional Reynolds number is defined as:

$$Re = \frac{UL}{\nu},$$

where U is the towing speed, L is a characteristic length (which here is taken as 3 ft (0.91 m)), and ν is the fluid's kinematic viscosity.
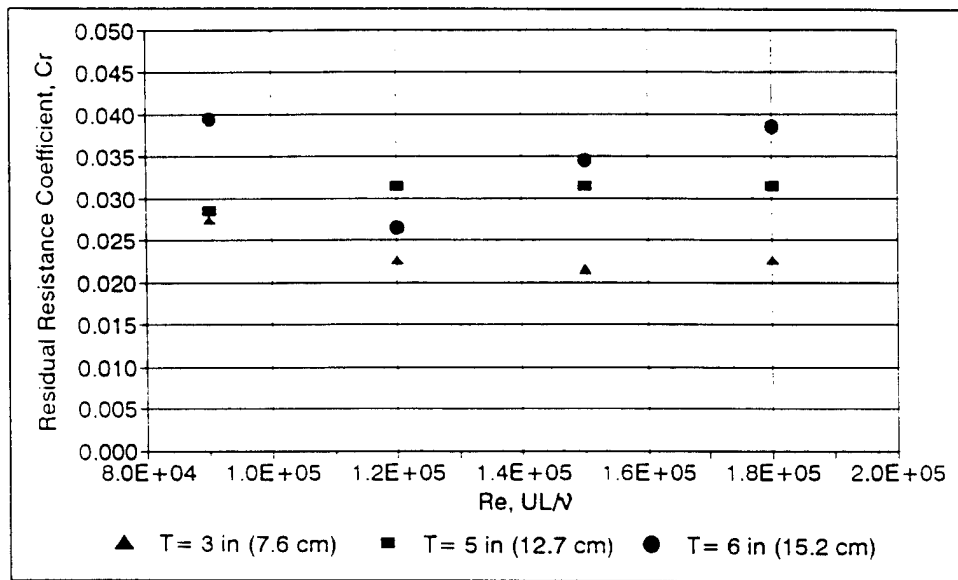
Figure 17: Plot of Unstratified Test Residual Resistance, $C_{r, unstratified}$, vs. Reynolds Number from Floe #1

34
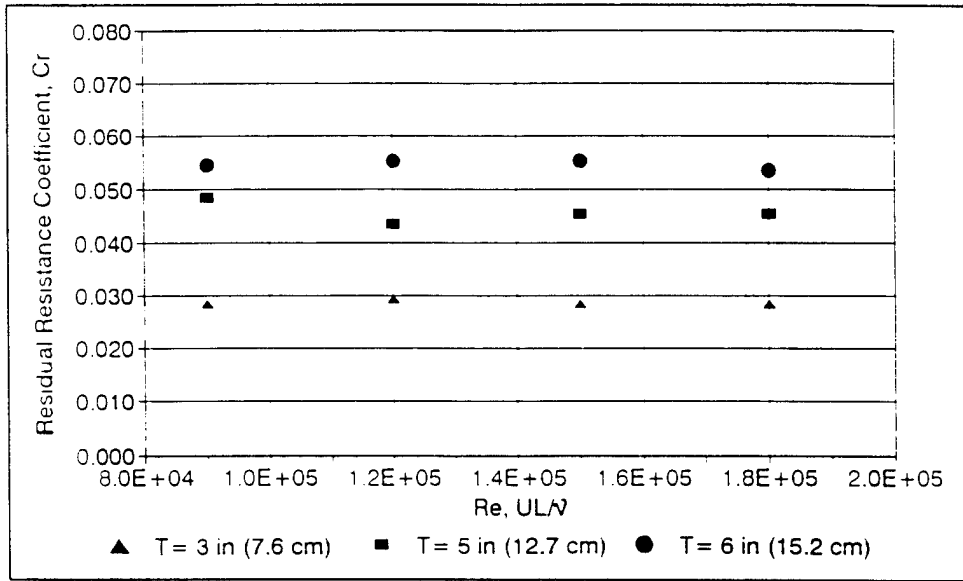
Figure 18: Plot of Unstratified Test Residual Resistance, $C_{r,\,unstratified}$, vs. Reynolds Number from Floe #2

One interesting observation of these results is that the residual resistance (which, in this case, is directly proportional to form drag) is approximately constant with Reynolds number. As Bruno (1992) discussed, this effect may be explained by considering form drag dynamics of bluff bodies. The form drag of a bluff body depends on Reynolds number only to the extent to which the boundary layer flow becomes turbulent and the flow separation pattern is complete. After that point, there is little dependence on Reynolds number. Since the Reynolds numbers during the model tests were sufficiently high (order of 10^5), it is assumed that this critical point has been surpassed. Therefore, the form drag, and here the residual resistance, C_r, should not vary significantly with Reynolds number.

The average residual resistance ($C_{r,\,unstratified}$) values are plotted versus draft in Figure 19. As expected, the floe with the periodic bottom (Floe #2) exhibits significantly greater residual resistance than the flat-bottom floe (Floe #1) at all drafts.

35
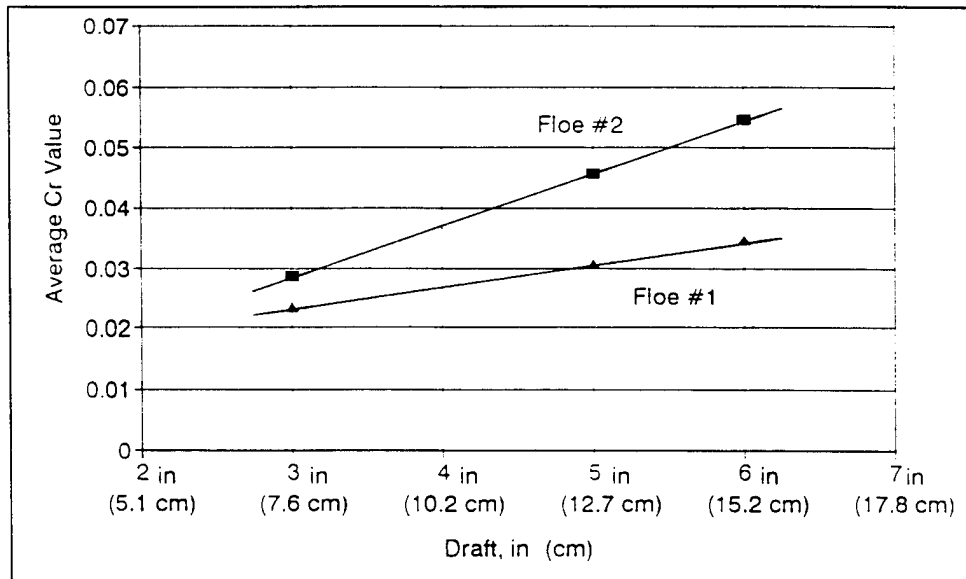
Figure 19: Average $C_{r, \text{unstratified}}$ Values from Floes #1 and #2
Plotted Versus Floe Draft

Stratified Tests

The corresponding run number is indicated next to each data point for all plots in this section to facilitate easy reference to Table 1 (in the Test Matrix section). The sketched curves in each plot are intended to point out noticeable trends in the total resistance with respect to the parameters varied during the tests.

Figures 20 through 23 present the total resistance coefficients from the stratified tests ($C_{t, \text{stratified}}$) plotted versus Reynolds number (as defined previously). An immediate observation of the trends in the total resistance is that the C_t values "peak" at certain Reynolds numbers for each floe. Figure 24 shows the extracted internal wave resistance component, C_{iw}, for Floe #2. These values were obtained by subtracting the unstratified test results from the stratified test results. It is evident from this plot that the internal wave effect diminishes at both low and high Reynolds numbers.

There are several ways of presenting the data for further interpretation. Figures 25 through 28 plot the $C_{t, \text{stratified}}$ data versus a non-dimensional floe velocity, U/C_1, where C_1 is defined as the first-mode interfacial phase speed. The

36

more general C_1 relation,

$$C_1^2 = \frac{g\,\Delta\rho}{k}\,\frac{1}{\rho_1\coth kh_1 + \rho_2\coth kh_2},$$

is the dispersion relation solved for a horizontally propagating gravity wave in a two-layer, inviscid fluid. In the shallow water, long wave case, both kh_1 and kh_2 approach zero; $\coth kh_{1,2} \rightarrow \dfrac{1}{kh_{1,2}}$, and the above equation may be approximated by:

$$C_1^2 = \frac{g\,\Delta\rho}{\rho_2}\,\frac{h_1 h_2}{h_1 + h_2}.$$

Non-dimensionalizing the results also accounted for density variations through the tests. Figure 29 shows selected data series from each floe plotted together. The similarity between the results is intriguing, considering the differing bottom complexities and different T/h_1 values represented.
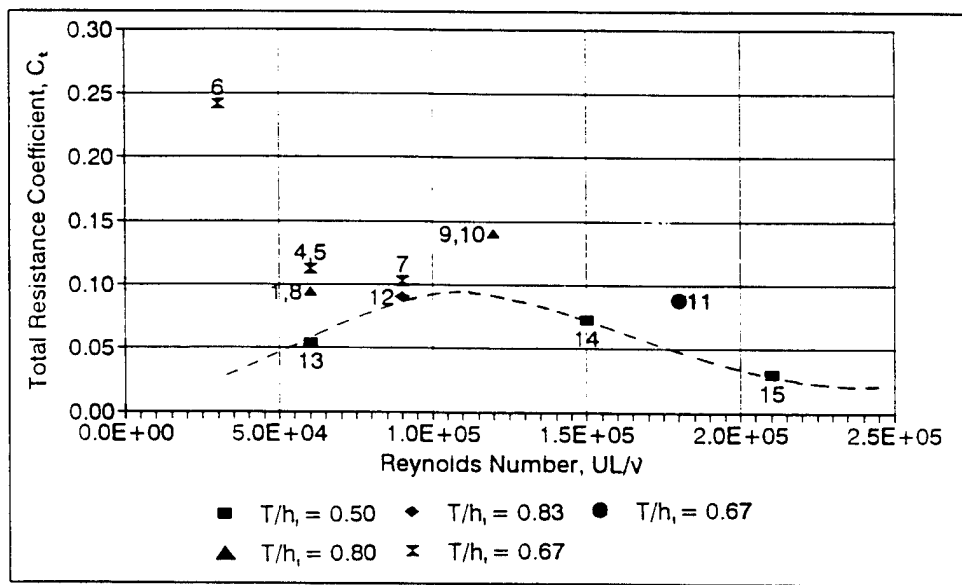
Figure 20: Plot of Stratified Test Total Resistance Coefficient, $C_{t,\text{stratified}}$, vs. Reynolds Number from Floe #1
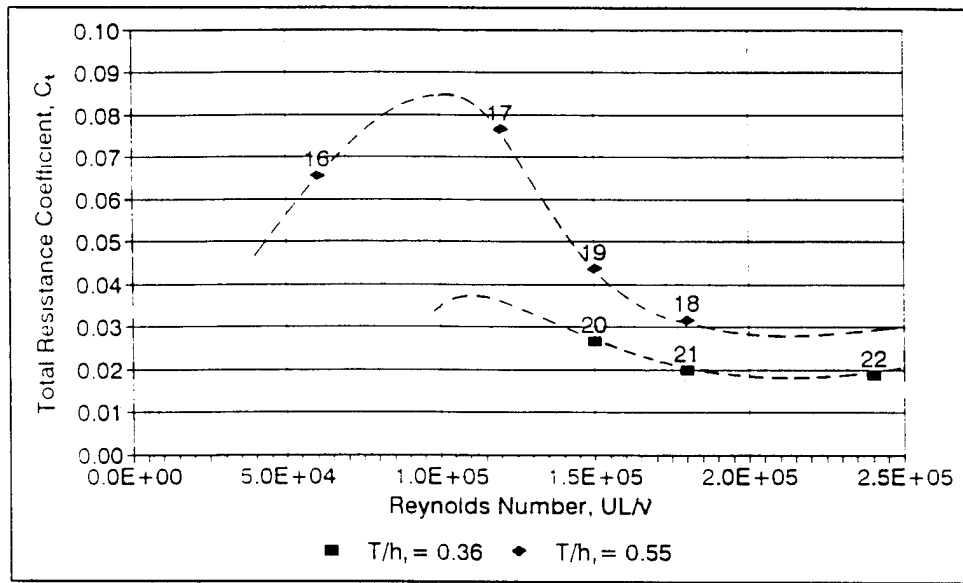
Figure 21: Plot of Stratified Test Total Resistance Coefficient, $C_{t, stratified}$ vs. Reynolds Number from Floe #2


Figure 22: Plot of Stratified Test Total Resistance Coefficient, $C_{t, stratified}$ vs. Reynolds Number from Floe #3

38
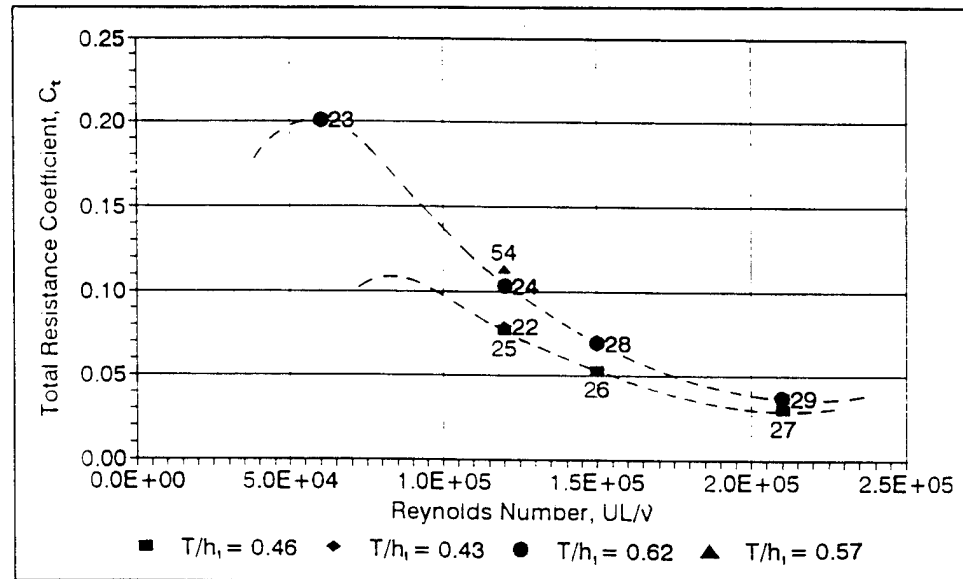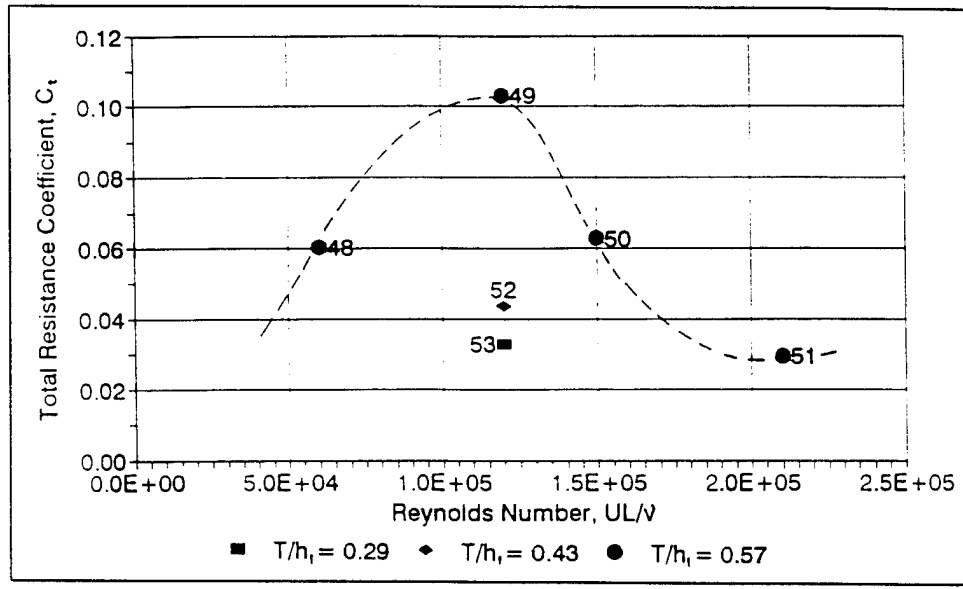
Figure 23: Plot of Stratified Test Total Resistance Coefficient, $C_{t, stratified}$, vs. Reynolds Number from Floe #4
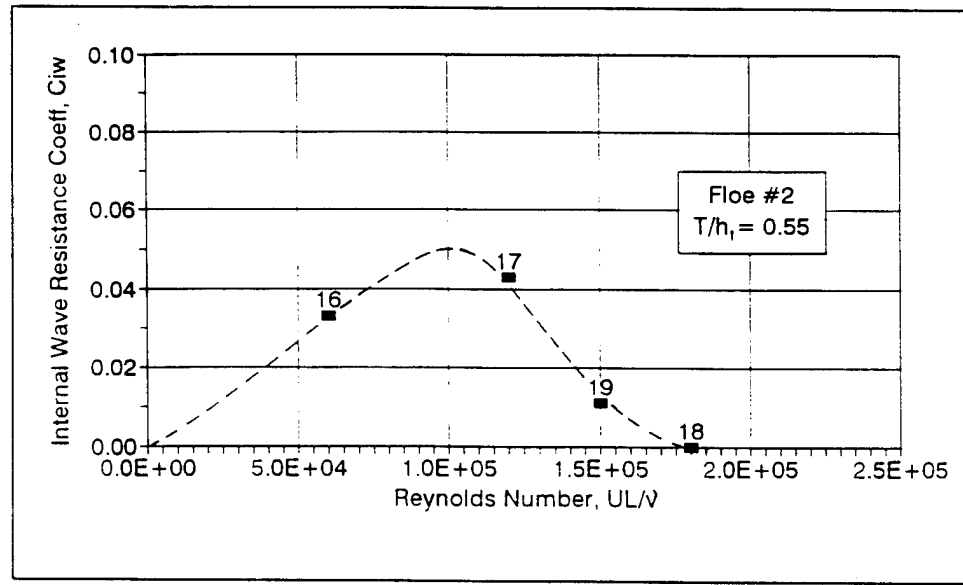
**Figure 24:** Plot of Internal Wave Resistance, C_{iw}, vs. Reynolds Number from Floe #2

39
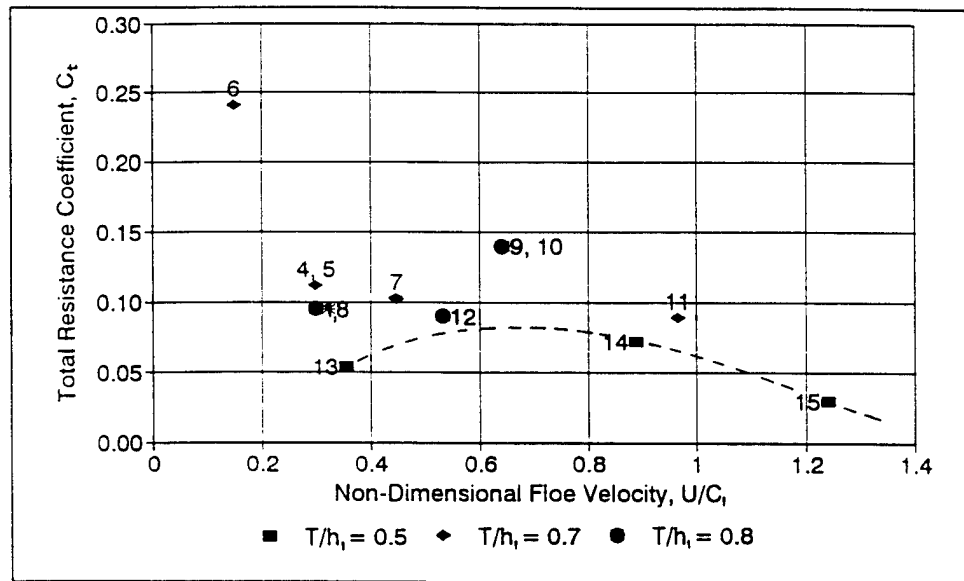
Figure 25: Plot of Stratified Test Total Resistance, $C_{t, stratified}$ vs. Non-Dimensional Floe Velocity, U/C_1 from Floe #1
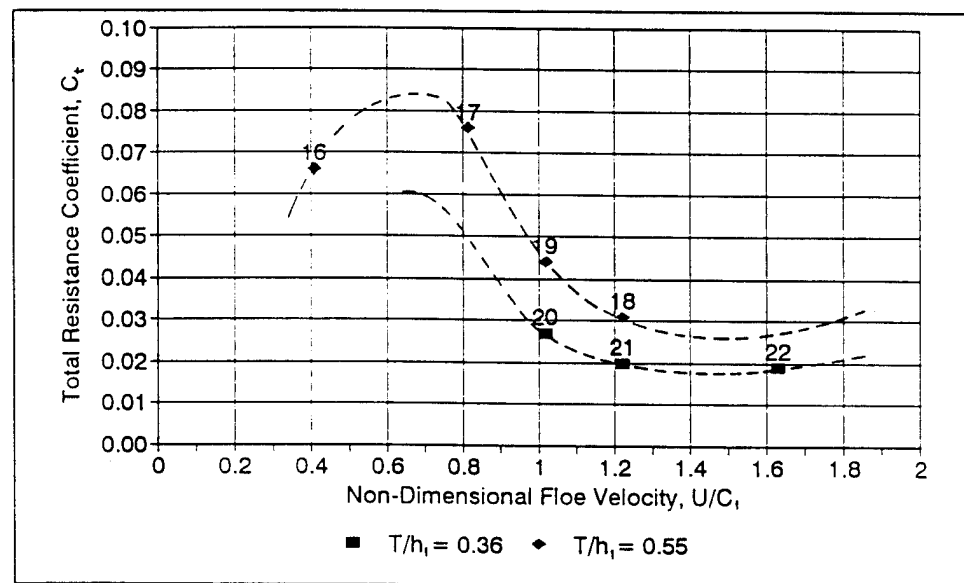

Figure 26: Plot of Stratified Test Total Resistance, $C_{t, stratified}$ vs. Non-Dimensional Floe Velocity, U/C_1 from Floe #2
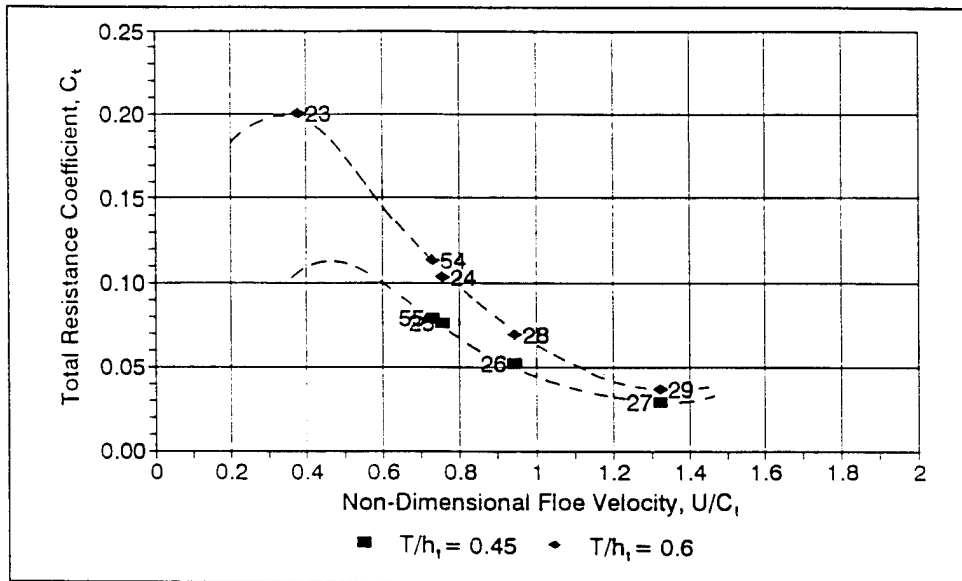
Figure 27: Plot of Stratified Test Total Resistance, $C_{t, stratified}$, vs. Non-Dimensional Floe Velocity, U/C_1 from Floe #3
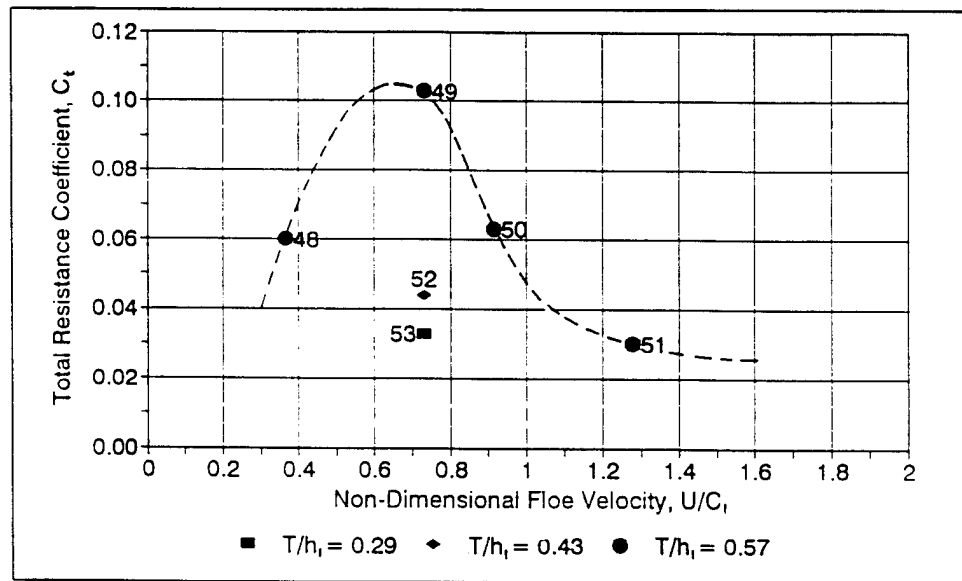
Figure 28: Plot of Stratified Test Total Resistance, $C_{t, stratified}$, vs. Non-Dimensional Floe Velocity, U/C_1 from Floe #4

41
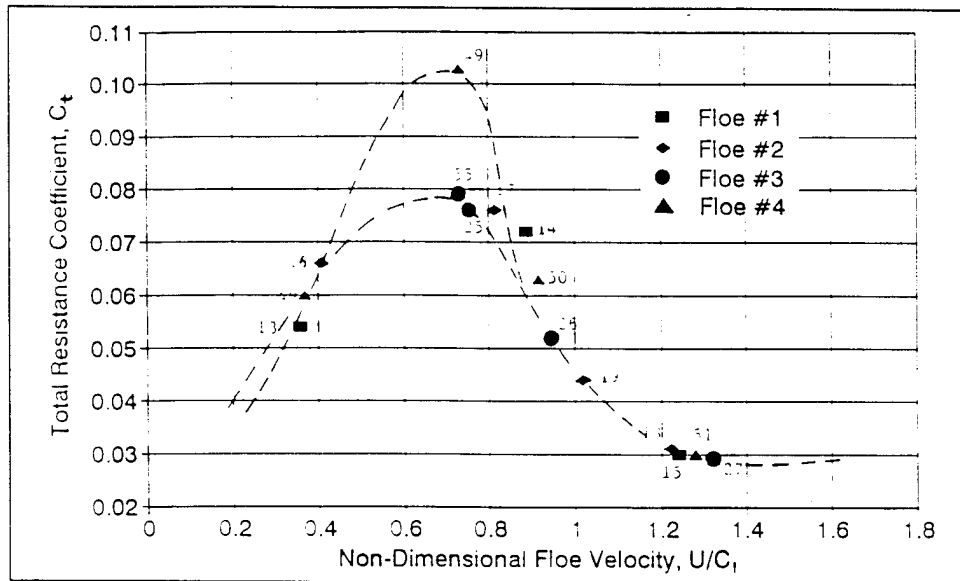
Figure 29: Plot of Stratified Test Total Resistance, $C_{t, stratified}$, vs. Non-Dimensional Floe Velocity, U/C_1, Selected Data from Each Floe

Finally, Figure 30 is a plot of the stratified test total resistance coefficient, $C_{t, stratified}$, versus the draft to upper layer thickness ratio, T/h_1. The data presented, from Floe #1 and Floe #3 tests, illustrates a dependence of drag with respect to floe's proximity to the interface of the two fluids. Surprisingly, there appears to be a decline in the total resistance as the draft to upper layer ratio approaches unity for each floe. This may be due to modifications of the pressure disturbance below the floe by the presence of the fresh water / salt water interface.

The internal wave videotape recordings also supply some interesting observations. The characteristics of the internal wave generated by the moving ice floe appear less dependent on ice floe bottom topography than originally expected. One of the reasons for this occurrence may be that the internal wave has a much longer wavelength than the floe's length. Although the pressure distribution immediately beneath the floe differs for each bottom topography, small pressure variations have little effect on the characteristics of the generated wave, and the characteristics of the wave are dictated rather by the average pressure disturbance beneath the floe. It is also interesting that the phenomenon of internal wave "attachment" to the aft end of the ice floe (as illustrated in

42
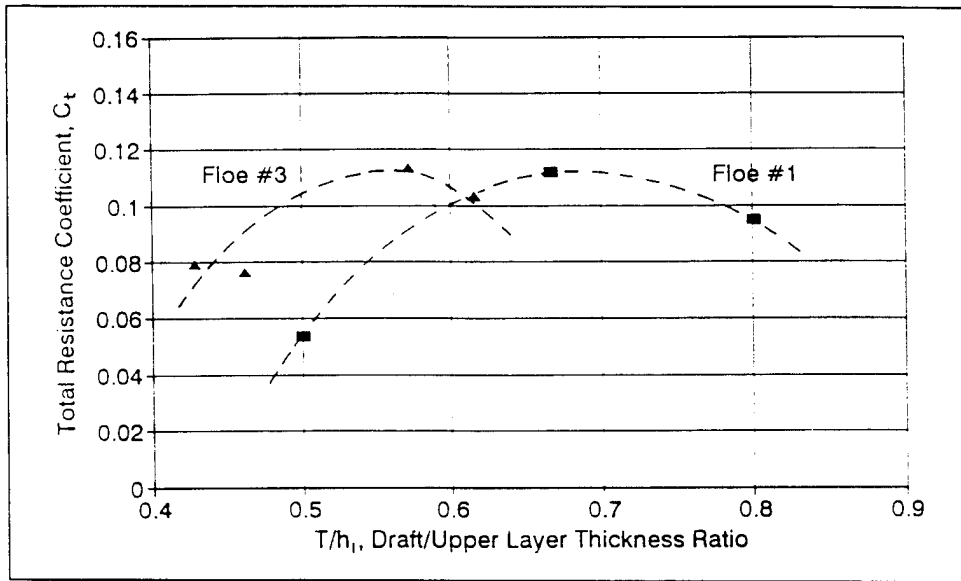
Figure 30: Plot of Stratified Test Total Resistance Coefficient, $C_{t, stratified}$, vs. Draft to Upper Layer Thickness Ratio, T/h_1

Figure 16, Test Results section) occurred with each of the four floes tested, and was always coincident with the peak resistance coefficient value. The association of maximum resistance and the "attachment" phenomenon is not surprising; production of the turbulent mixing evident at the aft end of the floe clearly adds significant resistance to the moving floe.

Conclusions

Although additional non-stratified tests still need to be completed, it may be concluded now that the contribution of internal wave creation on the total resistance of an ice floe moving in a stratified body of water has been proven, through laboratory experiments, to be significant and to show definite trends. It is apparent that, for a particular ice floe geometry, the additional resistance caused by the wave creation "peaks" at some optimal combination of draft to upper layer thickness ratio and velocity, and then tapers off and approaches the non-stratified values.

The ramifications of the results found in this study on ice floe numerical modelling is significant. The present methods for determination of ice-water drag coefficients should include dependencies on under-ice topographies, as well as water-body salinity profiles. This latter dependence should ideally be a dynamic one, as when the ice floe travels from waters with one salinity profile to another, the corresponding drag coefficient should also change.

It is clear that the interrelationship between the factors relating to ice floe movement is complex. Although certain correlations between ice-water resistance and several parameters have been identified, a great deal of work still needs to be completed to fully understand ice floe dynamics.

References

1   Ball, F. K., 1963. "Energy Transfer Between External and Internal Gravity Waves," Journal of Fluid Mechanics, Vol. 19, pp. 465-478.

2   Bourke, Robert H., and Alfred S. McLaren, 1992. "Contour Mapping of Arctic Basin Ice Draft and Roughness Parameters," Journal of Geophysical Research, Vol. 97, No. C11, pp. 17,715-17,728.

3   Bruno, M. S., 1992. "Quantifying Sea Ice Drag through Laboratory Experiments," Proceedings of The 11th OMAE Conference. pp. 5-9, ASME.

4   Bruno, Michael S., 1991."The Effect of Internal Waves on Sea Ice Drift," Proceedings of The 10th OMAE Conference, pp. 137-141, ASME.

5   Bruno, Michael S., and Ole S. Madsen, 1989. "Coupled Circulation and Ice Floe Movement Model for Partially Ice-Covered Continental Shelves," Journal of Geophysical Research, Vol. 94, No. C2, pp. 2065-2077.

6   Ekman, V. W., 1904. *The Norwegian North-Polar Expedition, 1893-1896, Scientific Results*, Vol. 5, edited by F. Nansen, pp. 1-152, Longmans, Green and Co., London.

7   Helfrich, Karl R. and W. K. Melville, 1986. "On Long Nonlinear Internal Waves Over Slope-Shelf Topography," Journal of Fluid Mechanics, Vol. 167, pp. 285-308.

8   Herrington, Thomas O., 1992. "Quantifying Sea Ice Drag in a Stratified Water Column Through Laboratory Experiments," Davidson Laboratory Technical Report SIT-DL-92-9-2681.

9   Hibler, William D. III, 1984. "Ice Dynamics," CRREL Monograph 84-3.

10 Kantha, L. H., and G. L. Mellor, 1989. "A Two-Dimensional Coupled Ice-Ocean Model of the Bering Sea Marginal Ice Zone," Journal of Geophysical Research, Vol. 94, pp. 10921-10936.

11 Lange, M. A. and H. Eicken, 1991. "The Sea Ice Thickness Distribution in the North Weddell Sea," J. Geophysical Research, Vol. 96, pp. 4821-4837.

12 Ma, Huamin and Marshall P. Tulin, 1992. "Experimental Study of Ship Internal Waves: The Supersonic Case," Proceedings of the 11th OMAE Conference, Vol.I-A, Offshore Technology, pp. 51-57, ASME.

13 Madsen, O. S. and M. S. Bruno, 1987. "A Methodology for the Determination of Drag Coefficients for Ice Floes," Journal of Offshore Mechanics and Arctic Engineering, Vol. 109, pp. 381-387.

14 McPhee, Miles G., 1982. "Sea Ice Drag Laws and Simple Boundary Layer Concepts, Including Application to Rapid Melting," CRREL Report 82-4.

15 McPhee, M. G. and L. H. Kantha, 1989. "Generation of Internal Waves by Sea Ice," Journal of Geophysical Research, Vol. 94, pp. 3287-3302.

16 Morison, James H., Miles G. McPhee and Gary A. Maykut, 1987. "Boundary Layer, Upper Ocean, and Ice Observations in the Greenland Sea Marginal Ice Zone," Journal of Geophysical Research, Vol. 92, No. C7, pp. 6987-7011.

17 Mowbray, D. E., 1967. "The Use of Schlieren and Shadowgraph Techniques in the Study of Flow Patterns in Density Stratified Liquids," Journal of Fluid Mechanics, Vol. 27, Part 3, pp. 595-608.

18 Muench, R. D., and L. E. Hachmeister, 1984. "Internal Wave Forces in Ice Keels in the Marginal Ice Zone: Some Preliminary Laboratory Results," MIZEX Bulletin 3, CRREL Special Report 84-7, 83-90, U.S. Army Cold Regions Research and Engineering Laboratory, Hanover, N.H.

19 Pritchard, R. S., A. C. Mueller, D. J. Hanzlick, and Y. S. Yang, 1990. "Forecasting Bering Sea Ice Edge Behavior," Journal of Geophysical Research, Vol. 95, pp. 775-788.

20 Sandven, Stein and Ola M. Johannessen, 1987. "High Frequency Internal Wave Observations in the Marginal Ice Zone," Journal of Geophysical Research, Vol. 92, No. C7, pp. 6911-6920.

21 Watson, G., R. D. Chapman and J. R. Apel, 1992. "Measurements of the Internal Wave Wake of a Ship in a Highly Stratified Sea Loch," Journal of Geophysical Research, Vol. 97, No. C6, pp. 9689-9703.

22 Yih, Chia-Shun, 1960. "Gravity Waves in a Stratified Fluid," Journal of Fluid Mechanics, Vol. 8, pp. 481-508.

23 Zhu, Jinlin, Theodore Y. Wu and George T. Yates, 1987. "Internal Solitary Waves Generated by Moving Disturbances," Proceedings of the Third International Symposium on Stratified Flows, pp. 74-83.

Appendix A

Test Data

DAVIDSON LABORATORY

By: _T. HERRINGTON_   Project No: _5422/104_   Date: _18 DEC 1993_

Facility: _TANK 3_   Page: _1 OF 1_

FLAT BOTTOM FLOE

RUN #	DRAFT	SET POINT		TIMING DISTANCE	TIME	SPEED		DRAG			
	in	ft/s		ft	s	ft/s		lb			
1	6.0	*		50	—	—		0.1211			
		* SET POINT INITALLY 0.05 ft/s RESET TO 0.1 ft/s AFTER E-STOP									
		DURING RUN									

DAVIDSON LABORATORY

By: _T. HERRINGTON_   Project No: _5422/104_   Date: _21 DEC 1992_

Facility: _TANK #3_   Page: _1 OF 1_

FLAT

RUN #	DRAFT	SET POINT		TIMING DISTANCE	TIME	SPEED		DRAG	
	in	ft/s		ft	s	ft/sec		MEAN lb	
~~1~~ 4	6.0	0.20		50	249.49	0.200		0.1355	
~~2~~ 5	6.0	0.20		50	248.00	0.202		0.1313	
6	6.0	0.10		50	496.032	0.101		0.0677	
7	6.0	0.30		50	165.289	0.302		0.2708	
~~8~~	~~60~~	~~0.40~~		~~50~~	~~124.4~~			~~0.6506~~	
		PROBE ≈ 3'		FROM EDGE OF TANK					
*	RUNS	2 AND 3		WHERE DUMMY RUNS					

DAVIDSON LABORATORY

By: T Herrington   Project No: 5422 /104   Date: 22 Dec 1992

Facility: Tank 3   Page: 1 of 1

FLAT

Run #	Draft IN.	Set Point ft/s	Timing Distance ft	Time s	Speed ft/s	Drag lb	Video Count Start	Video Count Stop
							~~35:37~~	~~42:52~~
8	6	0.2	50	248.226		0.1095	35:37	42:52
9	6	0.4	50	124.456		0.6506	42:52	51.14

* PROBE NEAR SIDE OF THE TANK FOR RUNS 8 AND 9

DAVIDSON LABORATORY

By: T HERRINGTON   Project No: 5422 /104   Date: 23 DEC 1992

Facility: TANK 3   Page: 1 of 1

FLAT

Run	Draft in	Set Point ft/s		Timing Distance ft	Time s	Speed ft/s		Drag		Video Count Start	Stop
10	6	0.4		50	124.314	0.402		0.6641		56.16	1.01.13
11	5	0.6		50	83.129	0.601		0.8660		1.01.13	1.10.33
12	5	0.3		50	165.726	0.302		0.2292		1.10.33	1.17.00
13	3	0.2		50	248.100	0.201		0.0535		1.17.00	1.24.17
14	3	0.5		50	99.622	0.507		0.4246		1.24.17	1.31.08
15	3	0.7		50	71.306	0.701		0.3434		1.31.08	1.36.03

5422/104

5 JAN 1993

DRAG CALIBRATION   1400

FILE: DRAGCAL.ASU
CHANNEL: 00   ± 10 V
SAMPLE FREQ: 5 Hz   DURATION 10 s

DISK ACQUISITION

	FILE	DRAG	VOLTS
1.	CAL 1 00	0 lbs	MEAN VOLTS = 0.1357 V
2.	CAL 1 02	0.2 lbs	" " = 0.182 V
3.	CAL 1 04	0.4 lbs	= 0.321 V
4	CAL 1 06	0.6 lbs	= 0.469 V
5.	CAL 108	0.8 lbs	= 0.619 V
6.	CAL 110	1.0 lbs	= 0.798 V
7.	CAL 112	1.2 lbs	= 0.943 V
8	CAL 114	1.4 lbs	= 1.093 V
9	CAL 116	1.6 lbs	= 1.241 V
10.	CAL 118	1.8 lbs	= 1.386 V
11.	CAL 120	2.0 lbs	= 1.532 V
12.	CAL 10e	0.0 lbs	= 0.045 V

DRAG CALIBRATION

15 JAN 1995
AIR ICE FLOE PROJECT
TANK #3
Inc. (Global Lab Enterprise)

(lb)	(V)
0	0.045
0.2	0.182
0.4	0.321
0.6	0.459
0.8	0.619
1.0	0.718
1.2	0.943
1.4	1.093
1.6	1.241
1.8	1.886
2.0	1.532

SLOPE = 0.73 V/lb

VOLTS (X): 1,600 1,500 1,400 1,300 1,200 1,100 1,000 900 800 700 600 500 400 300 200 100

LBF: .2 .4 .6 .8 1.0 1.2 1.4 1.6 1.8 2.0

A - 6
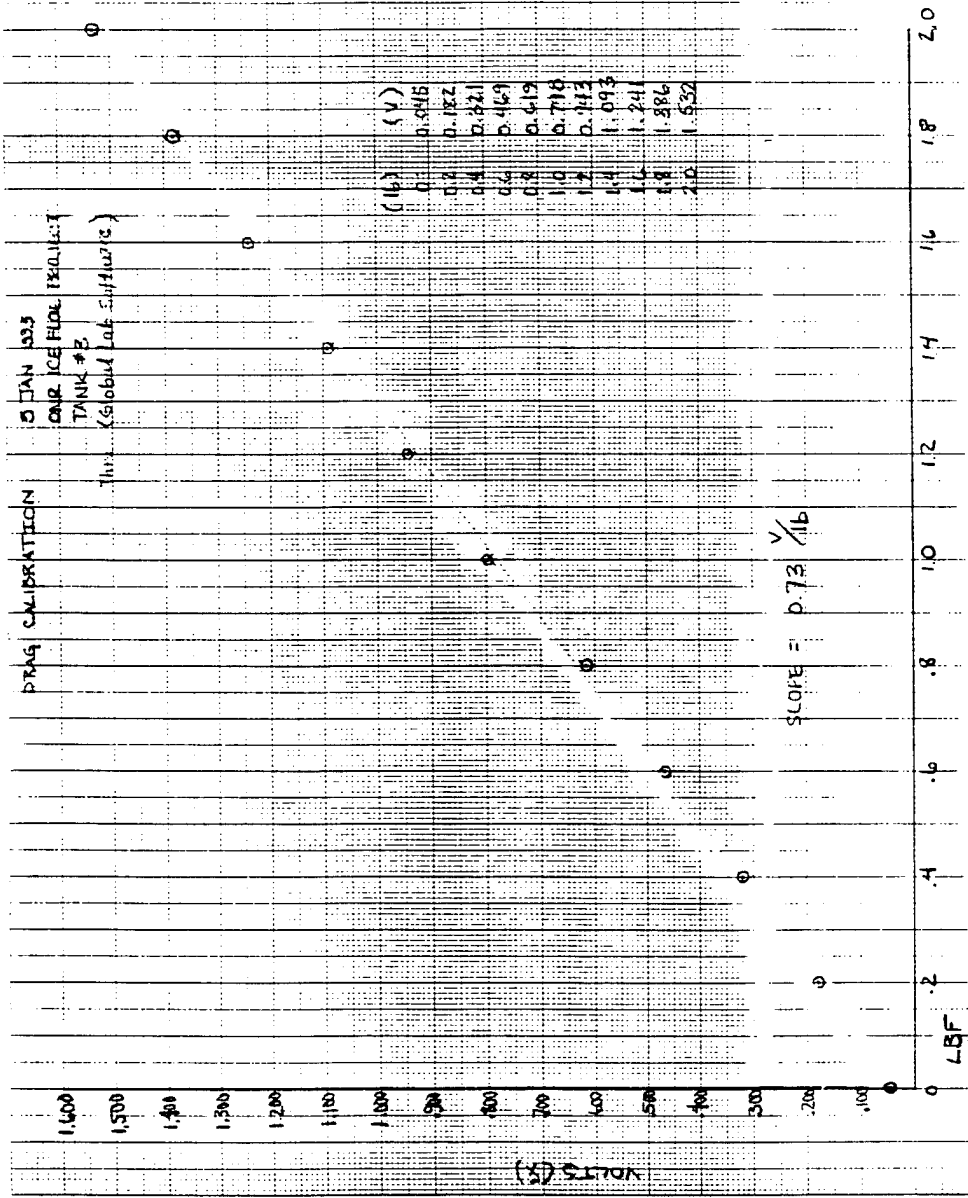
5422/104   5 JAN 93

WAVE PROBE CALIBRATION   1500

FILE: WAVECAL.ASU

CHANNELS 01   ± 10 VOLTS

SAMPLE FREQ: 5 HZ   DURATION 10 s

DISK ACQUISITION

FILE   DEPTH   MEAN VOLTS

WCAL10   0 in   0.013 √   VOID

WCAL15   0.5 in   0.250 √

WCAL11   1.0 in   0.526 √

WCAL18   1.5 in   0.467 √

WCAL12   2.0 in   0.705 √

WCAL20
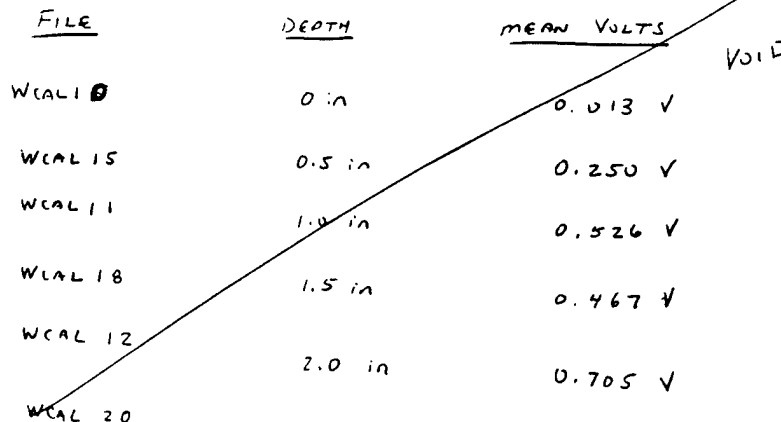
FILE: WAVECAL2.ASU

WC200   0.0   0.085

WC205   0.5   0.503

WC210   1.0   0.967

WC215   1.5   1.342

WC220   2.0   1.421

WC20m   0.0   -0.001

A - 7

WC2n05   -0.5   -0.541

WC2n10   -1.0   -1.095

WC2n15   -1.5   -1.745

WC2n20   -2.0   -2.375

WC2n00e   0.0   -0.332

---

run 16 z   zero run   drag mean = -0.320

run 16   mean = -0.272   0.048 v

---

run 17 z   zero run   drag mean = -0.320

run 17   drag = -0.118   0.202 v

---

run 18 z   zero run   drag mern = -0.302

run 18   drag = -0.114   0.188 v

---

run 19 z   zero run   drag mean = -0.307

run 19   drag = -0.126   0.181

---

run 20 z   = -0.311

run 20   = -0.210   0.101

Run 21 z   = -0.303

run 21   = -0.195   0.108

run 222   −0.303
Run 22   −0.118   0.185

1 PERIOD SIN FLOE

RUN ♯	DRAFT	SET POINT		Time DIST	TIME	SPEED		DRAG				
	in	ft/s		ft	s	ft/s		lb				
16	3	0.2		50	—	—		0.066				
17	3	0.4		50	124.33	0.402		0.277				
18	3	0.6		50	83.07	0.602		0.257				
19	3	0.5		50	99.71	0.501		0.248				
20	2	0.5		50	99.66	0.502		0.138				
21	2	0.6		50	93.04	0.602		0.148				
22	2	0.8		50	62.50	0.800		0.253				

∗ SALT - WATER INTERFACE AT 5½ in Depth

DAVIDSON LABORATORY

By: _T. HERRINGTON_   Project No: _5422/104_   Date: _6 JAN 1993_

Facility: _TANK #3_   Page: _1 OF 1_

2 PERIOD SIN FEEE

RUN #	DRAFT	SET POINT		TIMING DIST.	TIME	SPEED		DRAG			
	in	ft/s		ft	s	ft/s		lb			
23	4	0.2		50	247.76	0.202		0.195			
24	4	0.4		50	124.16	0.403		0.408			
25	3	0.4		50	—	—		0.283			
26	3	0.5		50	99.46	0.503		0.298			
27	3	0.7		50	—	—		0.326			
28	4	0.5		50	—	—		0.434			
29	4	0.7		50	71.32	0.701		0.448			
*	INTERFACE	(FRESH-SALT)		AT ~		6.5	in				

A - 11

DAVIDSON LABORATORY

By: _T. Harrington_   Project No: _5422/104_   Date: _7 Jan 1993_

Facility: _Tank # 3_   Page: _1 of_

Temp = 55°F @ 3" below surface
65°F @ 24" below

Run #	Draft	Set Point		Timing Dist.	Time	Speed		Drag				
	in	ft/s		ft	s	ft/s		lb				
* 46										Dummy Run		Drag
47										Dummy Run		Drag
48	4	0.2		50	247.93	0.202		0.062				
49	4	0.4		50	—	—		0.408		Irregular Floe Star		
50	4	0.5		50	99.48	0.503		0.392				
51	4	0.7		50	—	—		0.363				
52	3	0.4		50	124.25	0.402		0.165				
53	2	0.4		50	124.35	0.402		0.108				
54	4	0.4		50	124.35	0.402		0.447	}	2L Sin.		
55	3	0.4		50	—	—		0.293				

* Run #'s 30 → 45 Skipped due to Masscomp Error - Files Already Exist

A - 12

Appendix B

Internal Wave Strip Chart Recordings

Notes on internal wave wire strip-chart recordings:

- The internal wave wire was mounted (stationary) along the side of the tank, approximately 20 feet (6 m) into the data collection portion of the test run.

- Each internal wave record shown here is from the period during which the ice floe model was within the 50 ft (15.24 m) data collection length.

- The horizontal scale for all recordings is
                1 mm = 1 sec.

- Internal wave wire recordings were not obtained for Runs 23-29 due to malfunctions with the instrument.
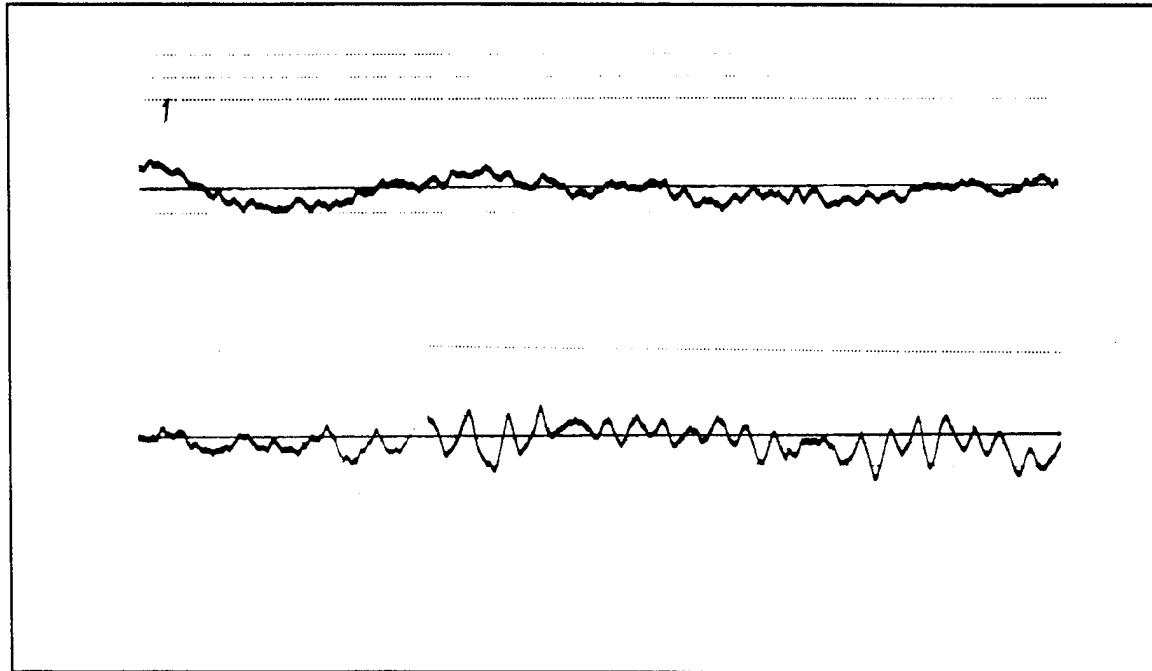
Run 1
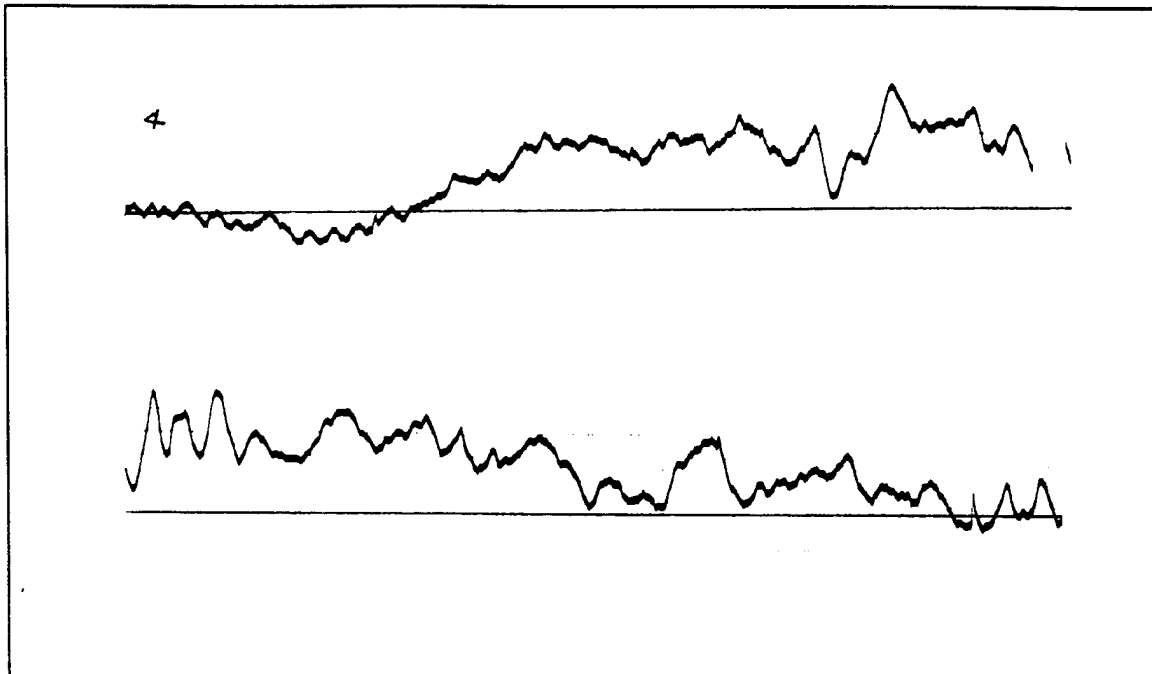
Run 4
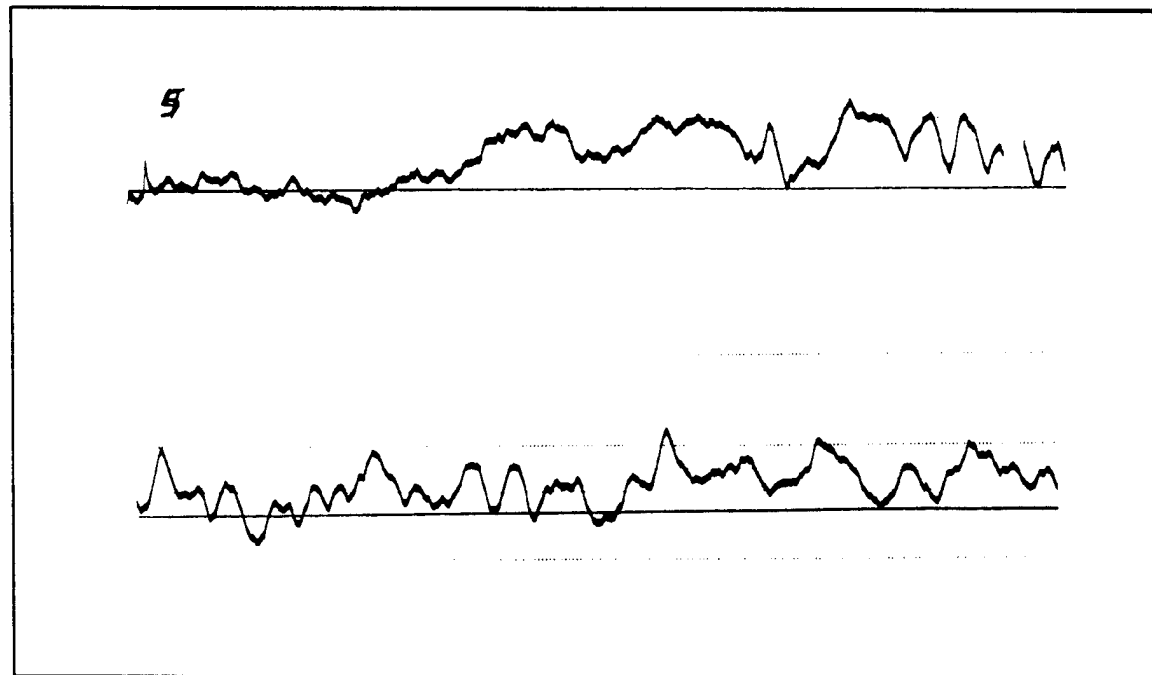
Run 5
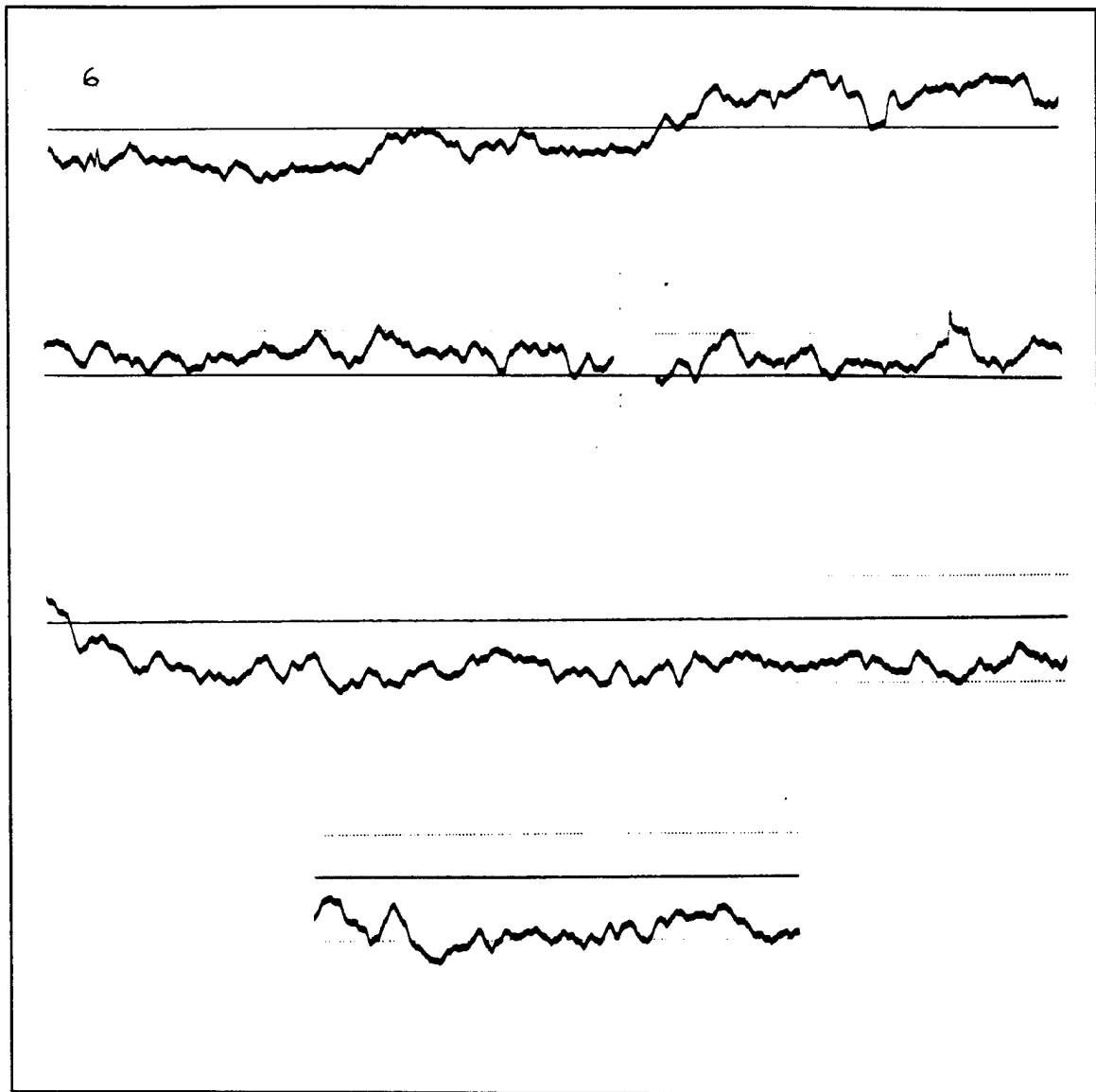
Run 6
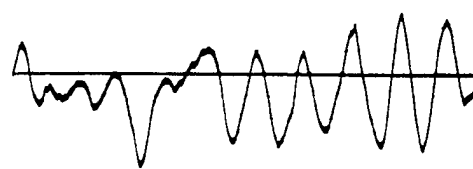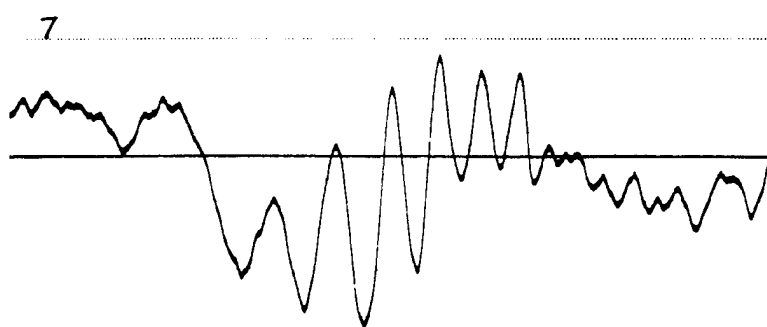
Run 7

Run 8

Run 9

Run 10

Run 11

Run 12

Run 13

Run 14

15

Run 15

16 (Drag signal is super-imposed)

Run 16

B - 8
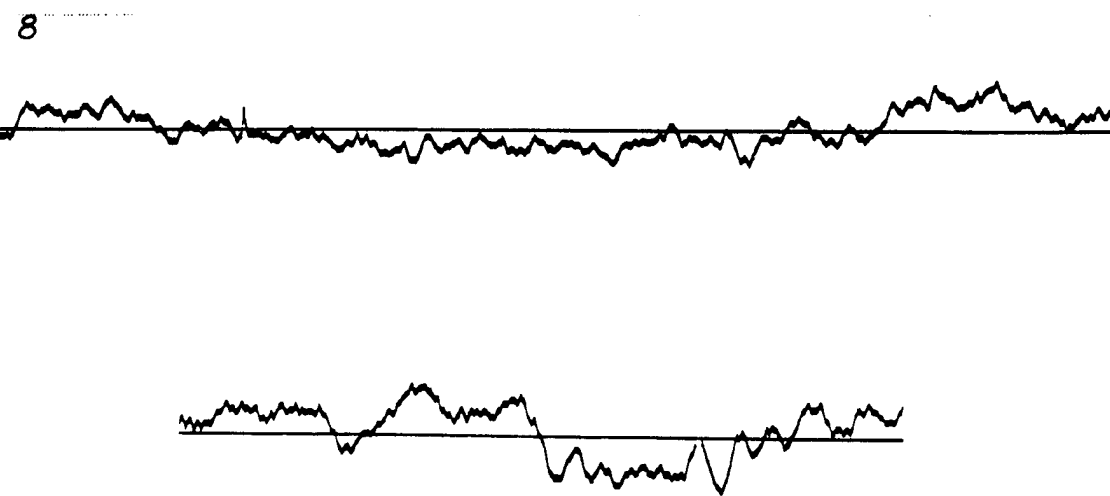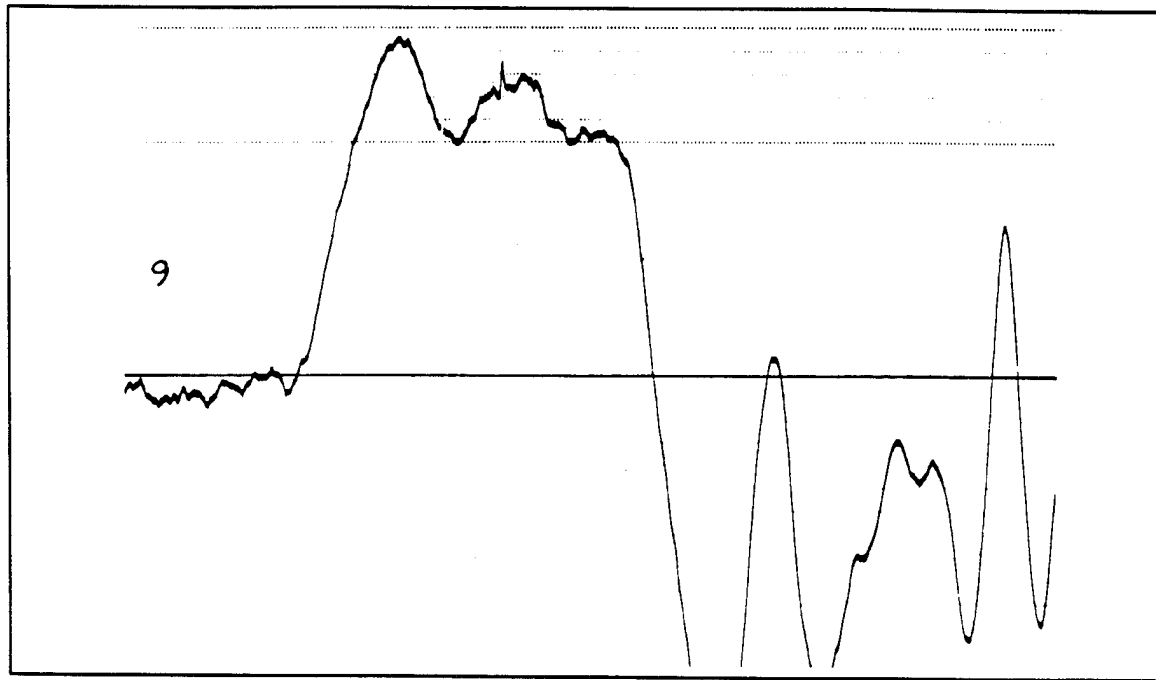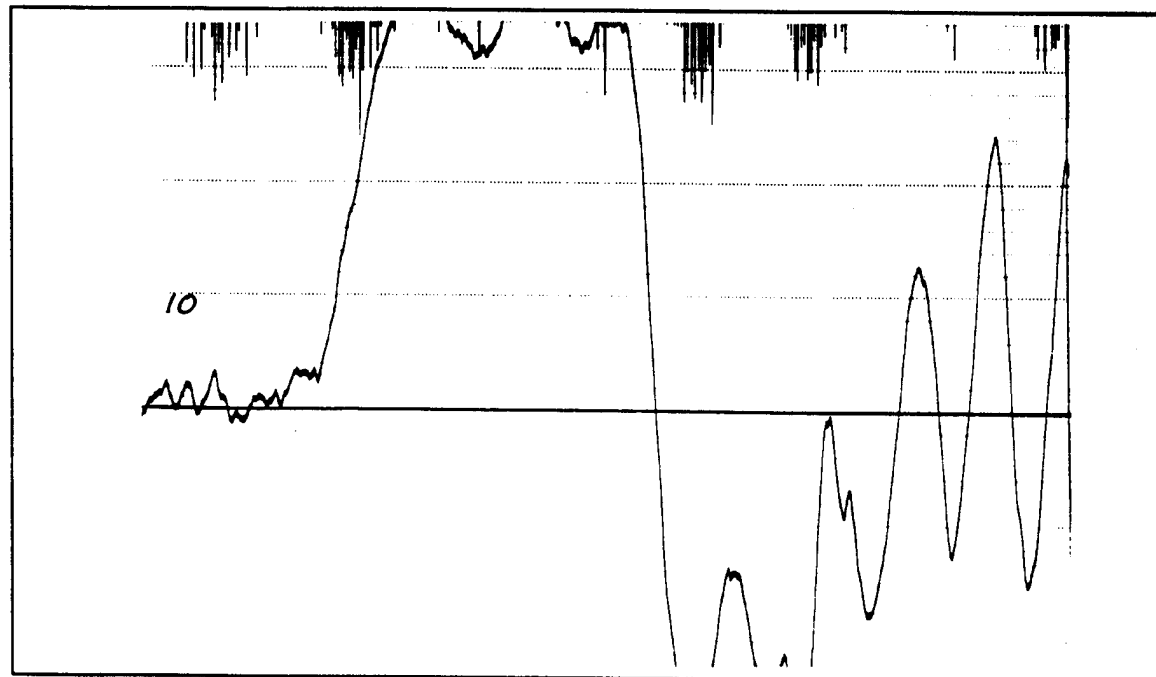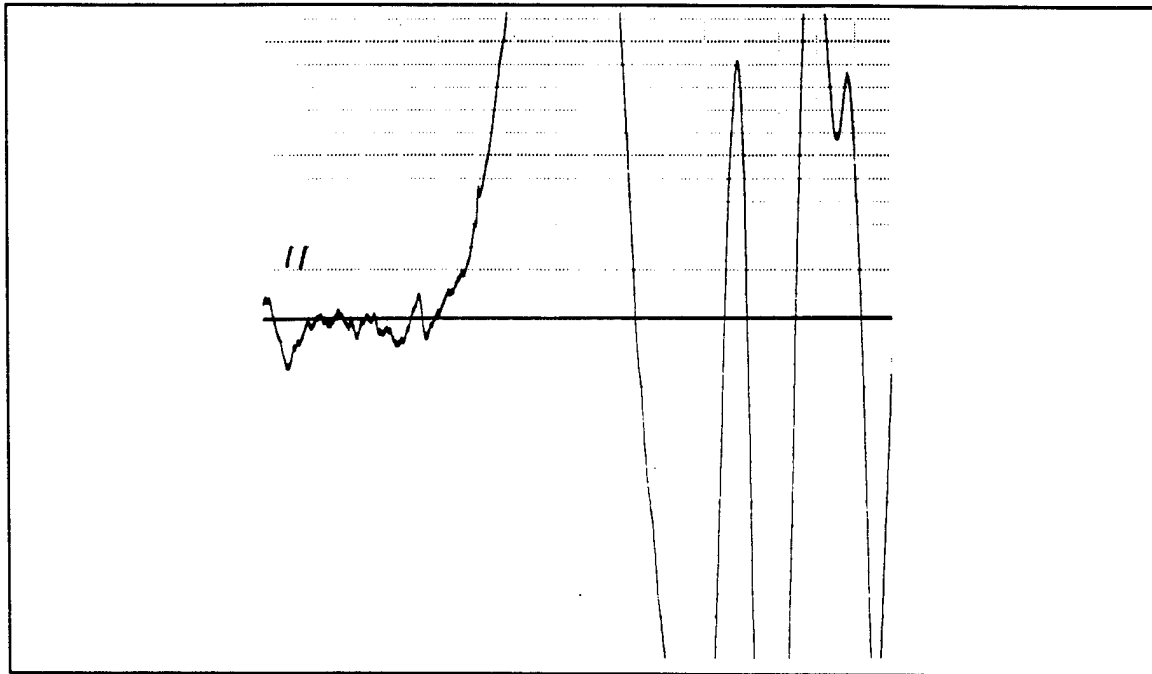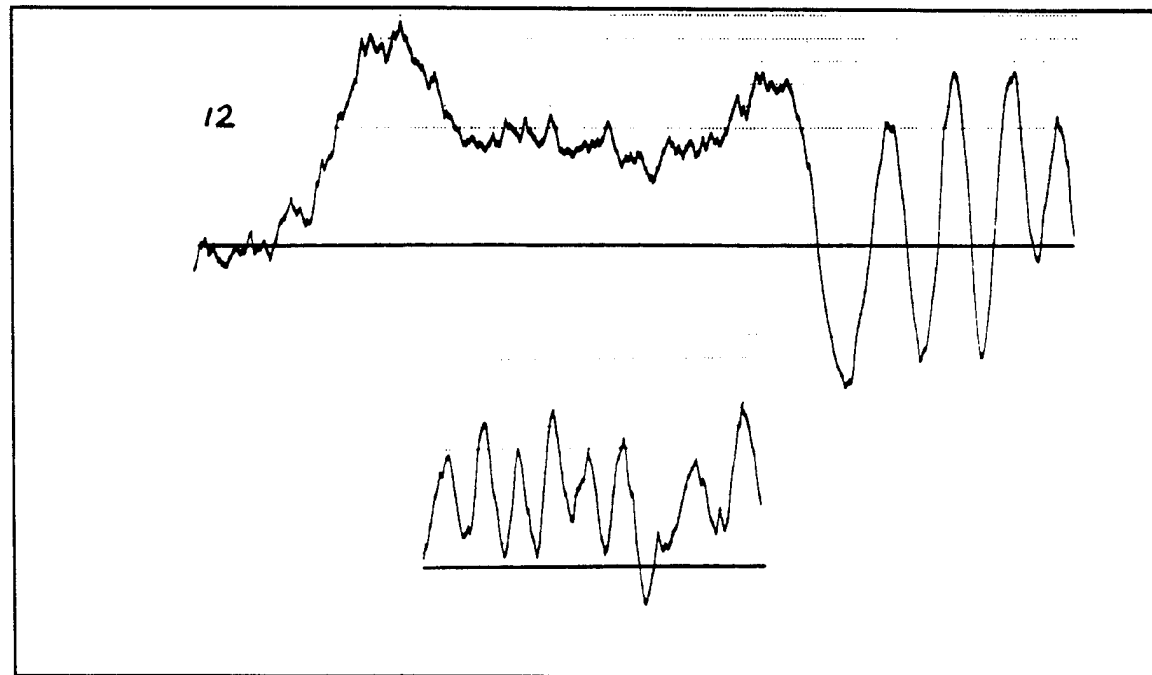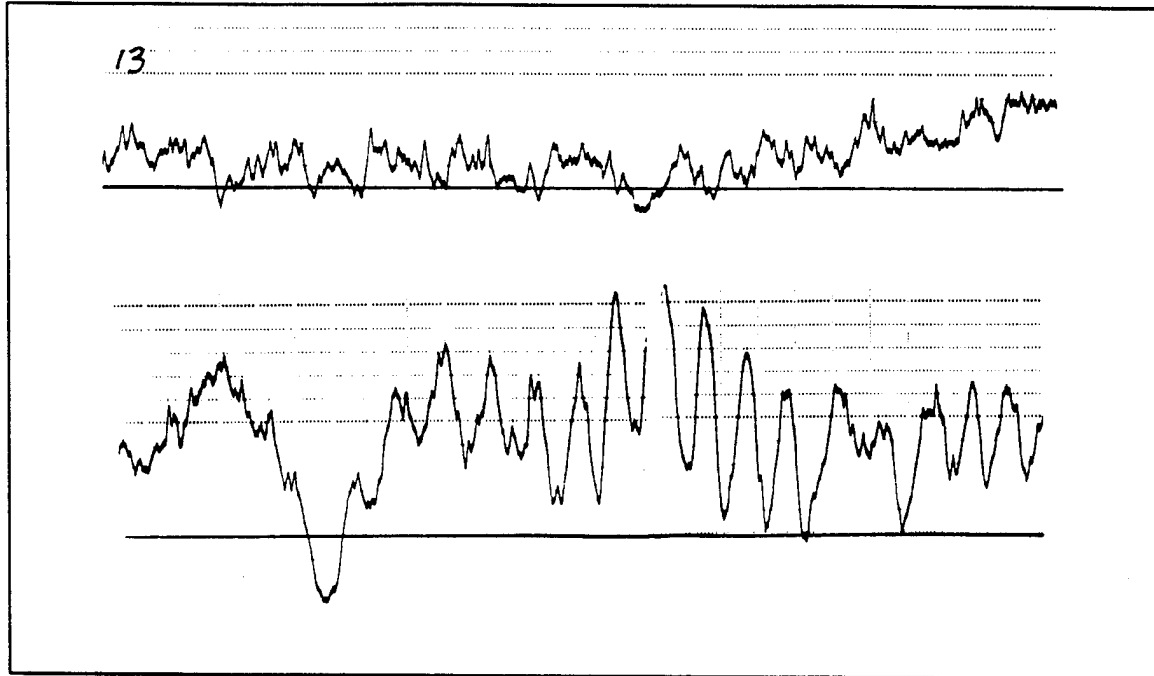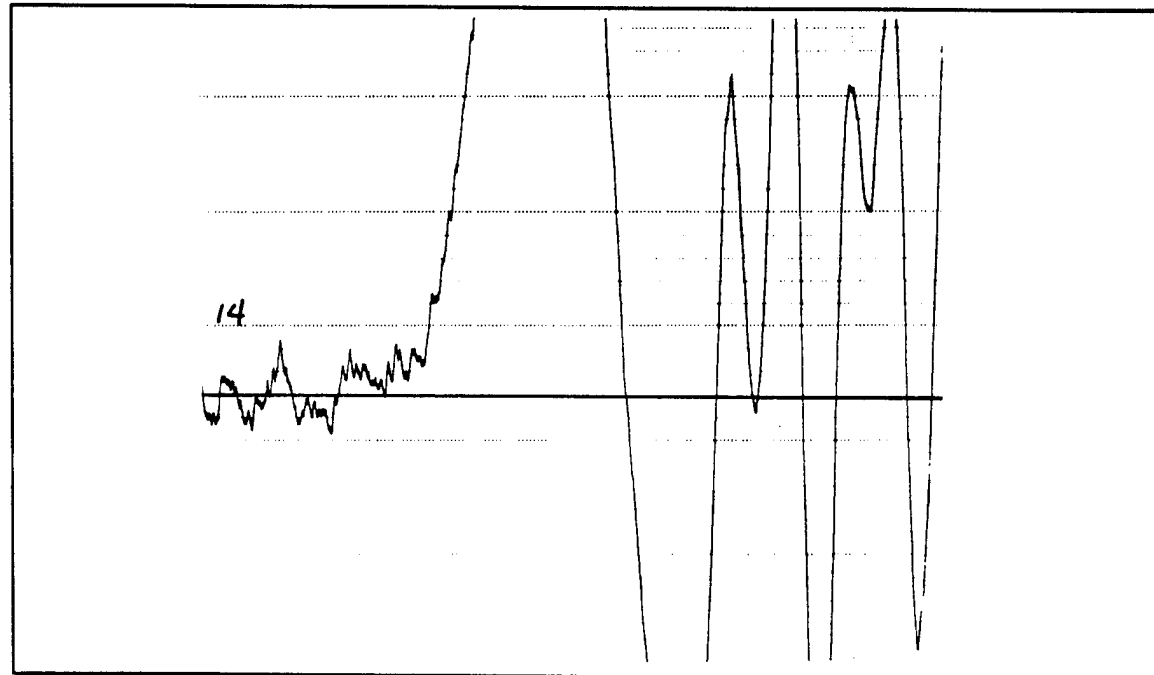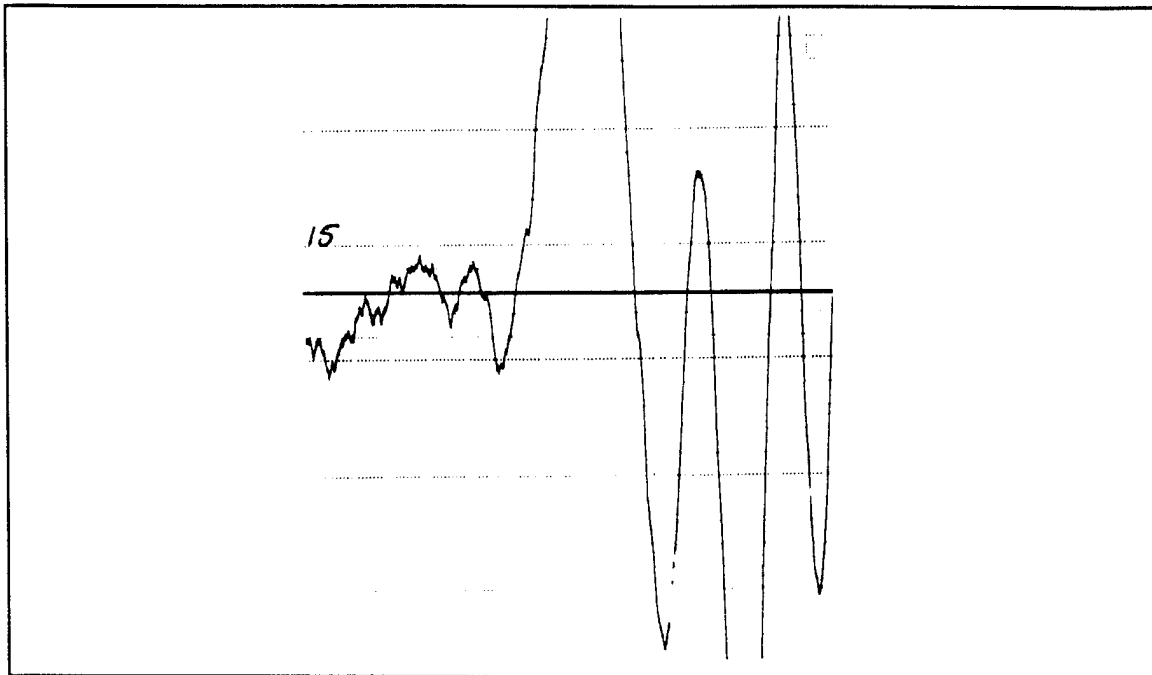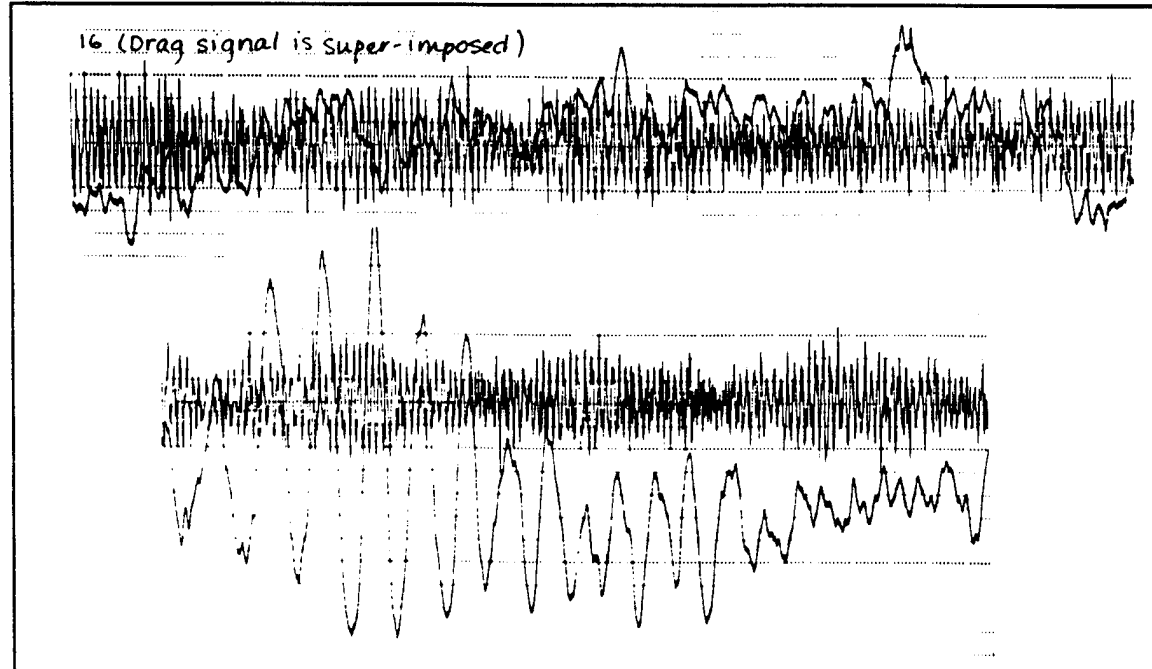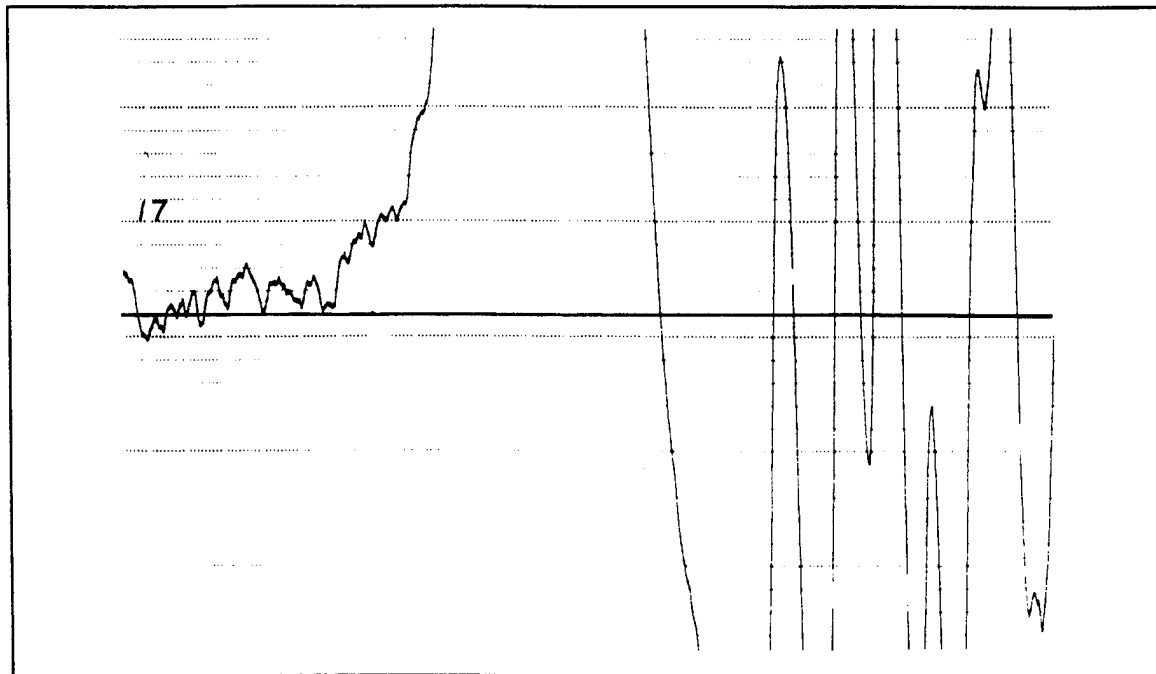
Run 17

Run 18

Run 19

Run 20

Run 21

Run 22

Run 48

Run 49

B - 12

Run 50

Run 51

B - 13

Run 52

Run 53

B - 14

54

Run 54

55
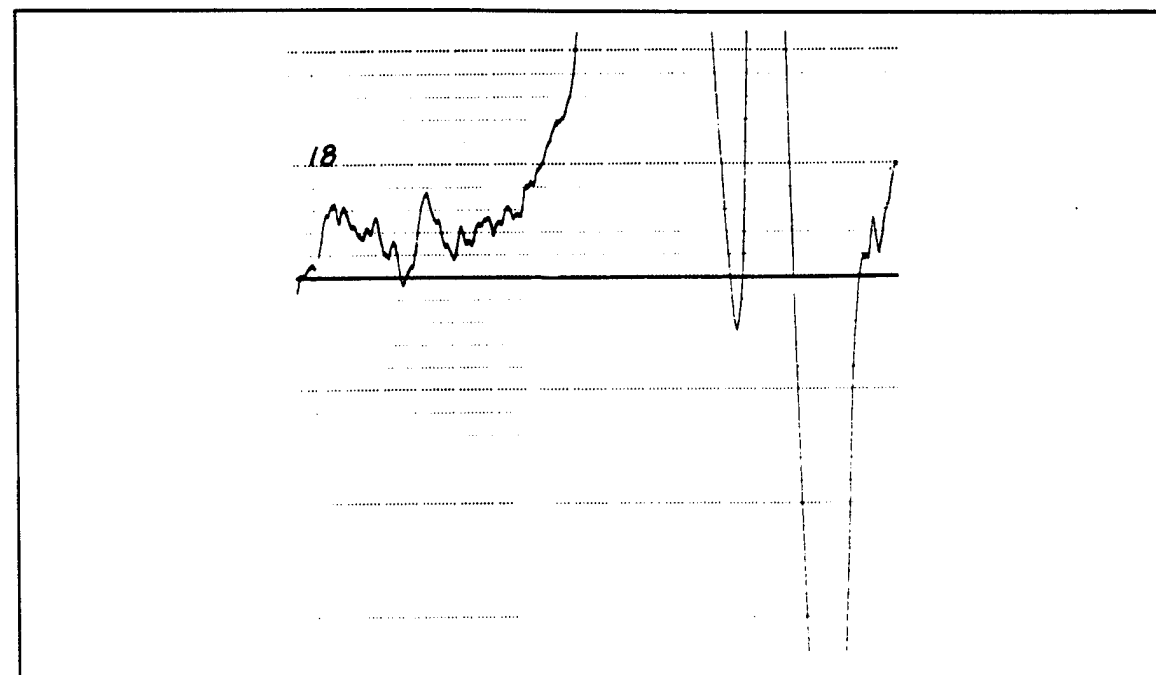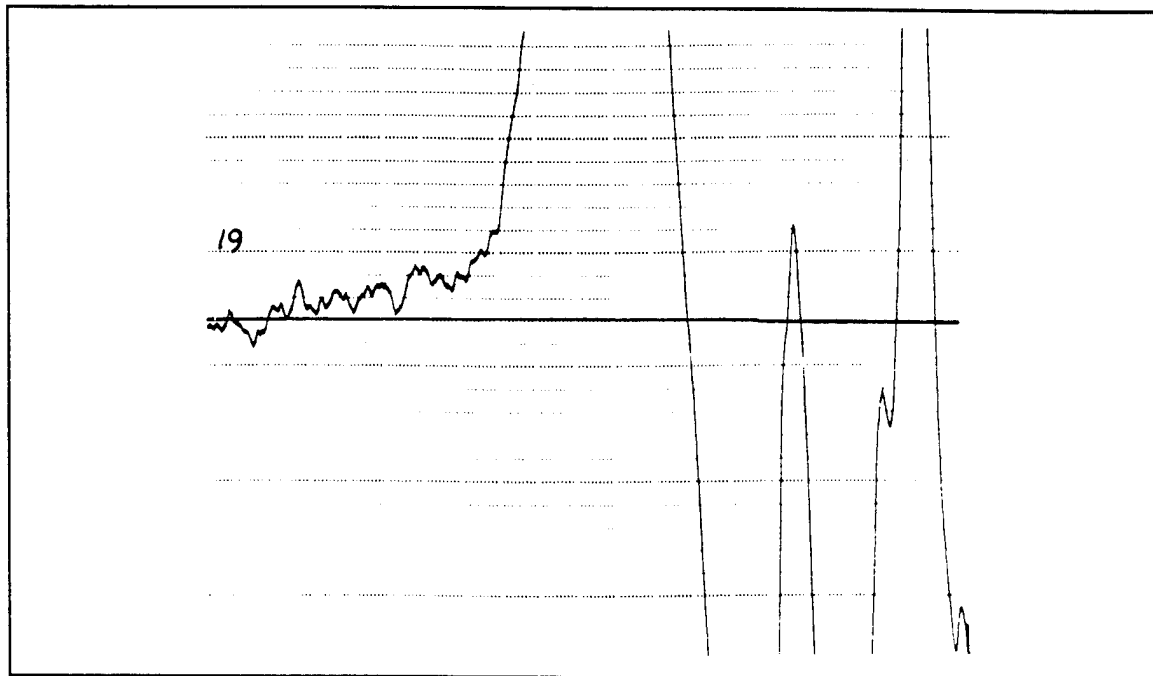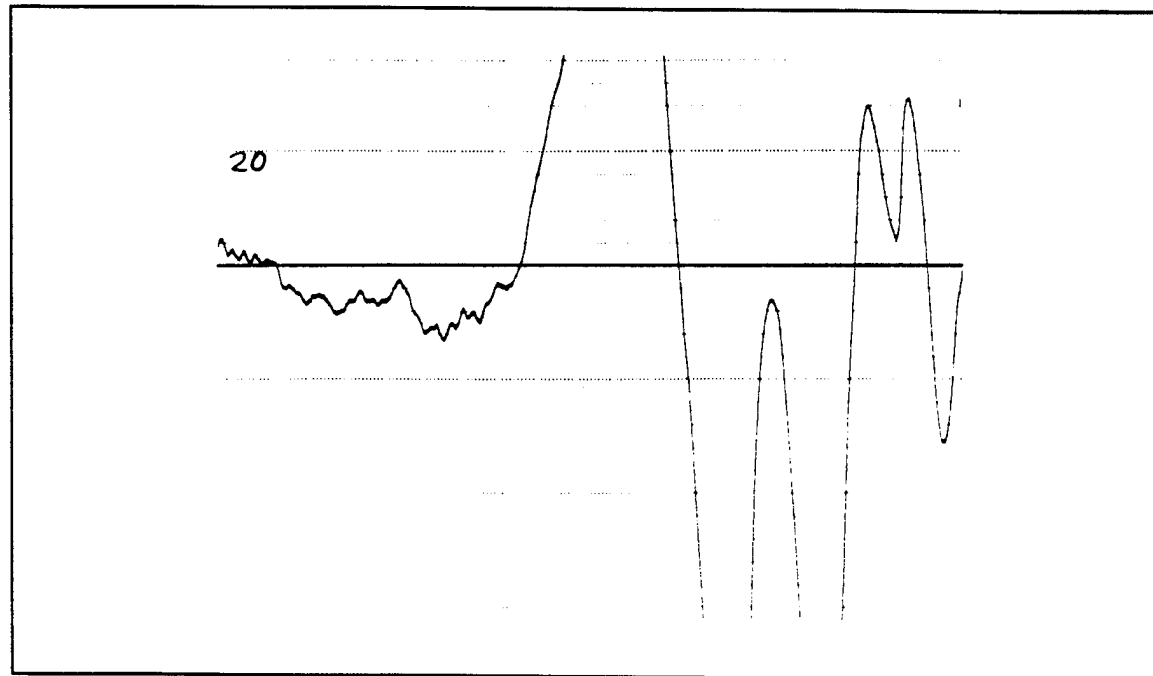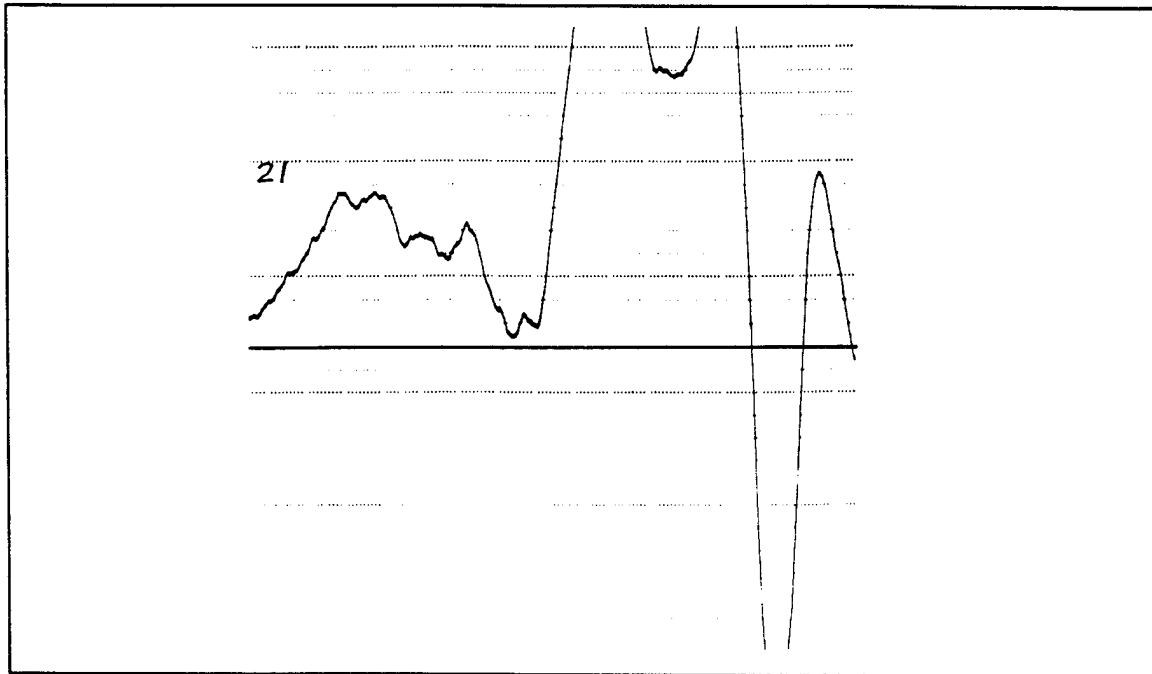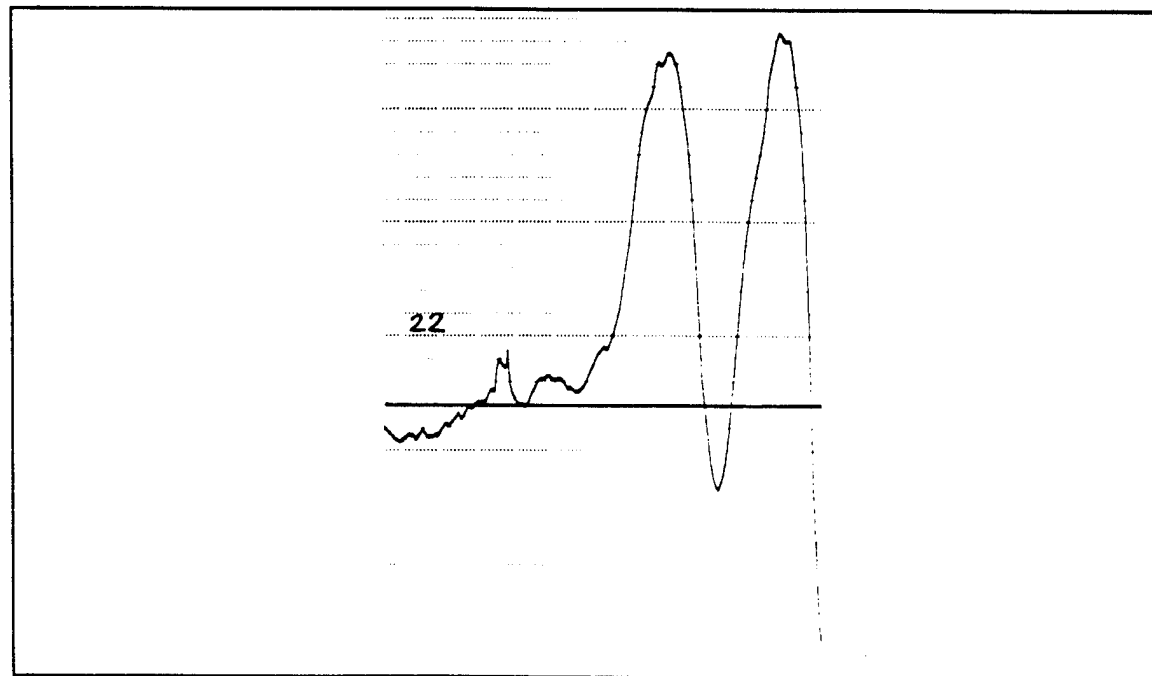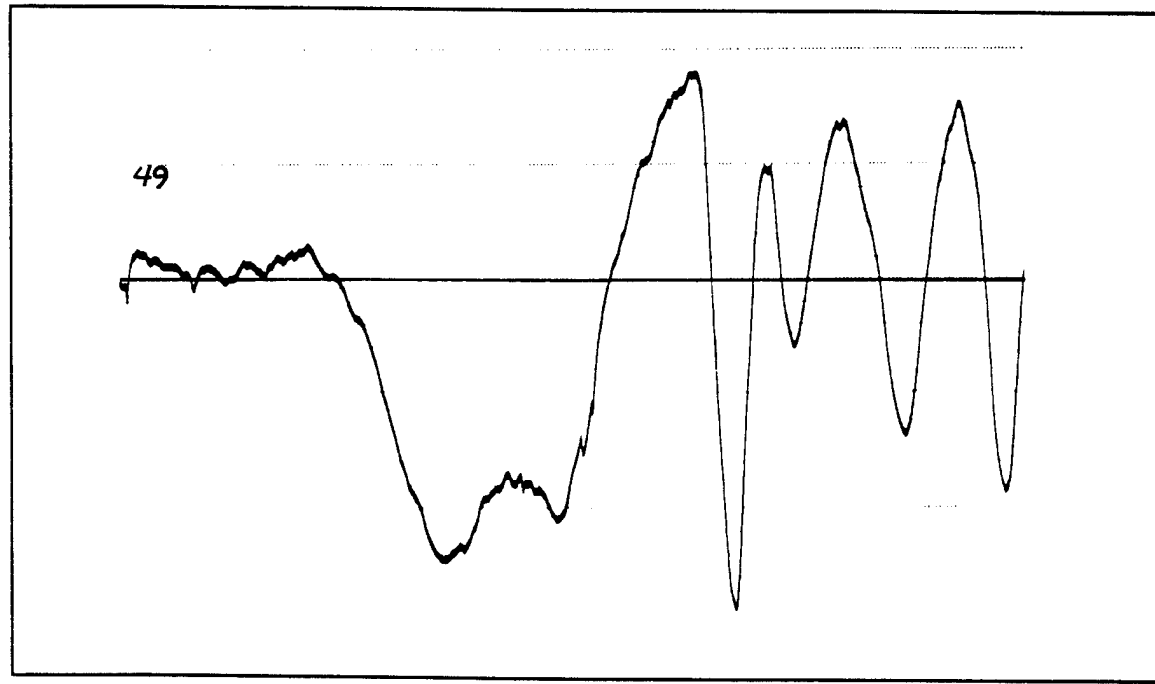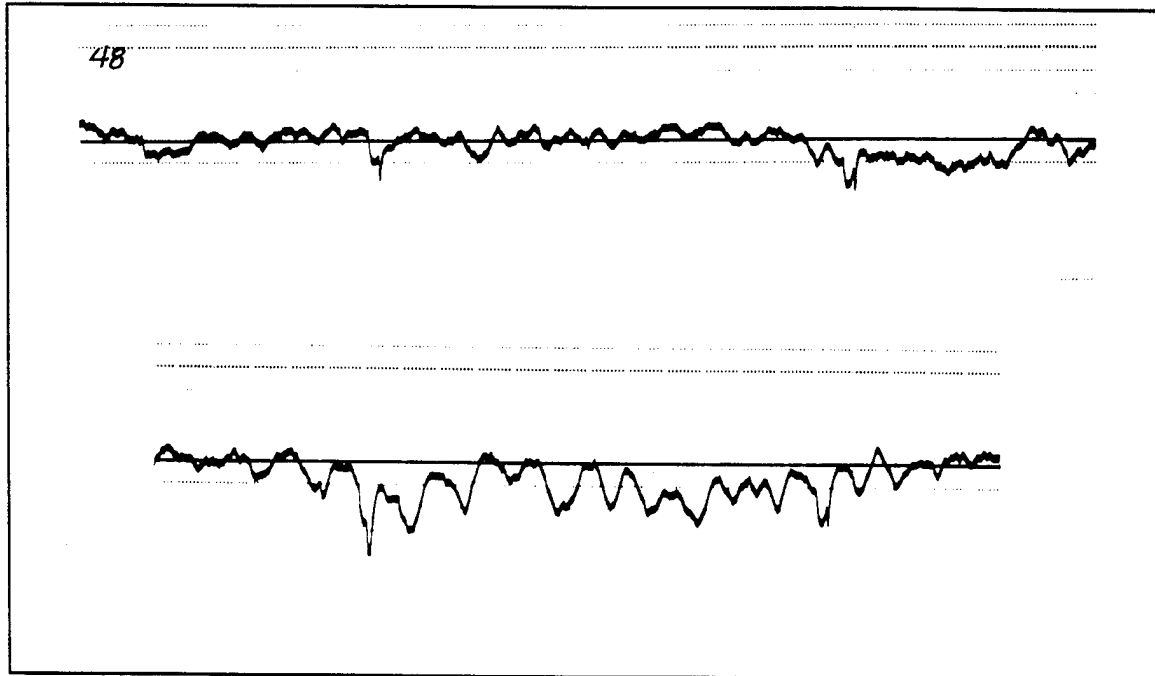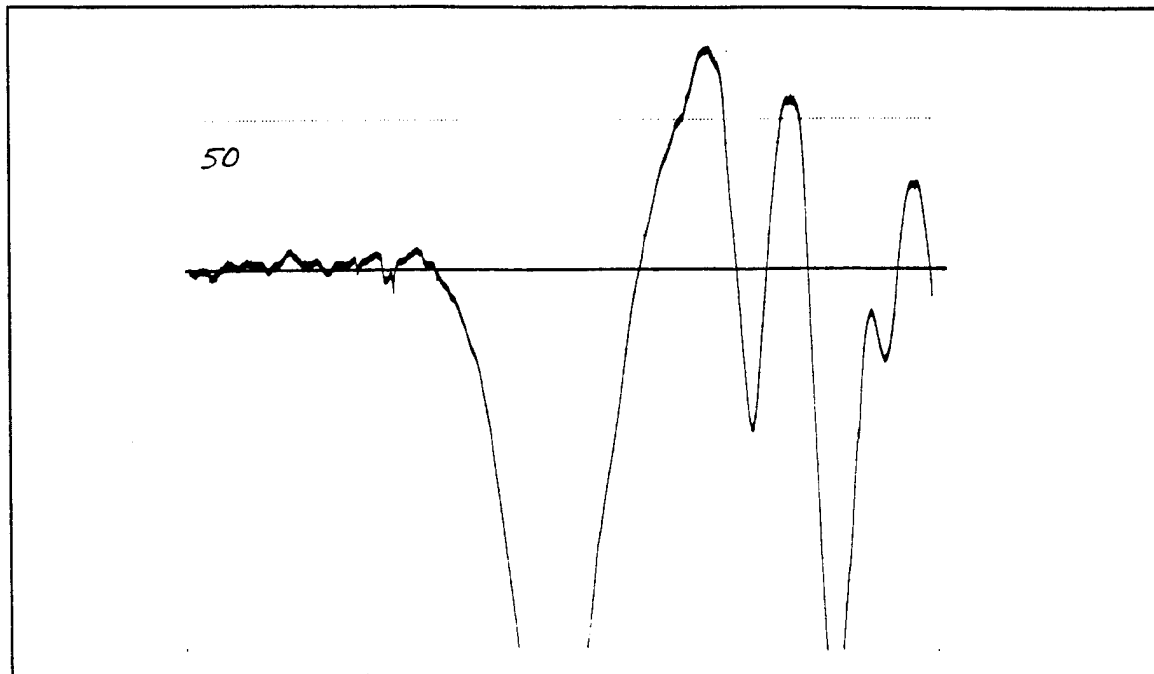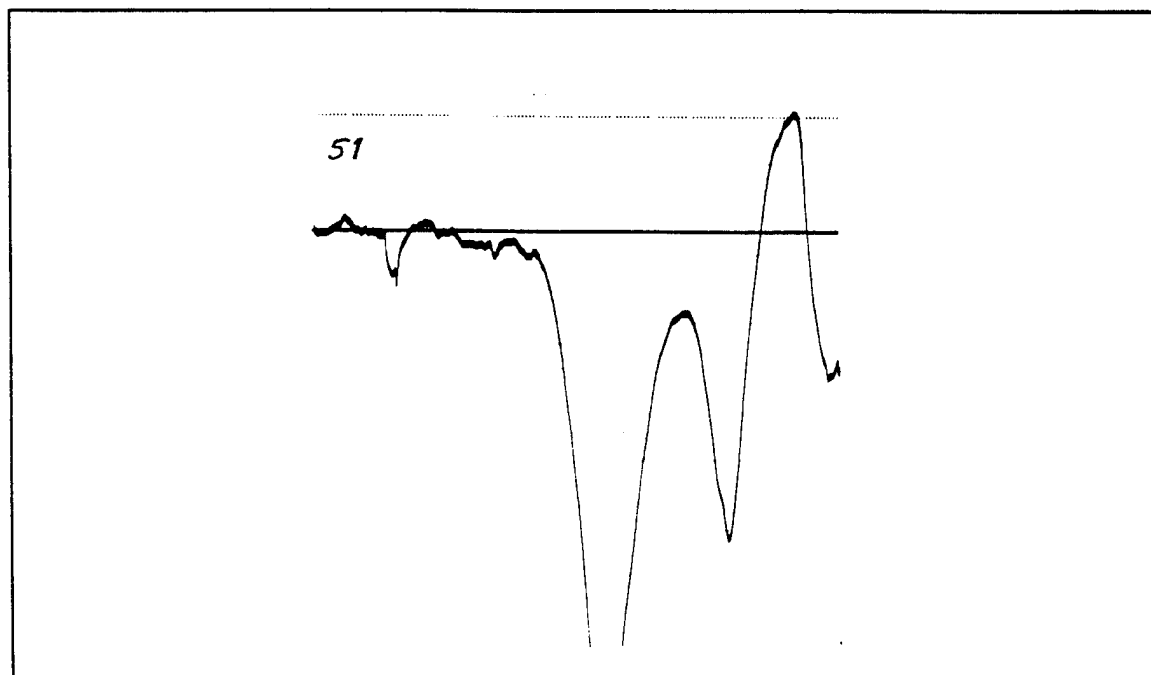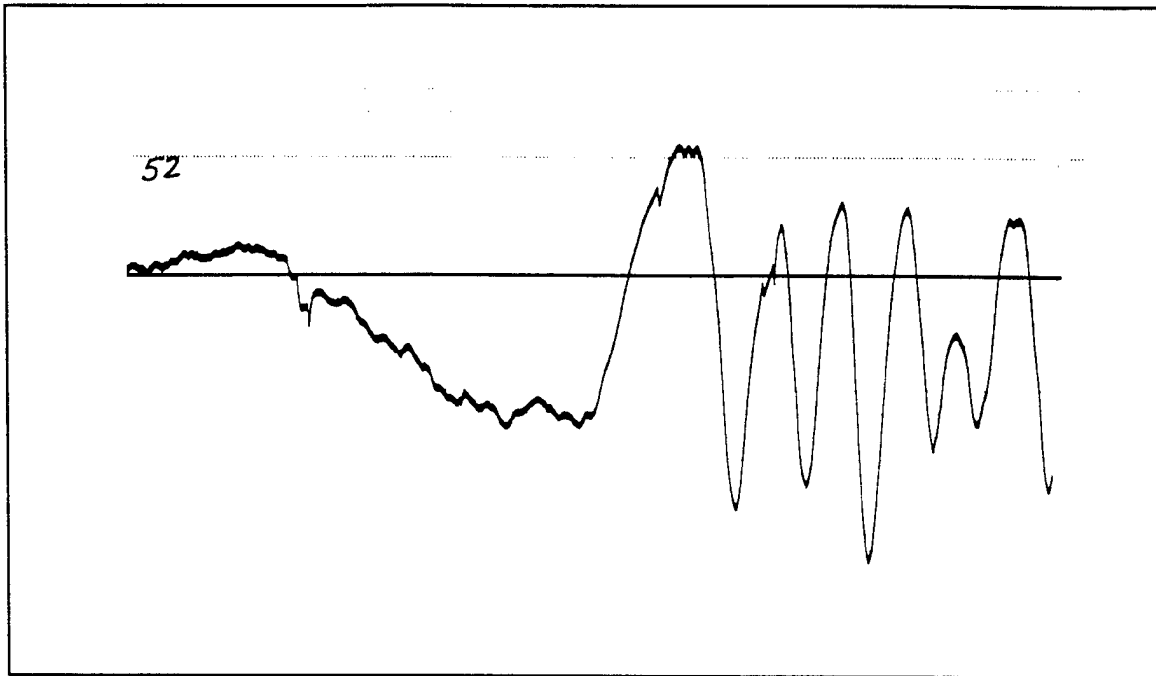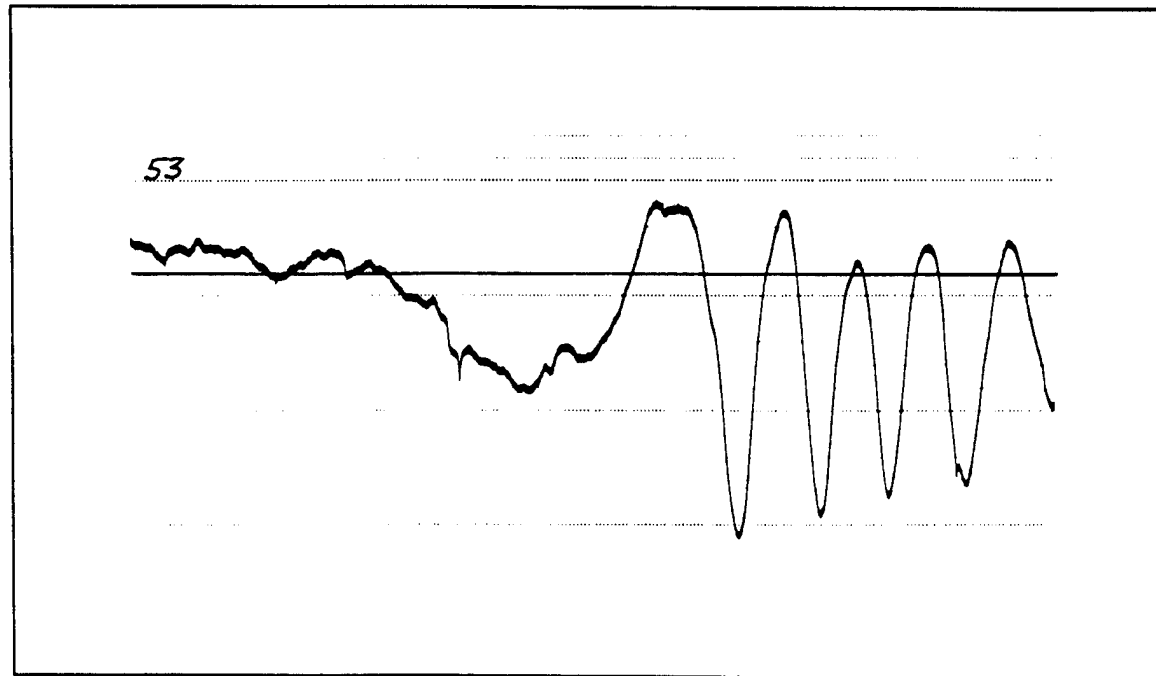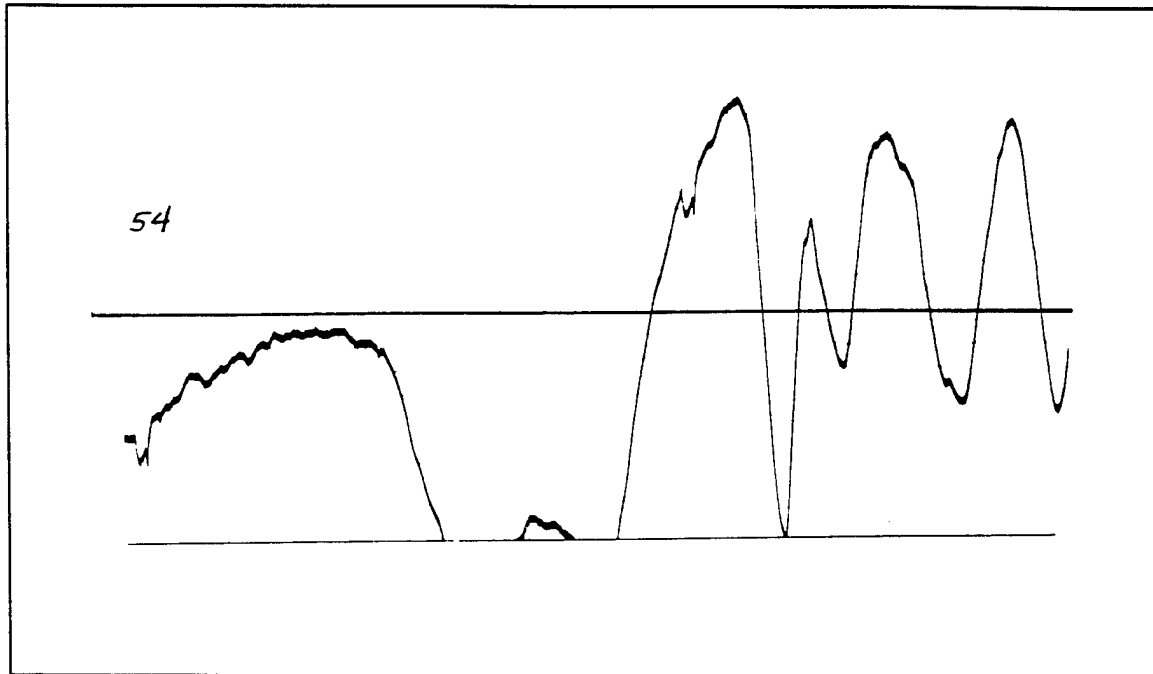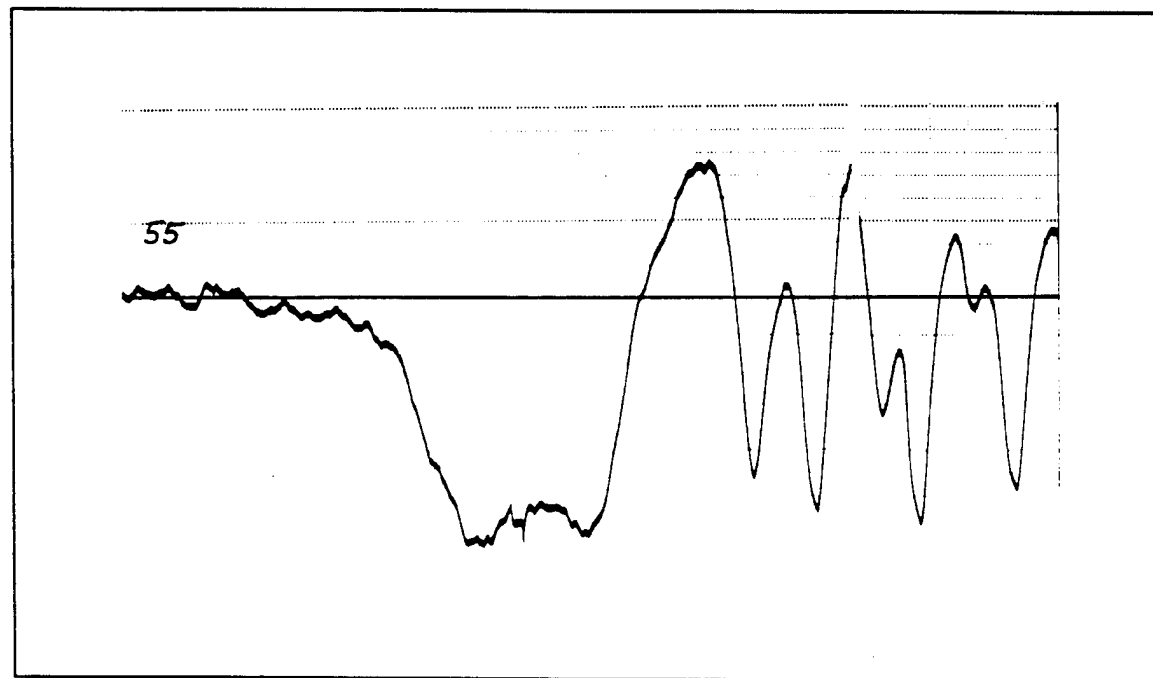
Run 55

Appendix C

Salinity Profile Data and Plots

Data for
SALINITY PROFILE PLOTS
(Run #s 8-15)

(Note: Salinity profiles for Runs #1-7 were acquired using a point conductivity probe.
Because of problems with the probe, the data obtained from the instrument
was discarded.)

Depth		Salinity, ‰							
in	cm	before Run #8	before Run #9	after Run #10	after Run #11	after Run #12	after Run #13	after Run #14	after Run #15
0.0	0.00	0	0	0	0	0	0	0	0
0.5	1.27	0							
1.0	2.54	0			0				
2.0	5.08	0	0	0	0	0	0	0	0
3.0	7.62	0			0				
4.0	10.16	0	0	2	0	0	0	0	2
5.0	12.70	0	0		2	2			9
5.5	13.97								17
6.0	15.24	1	4	5	6	8	5	5	22
6.5	16.51	6	7	5	10	8	9	10	23
7.0	17.78	12	12	11	11	10	10	11	23
7.5	19.05	12	12	18	17	14	15	15	
8.0	20.32	22	16	20	23	23	20	23	23
8.5	21.59		20	22	23	24			
9.0	22.86	25	22	24	27	27	20	23	
10.0	25.40	30	28	28	29	29	26	28	
12.0	30.48	30	30	28	29		26	28	23
14.0	35.56			30	29				
16.0	40.64				30				
22.0	55.88								
24.0	60.96	31							24
48.0	121.92								

Data for
SALINITY PROFILE PLOTS
(Run #s 16-23)

Depth		Salinity, ‰							
in	cm	after Run #16	after Run #17	after Run #18	after Run #19	after Run #20	after Run #21	before Run #23	after Run #23
0.0	0.00	0	0	0	0	0	0	0	0
0.5	1.27								
1.0	2.54								
2.0	5.08	0	0	0	0	0	0	0	0
3.0	7.62								
4.0	10.16	2	2	5	3	3	2	1	0
5.0	12.70	8	8	10	8	11	11	4	4
5.5	13.97	11	15	15	15	18	15	7	
6.0	15.24	16	18	20	20	20	22	10	8
6.5	16.51	16	22	22	22	23	23	14	18
7.0	17.78	22	22	23	22	23	23	20	22
7.5	19.05								
8.0	20.32	22	22	23	23	24	23	22	22
8.5	21.59								
9.0	22.86								
10.0	25.40								
12.0	30.48	23	24	24	24	24	24		
14.0	35.56								
16.0	40.64								
22.0	55.88								
24.0	60.96								25	25
48.0	121.92								

Data for

SALINITY PROFILE PLOTS

(Run #s 24-28, 48-49)

Depth		Salinity, ‰							
		after Run #24	after Run #25	after Run #26	after Run #27	after Run #28	before Run #48	after Run #48	after Run #49
in	cm								
0.0	0.00	0	0	0	0	0	0	0	0
0.5	1.27								
1.0	2.54								
2.0	5.08	0	0	0	0	0	0	0	0
3.0	7.62								
4.0	10.16	0	2	2	2	2	0	0	0
5.0	12.70	2	3	5	5	4			
5.5	13.97	5							
6.0	15.24	8	9	8	11	9	3	4	3
6.5	16.51	18	15	13	15	15	9	7	7
7.0	17.78	20	19	20	18	17	12	12	14
7.5	19.05		20	20			15	17	18
8.0	20.32	21	21	21	20	20	17	19	19
8.5	21.59						19	20	
9.0	22.86	22				21	20	20	20
10.0	25.40								
12.0	30.48						22	22	22
14.0	35.56								
16.0	40.64								
22.0	55.88						24	25	25
24.0	60.96	24	24	23	23	23			
48.0	121.92								

Data for

SALINITY PROFILE PLOTS

(Run #s 50-54)

Depth		Salinity, ‰				
in	cm	after Run #50	after Run #51	after Run #52	after Run #53	after Run #54
0.0	0.00	0	0	0	0	0
0.5	1.27					
1.0	2.54					
2.0	5.08	0	0	0	0	0
3.0	7.62					
4.0	10.16	1	1	1	1	0
5.0	12.70					
5.5	13.97					
6.0	15.24	4	5	5	4	3
6.5	16.51	10	6	7	9	7
7.0	17.78	17	14	13	14	14
7.5	19.05	17	18	17	17	17
8.0	20.32	18	20	18	20	19
8.5	21.59					
9.0	22.86	20	20	18	20	
10.0	25.40					
12.0	30.48	22	22	22	22	22
14.0	35.56					
16.0	40.64					
22.0	55.88	25	25	25	24	24
24.0	60.96					24
48.0	121.92					

Salinity Profile
before Run #8
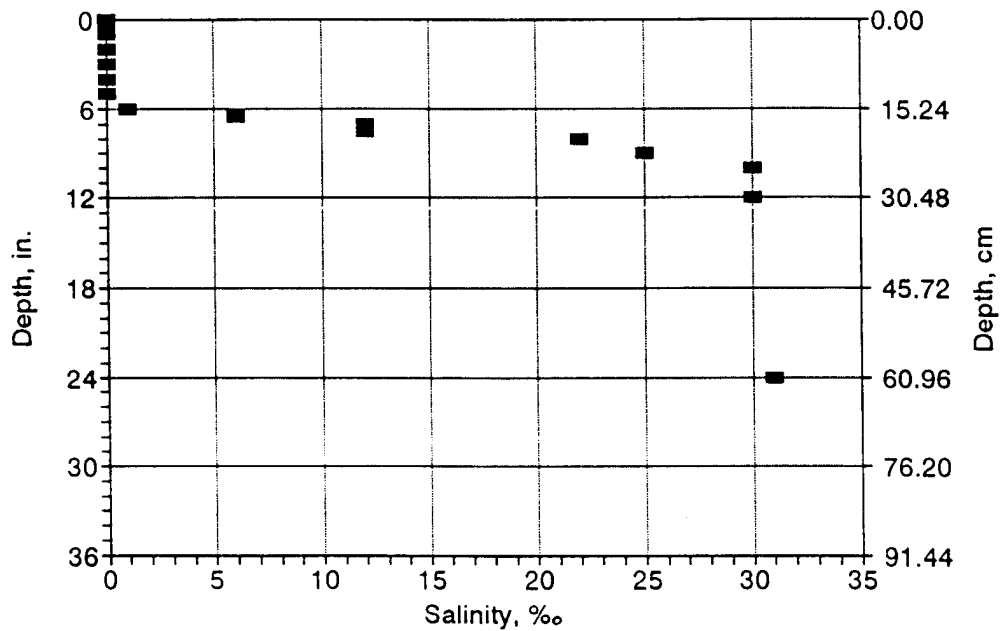
Salinity Profile
before Run #9
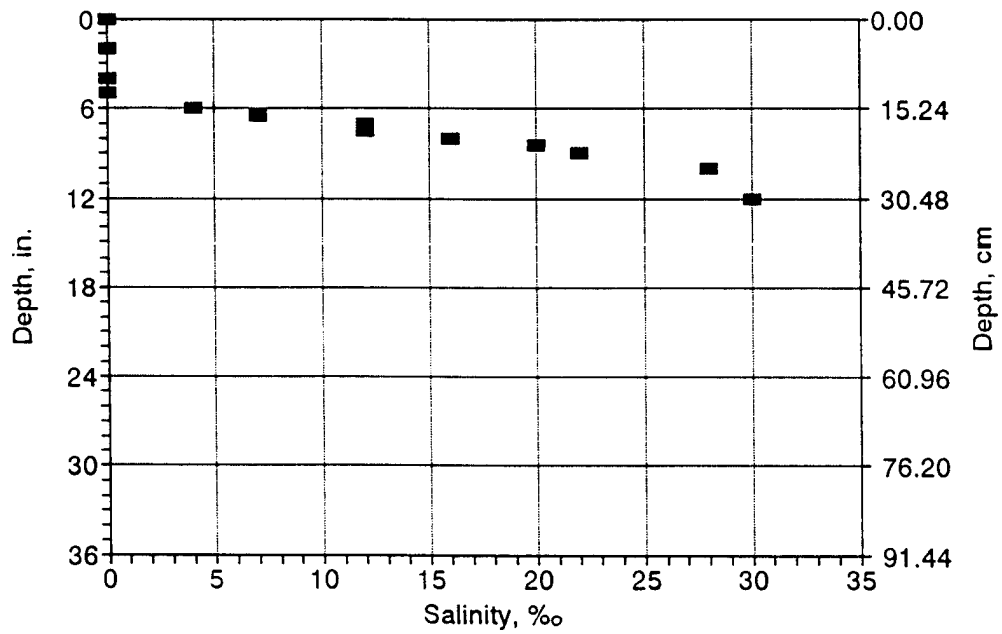
Salinity Profile
after Run #10
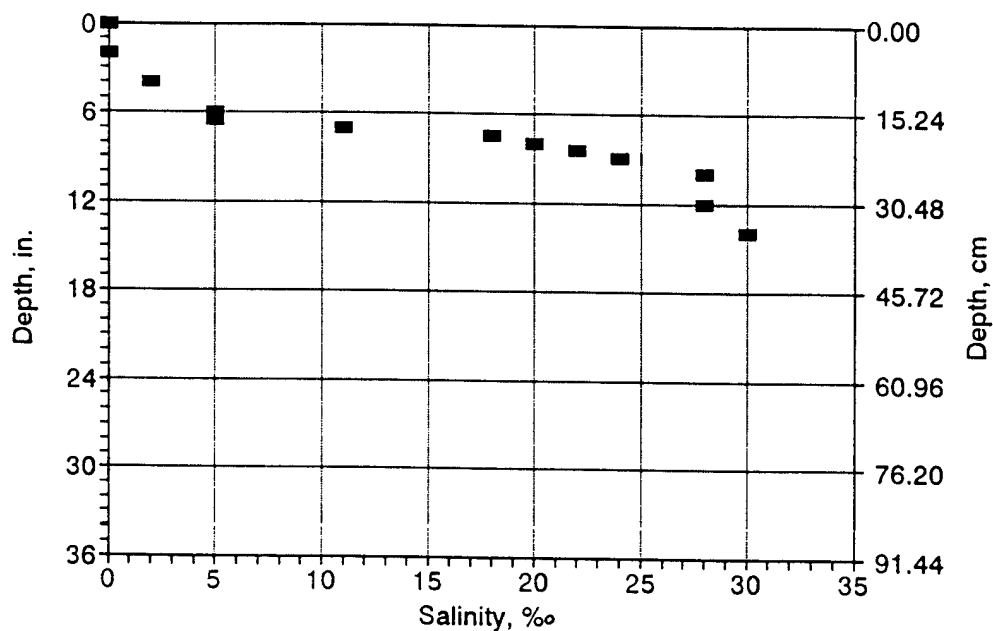
Salinity Profile
after Run #11
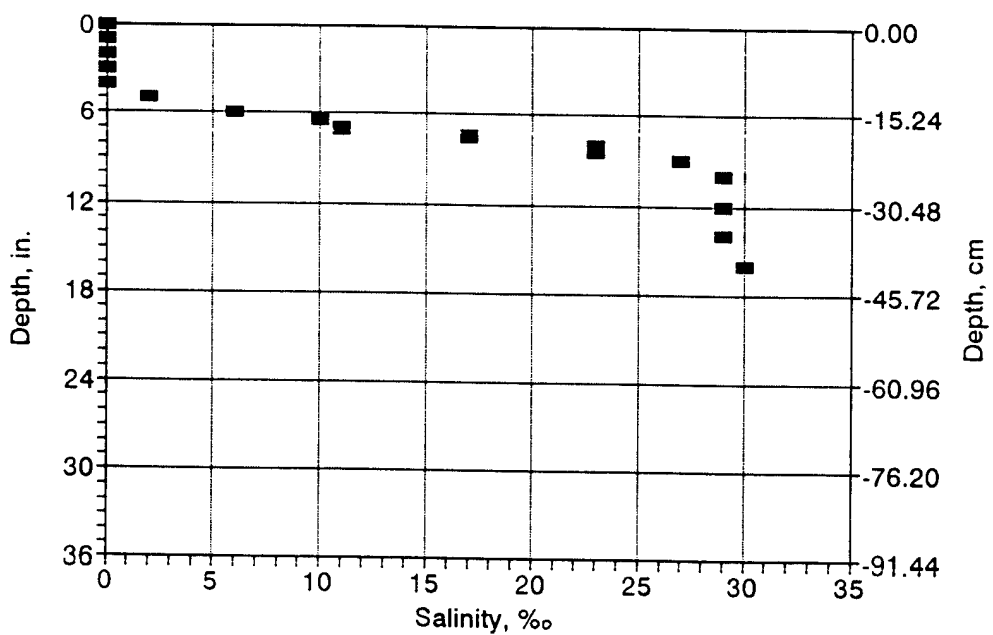
Salinity Profile
after Run #12
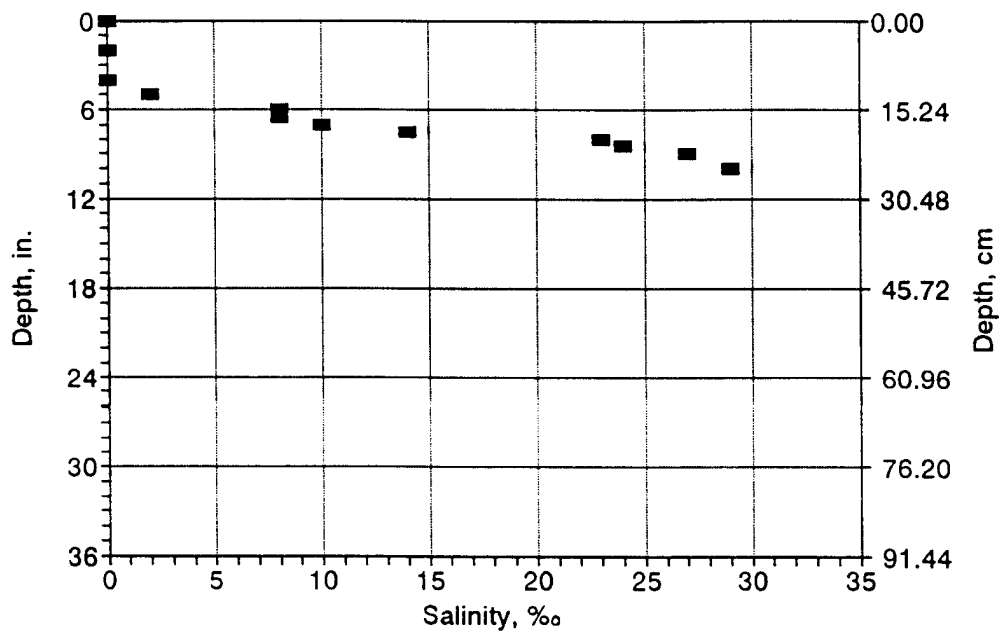
Salinity Profile
after Run #13
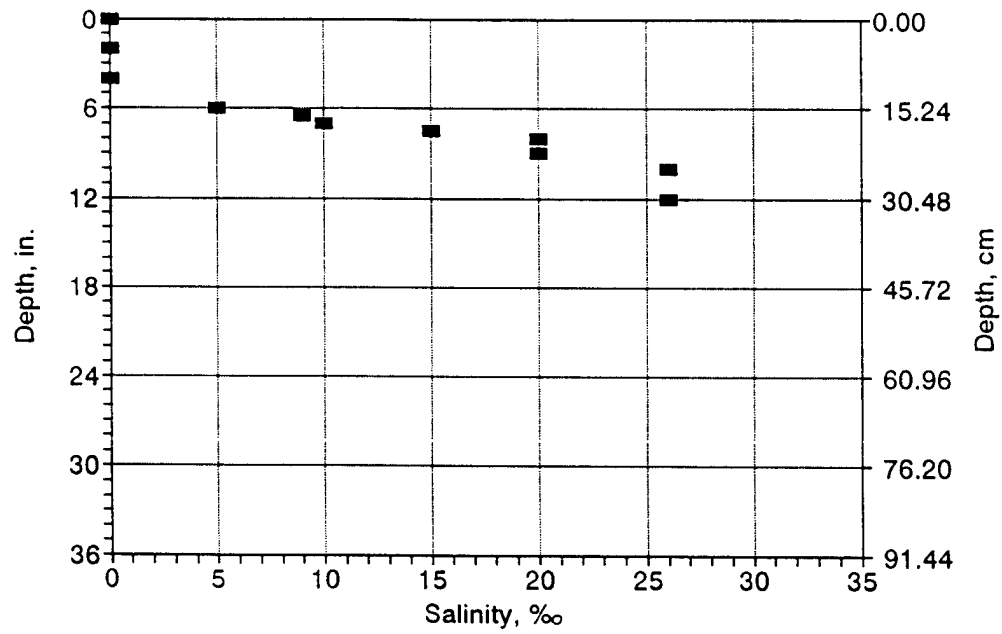
Salinity Profile
after Run #14
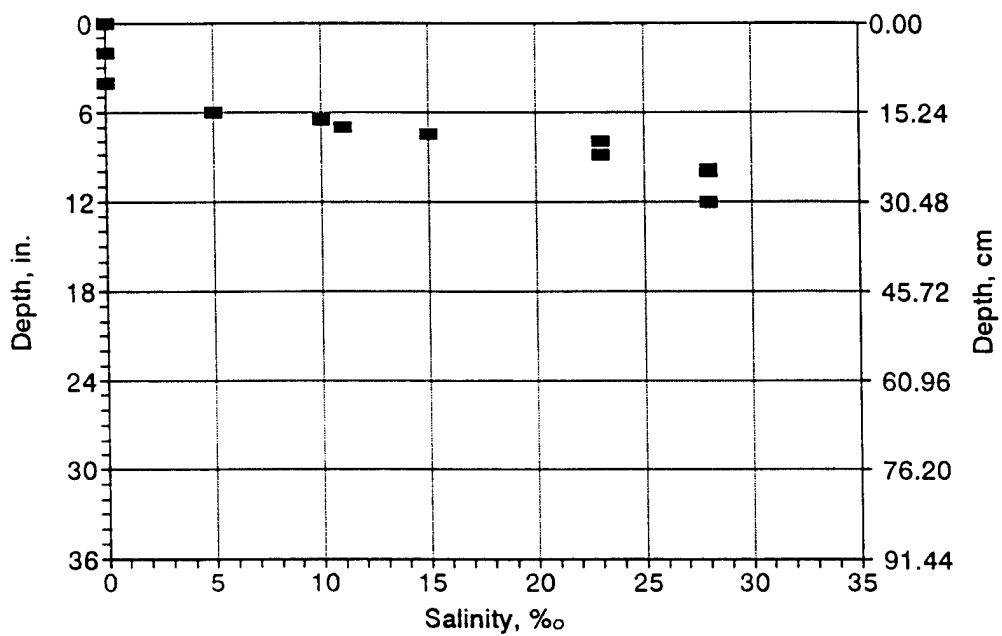

Salinity Profile
after Run #15
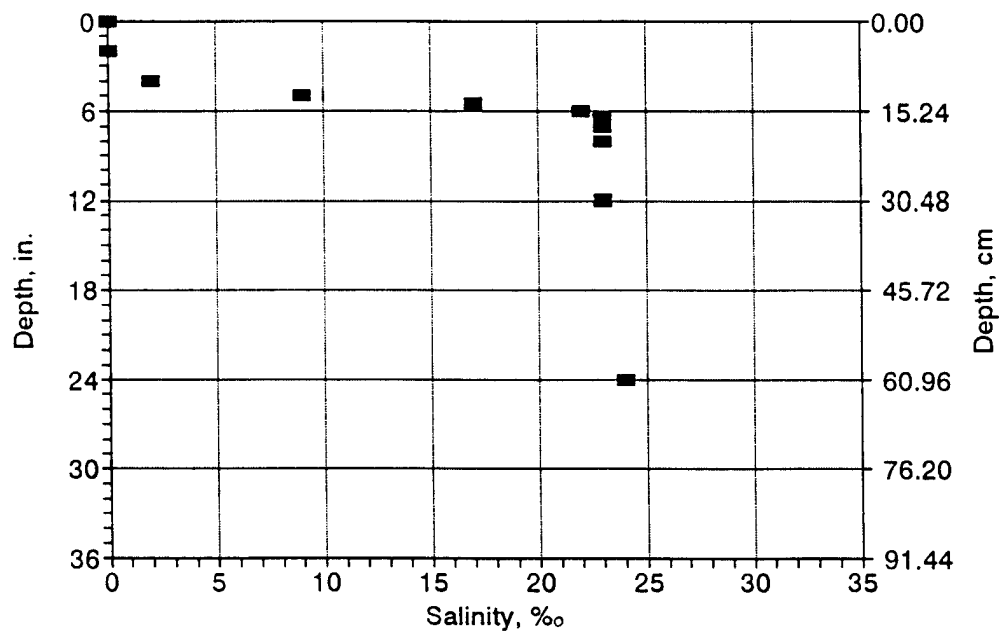
Salinity Profile
after Run #16
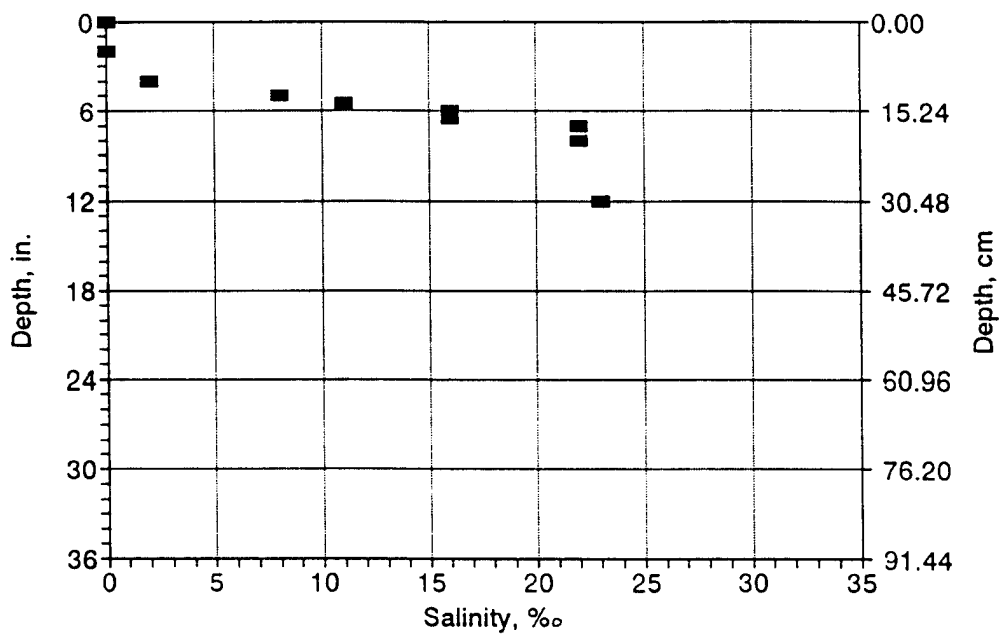
Salinity Profile
after Run #17

C - 9
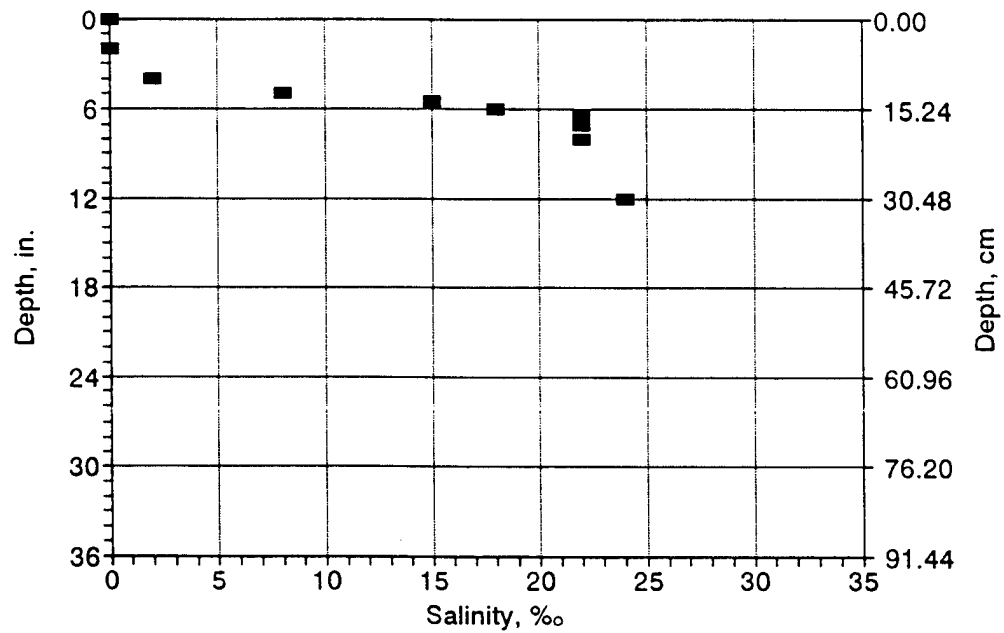
Salinity Profile
after Run #18
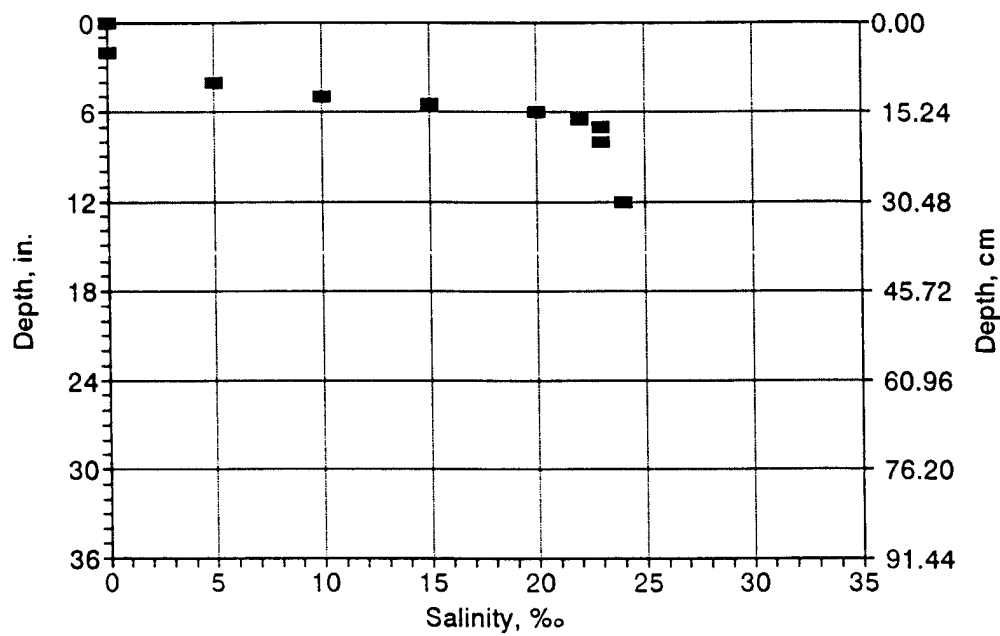
Salinity Profile
after Run #19
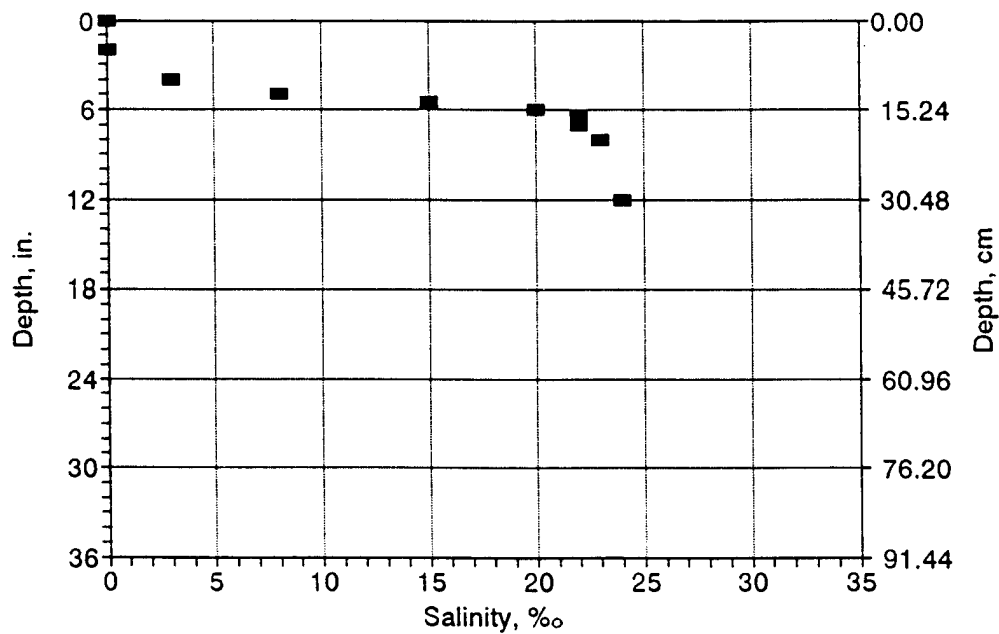
Salinity Profile
after Run #20
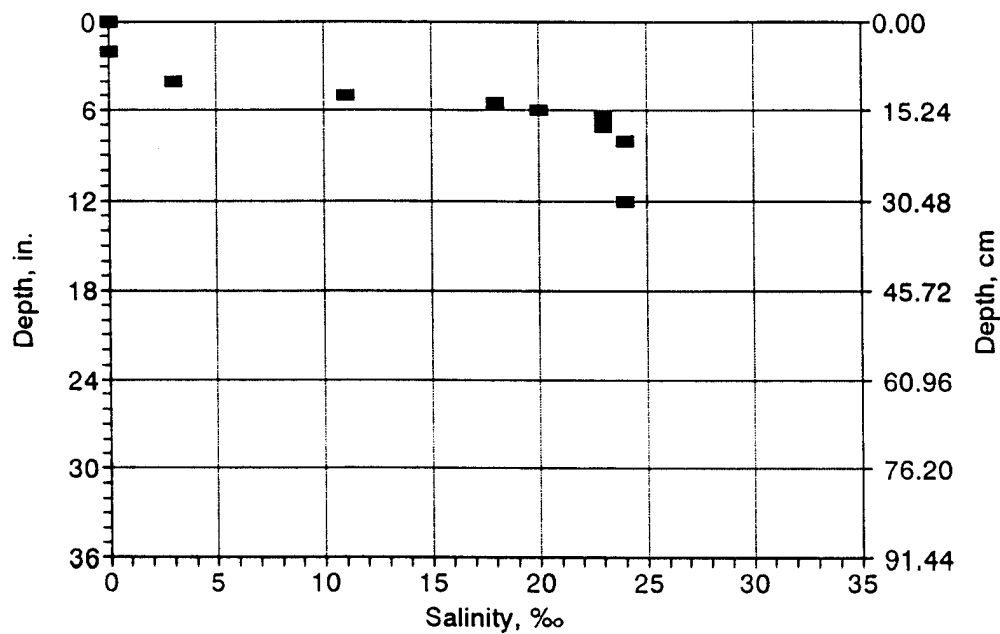
Salinity Profile
after Run #21

C - 11
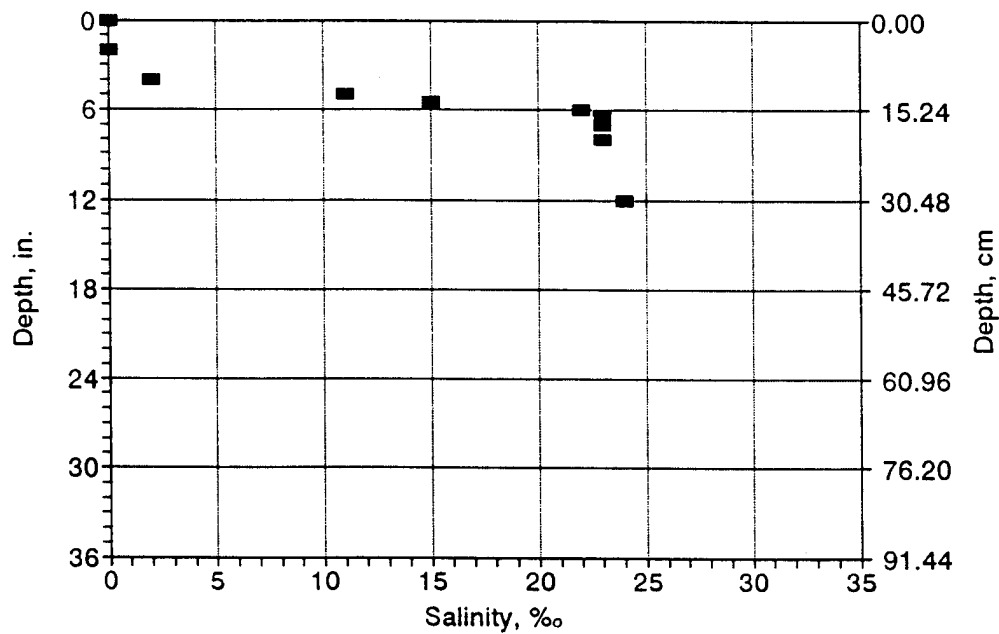
Salinity Profile
before Run #23
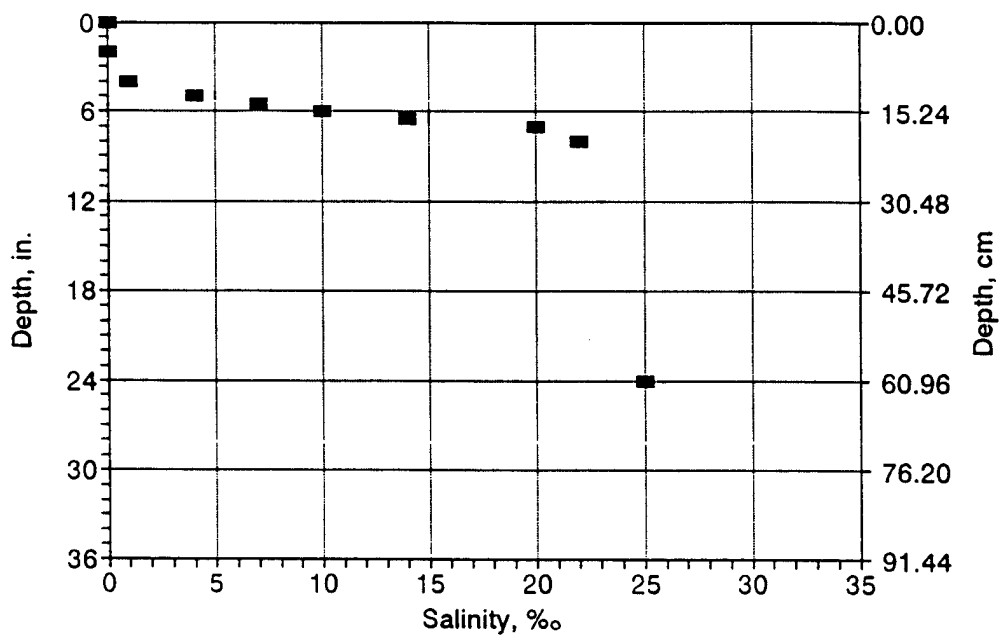
Salinity Profile
after Run #23

C - 12
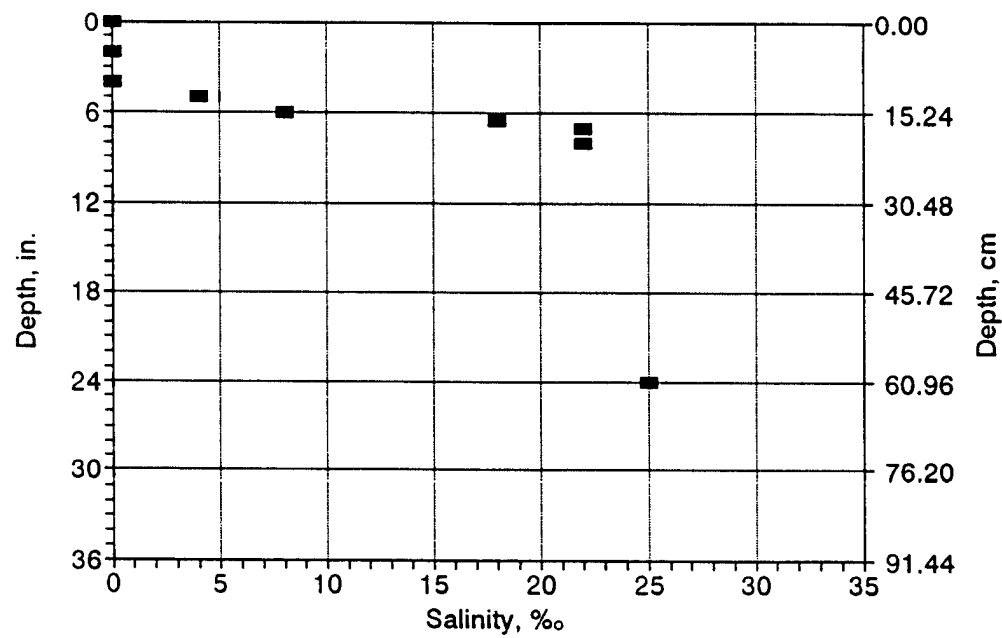
Salinity Profile
after Run #24
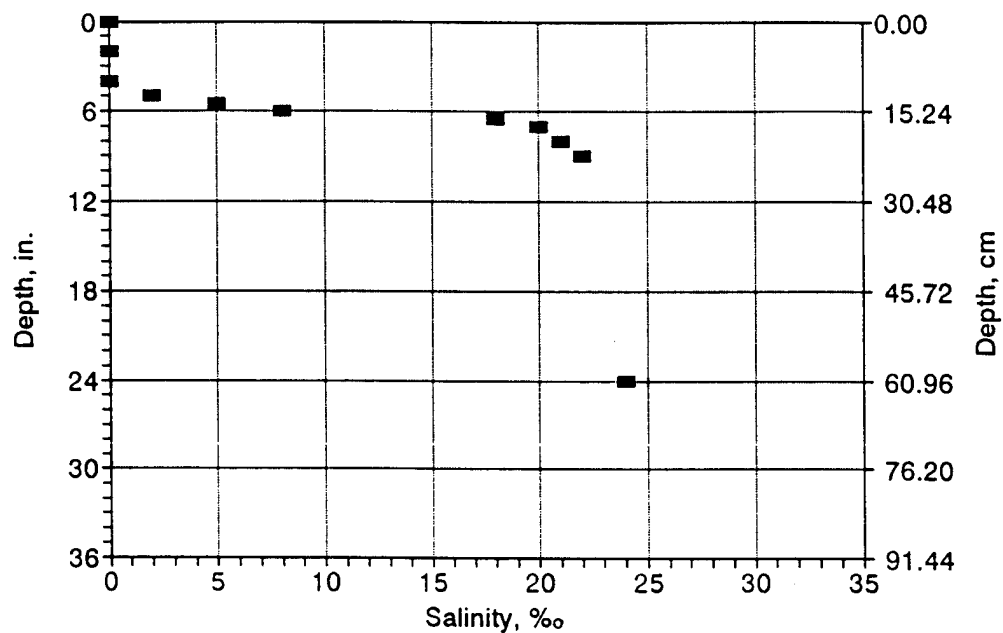
Salinity Profile
after Run #25
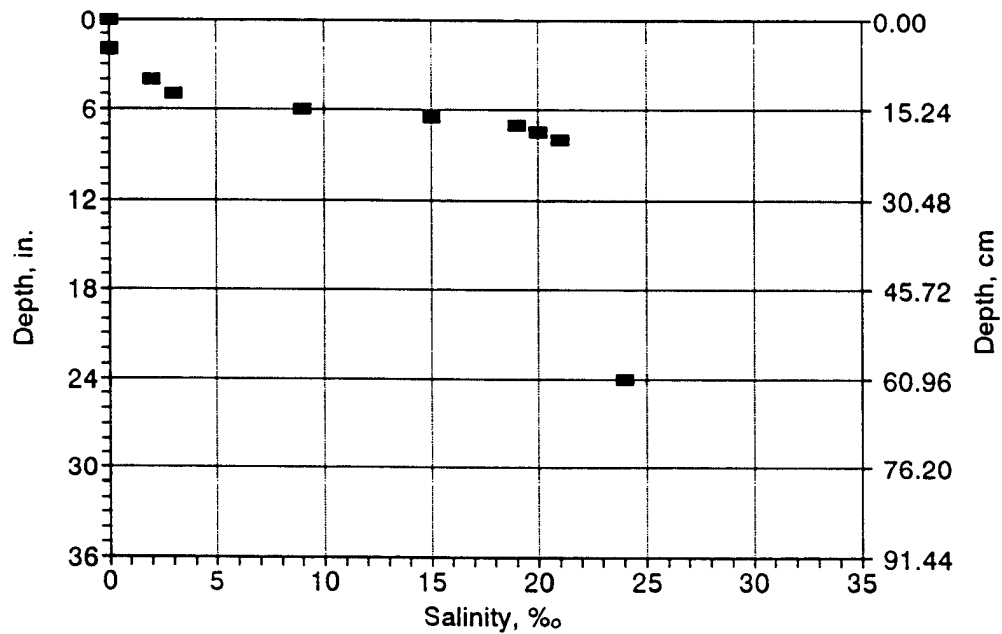
Salinity Profile
after Run #26
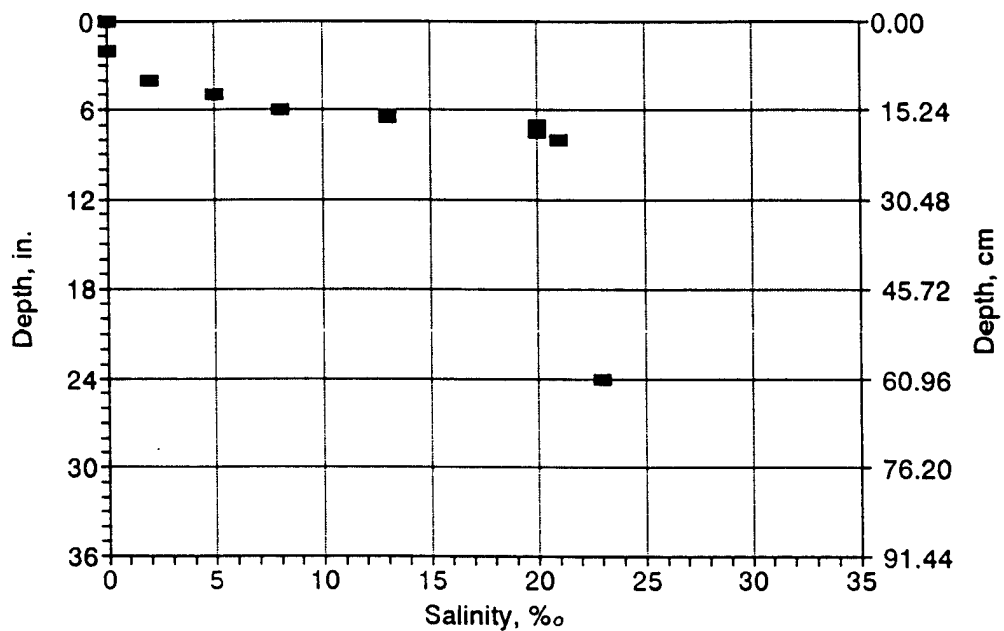
Salinity Profile
after Run #27
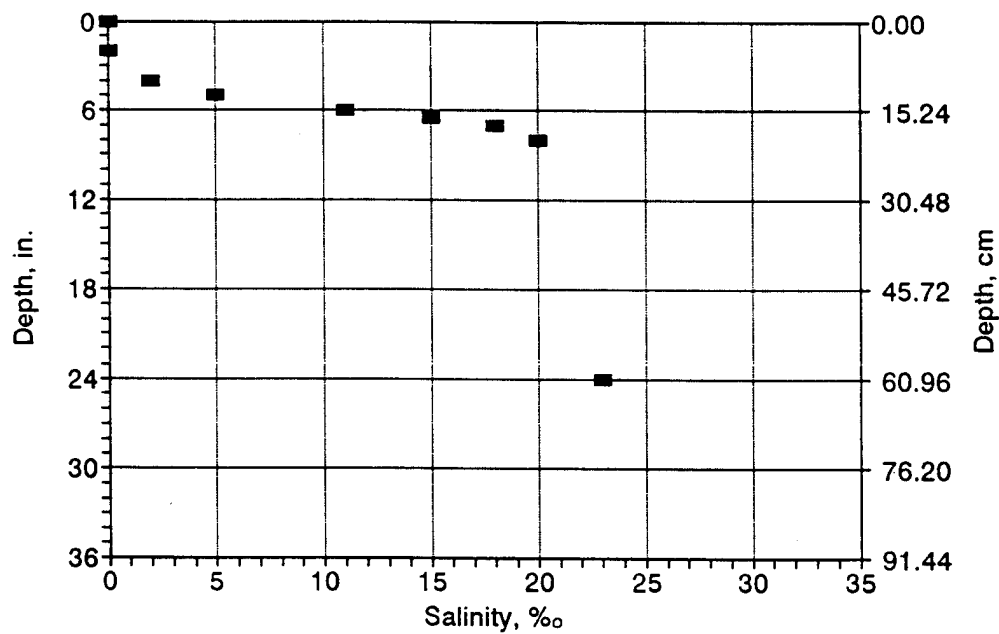
Salinity Profile
after Run #28
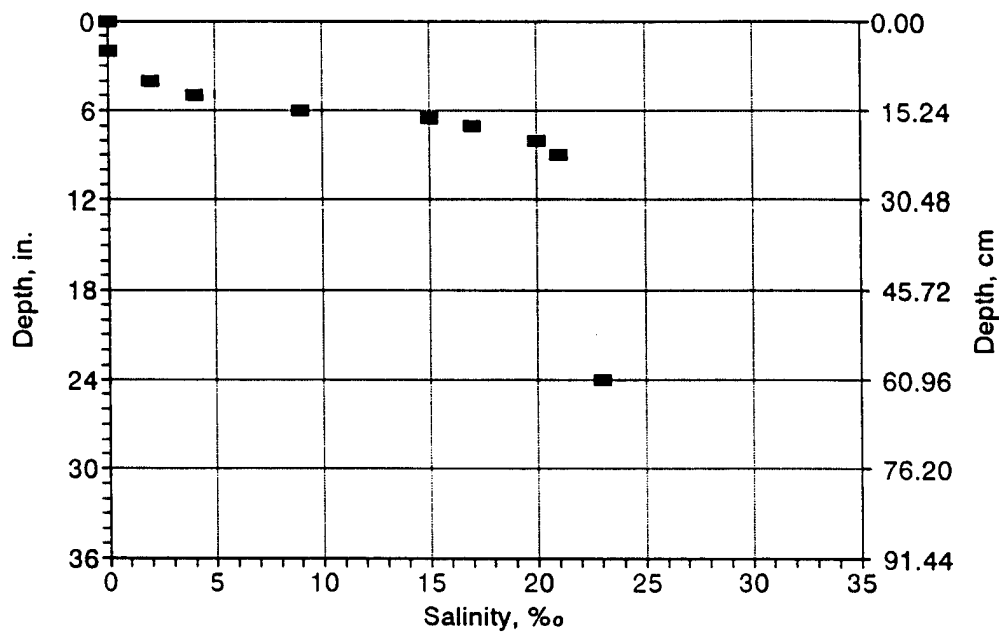
Salinity Profile
before Run #48
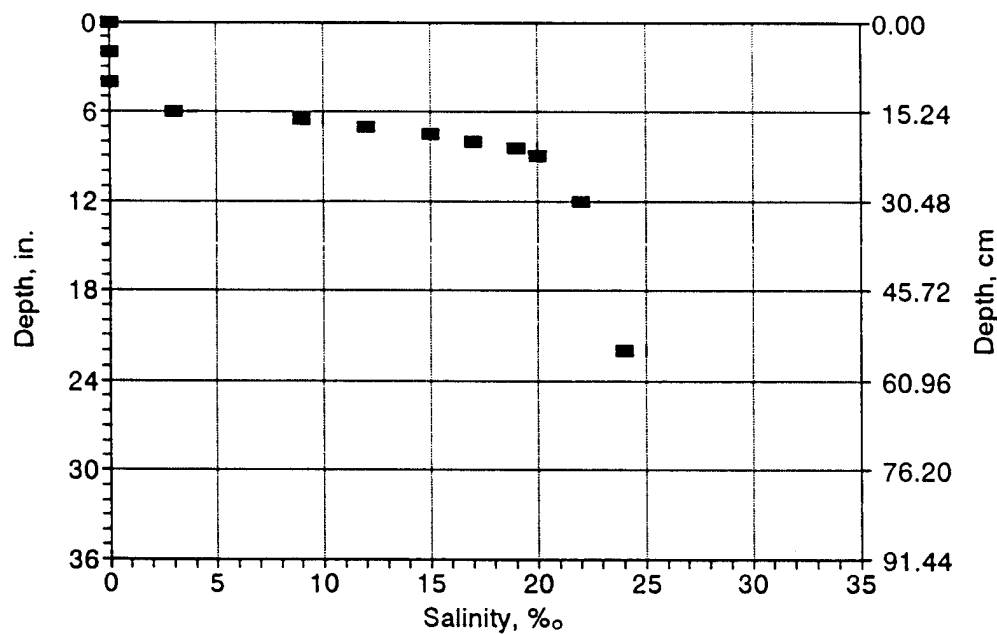
Salinity Profile
after Run #48
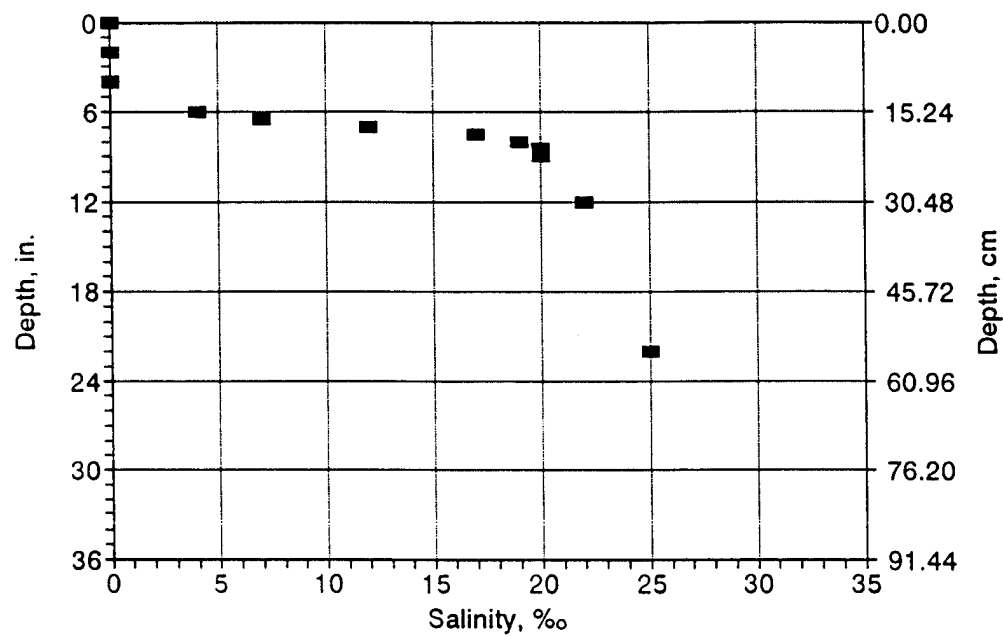
Salinity Profile
after Run #49
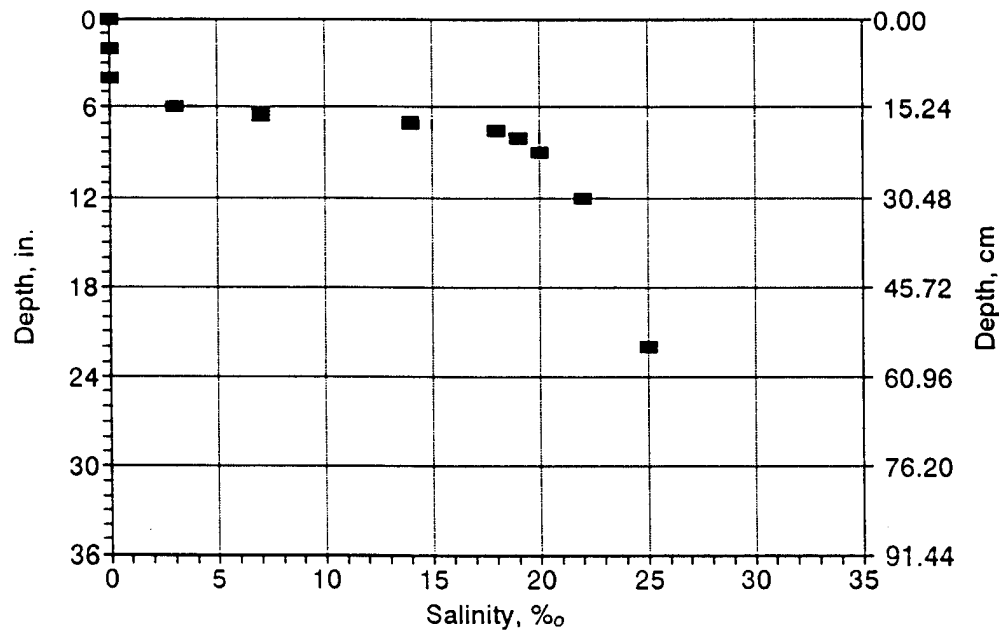
# Salinity Profile
after Run #50
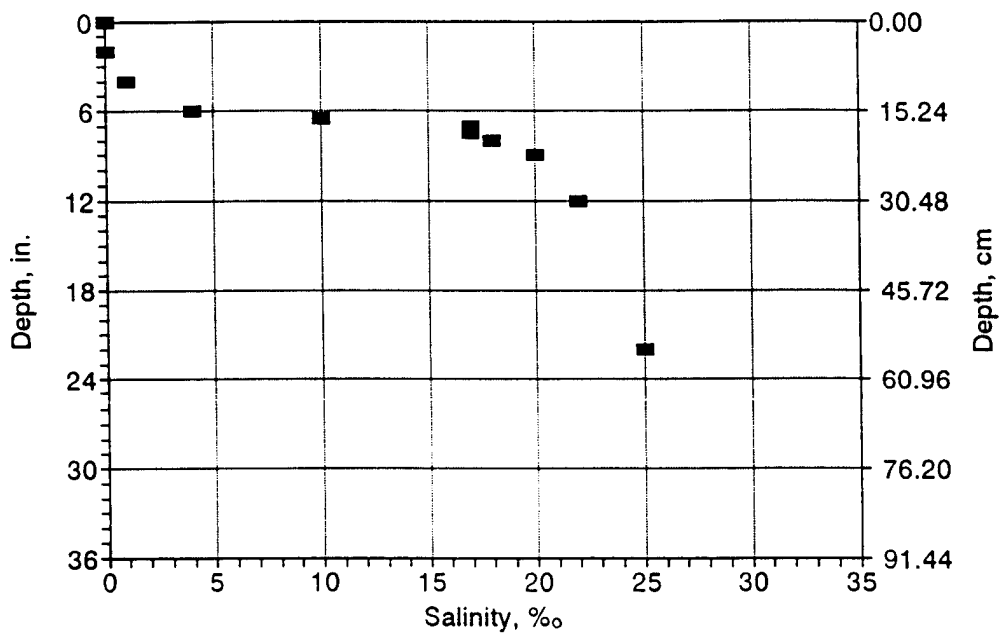
Salinity Profile
after Run #51
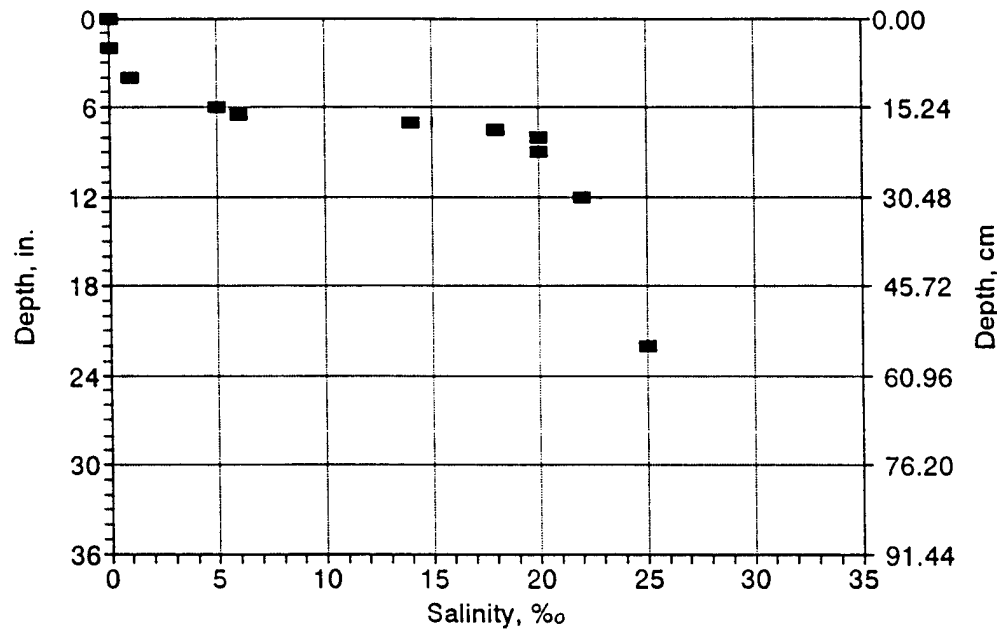
Salinity Profile
after Run #52
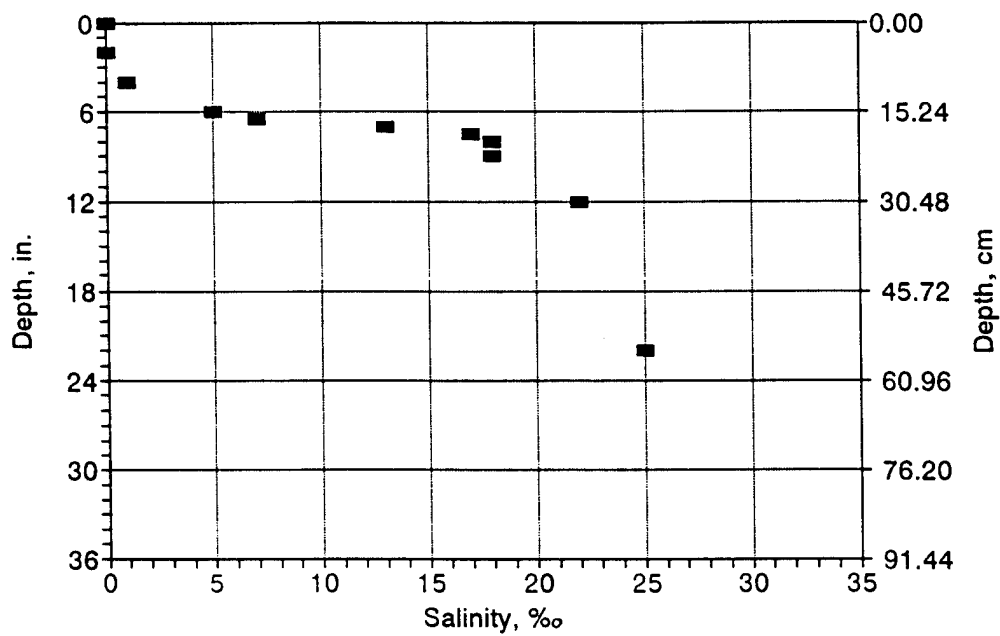
Salinity Profile
after Run #53

Salinity Profile
after Run #54